Understanding and Improving Locomotion: The Simultaneous Optimization of Motion and Morphology in Legged Robots

by

Yevgeniy Yesilevskiy

A dissertation submitted in partial fulfillment
of the requirements for the degree of
Doctor of Philosophy
(Mechanical Engineering)
in the University of Michigan
2018

Doctoral Committee:

Assistant Professor C. David Remy, Chair
Professor Keith W. Buffinton, Bucknell University
Professor Jessy Grizzle
Professor Greg Hulbert

Yevgeniy Yesilevskiy
yevyes@umich.edu
ORCID iD: 0000-0002-1181-1699

To that which was there when no one else was.
That warmed my soul when it was cold.
That brought light to the darkness of my mind.
That which brought me joy during my bleakest moments.
That's right.
To coffee.

ACKNOWLEDGEMENTS

Throughout my life I have had the great fortune to have caring family, friends, colleagues, and mentors at every stage. This work is an extension of their ceaseless support. It truly would not have been possible without them.

To begin, I want to give thanks to the mentors that I have had throughout the years. I am incredibly grateful for my Ph.D. advisor David Remy. The fundamental role of an advisor is to guide you through your research, teaching you the skills necessary to advance as a scientist and push towards novel achievements. That fundamental role only scratches at the surface of what David does. He is the rare person that can, in equal measures, have a serious scientific discussion, be a friend to joke around with, and be a source of constant support that I could turn to in my toughest moments. Thank you for everything David. I would also like to thank my mentors during my undergraduate days at The Cooper Union. Thank you to Alan Wolf and Eric Lima for the tutelage and opportunities that you gave me, you are the reasons that I have taken the graduate path I have.

Thank you to my colleagues in the RAMlab. The community that you have built in the lab made coming to work everyday something that I looked forward to. In particular, I want to single out my good friend Zhenyu Gan. You and I have worked on nearly every project together. It has been a daily honor and a privilege to work so closely with as curious, talented, and intelligent a person as yourself. Thank you also to William Yang and Nikko Van Crey for your tireless help in developing and running optimization studies.

Thank you to my many friends. I am truly lucky to be in the position that there are too many of you to name individually. Still, it would be remiss not to mention the special place that Dom, Fresc, and Brandon have. When I moved to Ann Arbor, I certainly worried that my ties to my friends from back in New York might fray. That has not been the case. If anything, they have become stronger. I talk to you each every single day. You three have always been there to help me through the bad times and to celebrate the good times. Dom and Fresc, we have a great time whether it is sitting on a beach in Bermuda telling jokes, contemplating the meaning of our place in the world over text messages, or daydreaming about opening up a coffee shop. Brandon, you are my oldest friend. All the more impressive considering

that we started as mortal enemies. To this day we spend more time laughing than saying actual words when we talk, which is the best thing I could ask for. Thank you also to Jason Damiano for always being there and always being up for an adventure exploring Europe. Thank you to Joey B, Ryan, and Jimmy for being a constant source of hilarity and camaraderie. Thank you to my many friends in Ann Arbor. In particular, thank you to Ben and Jeff, my constant companions throughout the Ph.D. process.

Most importantly, I want to thank my family. Mom, you are the hardest working person I know. You are a constant inspiration. I certainly don't tell you enough, but your love and support have meaning beyond words. Dad, from as early as I can remember, I always looked up to your quick mind. You always encouraged my inquisitiveness, and I am sure that led me to this scientific path. Helen, it has been incredible to watch you grow into the strong, intelligent, and independent woman you are today. Lastly, Mark, it is certainly a rarity that someone can call their brother their best friend, but with you, I am lucky enough to have that fortunate situation. You, and Jenny as well, have been a constant source of support and encouragement.

PREFACE

Chapters 2-5 have each been written as separate manuscripts. Given this, there may be some repetition of presented material, particularly in the methodology of the studies.

TABLE OF CONTENTS

LIST OF FIGURES

Figure

LIST OF TABLES

Table

ABSTRACT

There exist many open design questions in the field of legged robotics. Should leg extension and retraction occur with a knee or a prismatic joint? Will adding a compliant ankle lead to improved energetics compared to a point foot? Should quadrupeds have a flexible or a rigid spine? Should elastic elements in the actuation be placed in parallel or in series with the motors? Though these questions may seem basic, they are fundamentally difficult to approach. A robot with either discrete choice will likely need very different components and use very different motion to perform at its best. To make a fair comparison between two design variations, roboticists need to ask, is the best version of a robot with a discrete morphological variation better than the best version of a robot with the other variation?

In this dissertation, I propose to answer these type of questions using an optimization based approach. Using numerical algorithms, I let a computer determine the best possible motion and best set of parameters for each design variation in order to be able to compare the best instance of each variation against each other.

I developed and implemented that methodology to explore three primary robotic design questions. In the first, I asked if parallel or series elastic actuation is the more energetically economical choice for a legged robot. Looking at a variety of force and energy based cost functions, I mapped the optimal motion cost landscape as a function of configurable parameters in the hoppers [134]. In the best case, the series configuration was more economical for an energy based cost function, and the parallel configuration was better for a force based cost function. I then took this work a step further and included the configurable parameters directly within the optimization on a model with gear friction [133]. I found, for the most realistic cost function, the electrical work, that series was the better choice when the majority of the transmission was handled by a low-friction rotary-to-linear transmission. In the second design question, I extended this analysis to a two-dimensional monoped moving at a forward velocity with either parallel or series elastic actuation at the hip and leg [132]. In general it was best to have a parallel elastic actuator at the hip, and a series elastic actuator at the leg. In the third design question, I asked if there is an energetic benefit to having an articulated spinal joint instead of a rigid spinal joint

in a quadrupedal legged robot [135]. I found that the answer was gait dependent. For symmetrical gaits, such as walking and trotting, the rigid and articulated spine models have similar energetic economy. For asymmetrical gaits, such as bounding and galloping, the articulated spine led to significant energy savings at high speeds.

The combination of the above studies readily presents a methodology for simultaneously optimizing for motion and morphology in legged robots. Aside from giving insight into these specific design questions, the technique can also be extended to a variety of other design questions. The explorations in turn inform future hardware development by roboticists and help explain why animals in nature move in the ways that they do.

CHAPTER I

Introduction

1.1 Motivation

In recent years, the field of legged robots has made remarkable advances. Researchers have made great strides in achieving dynamic locomotion in legged robots [104, 44, 96, 116]. There have been significant improvements in legged robotic control [101, 127, 103, 32] and design [61, 43, 121]. Through all of these improvements, the field is steadily approaching the point where legged robots are able to perform a variety of tasks that will aid humans. They are approaching the ability to aid on disaster missions [74] and perform jobs that are unsafe for humans [60]. To continue pushing the field forward, energetics must also be improved. Though robots are becoming more energetically economical [13, 83, 58], the more versatile designs still do not yet approach the energy values of animals of comparable size [107]. Furthermore, the vast majority of legged robots that exist today depend on a wall outlet to provide power [81, 114, 93]. To get to the point that robots are able to help humans in our many tasks, we need to remove this tether.

Improving legged robot energetics is a fundamentally difficult problem. Within a robot, there are an immense amount of configurable parameters and actuation strategies. Many roboticists, seeking to take advantage of the energetically economical motion that animals exhibit across a wide range of speeds [57, 51, 85], design their robots based on animals [80, 10, 64]. The motivating idea is that features that are useful in nature should be similarly useful in robotics. However, nature has significant constraints that are not necessarily present in robotics. For example, quadrupedal animals have little movement in the anterior section of their spines [115], possibly due to their respiration systems, and favor the synchronization of breathing and locomotion [18]. Evolutionary pressures also constrain animals to particular morphologies

[36]. Furthermore, there are significant differences in elasticity and actuation between robotics and nature.

The differences between nature and legged robotics open up a fundamental design question: how should roboticists improve robotic energetics? There are two primary avenues that roboticists can take. Roboticists can improve robotic morphology, or, they can change the motion of the robot.

Broadly speaking, roboticists have two routes within the realm of robotic morphological changes. Within the robot there are many configurable parameters that can be adjusted to improve energy usage. First, they can change parameters that are able to vary smoothly. Roboticists can choose the motors that provide the best trade-off between weight, power, and efficiency. They can choose the transmission system that allows them to provide large torques without sacrificing speed. Masses of different segments can be reconfigured to best utilize inertial forces [10]. To avoid excessive motor torques, large inertias can be avoided, and mass can be moved closer to the actuation source [61]. Springs can be incorporated to store and release energy passively [131]. The spring constants and damping ratios can then be adjusted to obtain desired oscillations. Secondly, roboticists can also conduct discrete design comparisons. These represent fundamental structural changes in the robot that do not vary smoothly. For example, changing the configuration of a motor and a spring in a leg joint [45].

For a given robot, roboticists can also improve energetics by changing the motion to achieve desirable characeristics. Here they again have two routes. First, they can choose the best motion within a particular footfall pattern [13]. For example, choosing to apply increased torque during stance, or allowing the legs to oscillate during swing. Improved control strategies such as these can also be used to leverage motions that lower collision losses, decrease damping, and minimize the negative work performed by the motors. Roboticists can take advantage of the natural dynamics of their system to minimize motor input [83]. That is, they can use the passive interplay of gravity, inertia, and spring oscillation to move economically. Second, roboticists can improve legged robot energetics by utilizing multiple gaits [130]. This practice is inspired by nature [57], and allows efficient locomotion across a wide range of speeds.

In reality, the way that a robot moves and the way that is built are intrinsically related. The choice of parameters clearly affects the energetically optimal motion. Choosing a certain mass distribution affects the ways in which gravity will interact with the robot. Choosing certain springs will change the natural frequencies of oscillation of the robot, which will in turn affect how the springs can be used in an

economical way. The parameters and motion choice will decide which gaits are optimal at which speeds, and when one should transition among them. The two avenues mutually affect each other, and therefore, to build the most energetically economical robots, they must be modified simultaneously.

The central tenet of this proposal is that, to build the best possible legged robots, we must simultaneously optimize the motion and morphology of robots. In the process of exploring this simultaneous optimization, the goal is to understand the relationship between the two avenues and explore a set of basic questions. How do the parameter choices affect the motion? How much of the motion is driven by natural dynamics? Why are certain gaits favored over others? How can we compare different morphologies in order to find the best choice? Through exploring these broad questions, the goal is to improve legged robots, and also, to gain insight into why humans and animals move the way they do.

1.2 State of the Art

The vast majority of existing work in improving legged robots has focused on individually improving either the continuous or discrete aspects of morphology or motion respectively.

In the realm of improving continuous parameters, for example, different spine stiffness distributions were explored by [136] during quadrupedal bounding gaits to find the fastest running speed. [26] looked at the effect of changing passive exoskeleton spring constant values on metabolic cost. [10] optimized the structure of various leg components on the MIT Robotic Cheetah to minimize leg weight. [131] looked at various knee compliance values to improve the energetics of a bipedal robot. Other researchers have sought to compare discrete morphological variations. [45] compared different actuation and elasticity configurations to find which was most economical for a model of a human ankle joint exoskeleton. [49] compared two 2-dimensional quadrupedal bounding models.

Still others have looked at improving motion. Among the studies that sought to find the best motion within a particular footfall pattern, [66] optimized the motion of a central pattern generated bounding gait to optimize performance. [20] used offline optimization to select a feedback controller that improved the stability of their walking gait. [12] utilized optimization on a simple event-based controller to achieve human-like energetic economy in a walking gait. Similar to nature, these type of studies can take advantage of rigid inverted pendulum motion at low speeds [1] and spring loaded

inverted pendulum motion at higher speeds [15] to move passively. Researchers have also looked at utilizing multiple gaits on a single robot. Both humans [29] and horses [57] transition from one gait to another in order to move economically across a wide range of speeds. Similar gait changes could prove useful for robotics as well. [25] and [123] found that simple bipedal models also benefit from walking at low speeds and running at high speeds. [71, 125] have shown similar benefits to changing gaits in quadrupedal robot models. In our own work, we have also found a benefit to transitioning gaits in a conceptual quadrupedal robot model [130].

Ideally, roboticists would be able to, in a single study, simultaneously optimize for all aspects of robotic motion and morphology. They would be able to, at a given speed, automatically choose the best discrete morphology, with the best parameters, and the best motion, moving at the best gait. As far as we know, no studies have attempted this sort of combined optimization. The reason is because it is an incredibly complex problem. This section will illustrate that complexity through a discussion of robotic gait, and, introduce the studies that have begun exploring the notion of simultaneous optimization of motion and morphology.

Gait

During forward locomotion, humans and animals move in complex patterns. These patterns, known as gaits, involve a complex interplay of oscillations and precise foot placement that is periodically interrupted by collisions. The particular choice of gait depends on the animal, the speed of locomotion, and the terrain [22, 57, 86]. While the benefits and classification of these gaits have been researched in detail [52, 53], their origin is not well understood.

One hypothesis is that gaits arise due to energetic considerations. An important analysis of gait energetics was published by Hoyt & Taylor [57]. Hoyt & Taylor recorded the cost of transport (COT) of horses walking, trotting, and galloping on a treadmill. When plotting this COT as a function of locomotion speed and gait, one can identify three distinct curves. The walking and trotting curves show a clear minimum for different locomotion velocities (Fig. 1.1). Going faster or slower than this optimal speed, inevitably increases energy consumption. Furthermore, the curves intersect, meaning that at different speeds, different gaits require the least amount of energy. When the horses were allowed to self-select their velocity within a particular gait, they tended to move near the energetic minima. These experiments have been repeated by different groups [85], and extend to human locomotion [29], where they have shown that walking is more energetically economical at low speeds, and running

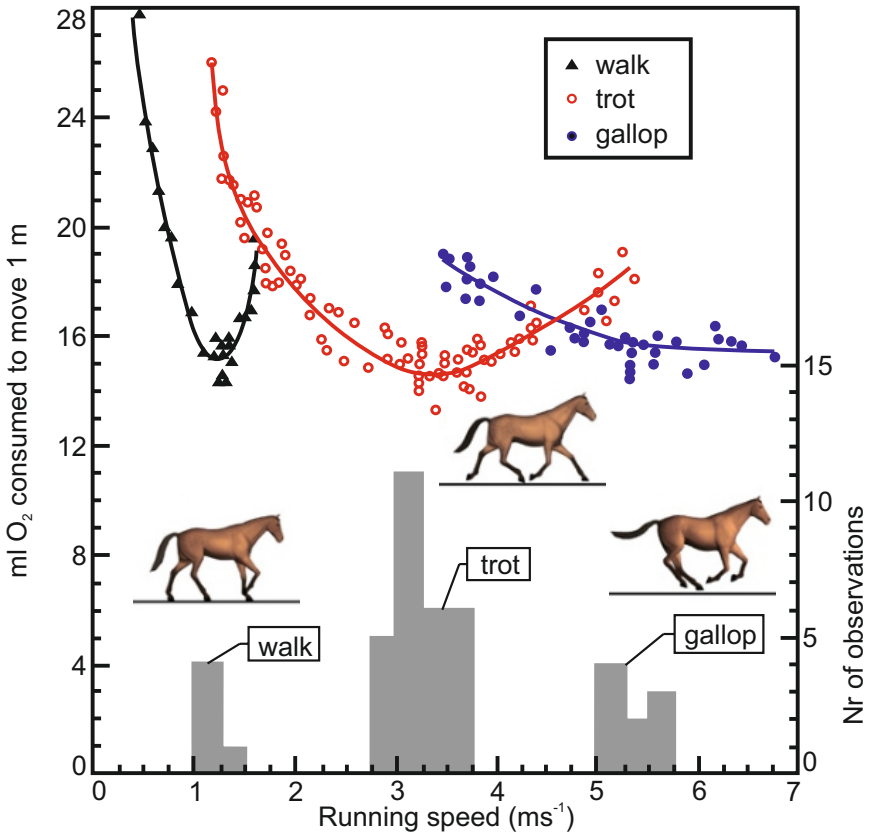

Figure 1.1: In this adaptation of a figure from Hoyt and Taylor [57], the metabolic cost of transport (COT) is shown as a function of forward speed and gait selection for horses moving on a treadmill. For each gait, an optimal velocity can be identified for which the COT is minimized. When allowed to self-select their locomotion speed (shown as the grey histograms), the animals choose velocities that correspond to these minima.

at higher speeds.

Any experiment like that of Hoyt & Taylor can only show a correlation of preferred locomotion speeds and energetic minima. It cannot explain causality, and allows for multiple interpretations of what is observed.

One line of reasoning is that some external factor causes the horses to prefer certain speeds. Through adaptation, they then become better at locomotion at those speeds. Such a factor could be, for example, the preferred locomotion speed of a herd of horses. This external influence would encourage horses to locomote primarily at certain speeds. Over time, they would learn better how to move at these speeds, making them inherently more efficient through a *neurological* adaptation. In this case, the energetic optima would only be a secondary effect. In this interpretation, the increase in energetic cost when going faster or slower is caused by forcing the

horses to execute a motion that they normally do not use and that they have not learned equally well. This idea requires a process of adaptation, and can be extended beyond simple learning.

A second line of reasoning is that some external factor causes certain speeds to be efficient. The horses then move at those speeds to minimize energy usage. This conclusion implies that this factor has nothing to do with the horses' preference. This factor could be a mechanistic explanation. That is, the biomechanical dynamics of the horses could *physically* favor certain locomotion speeds. Studies in nature have provided some evidence for this explanation. These studies state that an animal's structure and the way that it moves are closely linked [9, 55, 54]. Animals utilize the dynamics that arise from their morphology to move economically at a variety of speeds. For example, at low speeds, humans use a nearly straight stance leg in an inverted pendulum like motion [23]. At high speeds, they utilize the elasticity in their joints to move in a spring loaded inverted pendulum like motion [15]. Similarly, during the swing phase, humans utilize the passive double pendulum dynamics of their legs to swing forward and extend before touchdown [87]. Utilizing these principles, entirely passive mechanical walking machines have been made. These were explored conceptually in [87, 83] and shown in hardware by [27, 94] among others.

Ultimately though, it is difficult to isolate these mechanistic effects by studying nature. Model based studies could, however, focus exclusively on these effects. We propose an optimization-based approach. This approach finds the motions that are most economical for a given structure's dynamics, with no notion of that legged system's preference.

Optimal Control in the Study of Legged Locomotion

The role of energy in determining gait has been explored in a model-based approach. In these studies, the motion is entirely driven by the interplay of a chosen controller and the system dynamics; there is no adaptation influence. Optimization within these model-based studies provides an interesting tool that removes pre-defined motion bias from the energetics. [25] showed that for a simple actuated bipedal model with articulated knees, it is most economical to walk at low speeds, and run at high speeds. [123, 8] showed similar results on simple bipedal models. [71, 125, 92] demonstrated that quadrupedal robots could also potentially benefit from utilizing multiple gaits.

In our own work, we have explored the energetic utility of gaits on a significantly more complex model driven by optimal control [130]. I worked with my colleague

Weitao Xi as we built on the past studies discussed above, to see if the gait principles from nature held for a legged robotic model with added complexities such as elasticity, damping, and a motor model. To keep the results as general as possible, we looked at conceptual models with prismatic legs (Fig. 1.2). While these models are certainly simpler than a full robot, they are still capable of realistic robotic motion.

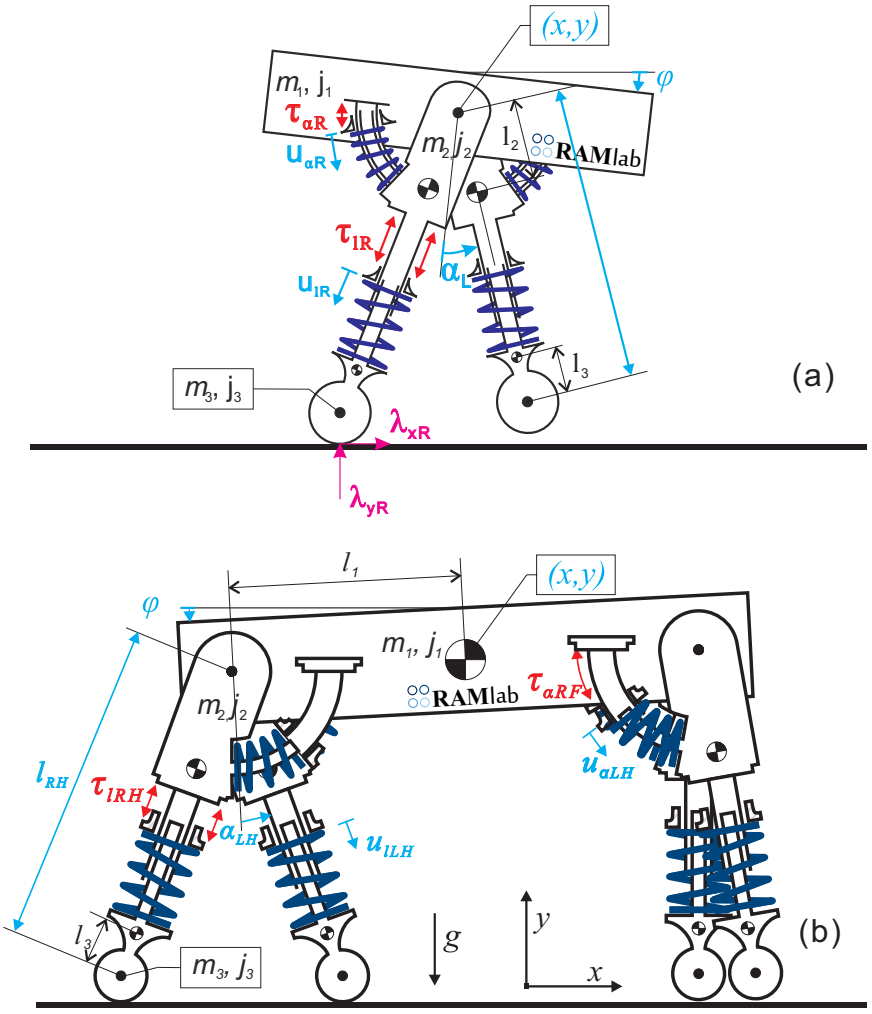

Figure 1.2: In [130], optimal gaits are identified for the planar models of a series elastic actuated biped (a) and quadruped (b). The results show that, similar to nature, switching gaits as locomotion velocity varies leads to considerable reductions in energy consumption.

For brevity, I will discuss only the quadrupedal model. This model has mass in the feet and upper legs, and therefore swing leg dynamics. When a contact closes, a collision happens and velocities change instantaneously. The system is therefore hybrid and has collision losses. The model has Series Elastic Actuators. For these

actuators, the proximal end of the spring in these models is driven by a DC motor, and we model its associated dynamics.

To obtain parameters and constraints necessary for the geared DC motor models, data was plotted from 132 Maxon motors in the RE and EC series. A logarithmic regression was then fit to that data. From there relationships were obtained among motor mass and the speed torque gradient, the rotational inertia of the motor rotors, the maximum torque of the motor, and the maximum speed of the motor. A motor mass was then chosen comparable to the value that we used in our previous hardware [112, 61].

The model also has springs that are capable of passively storing and releasing energy. These springs have associated damping losses. In total, the quadrupedal model has 19 generalized coordinates, corresponding to 38 continuous states and 24 parameters. Any optimization problem with a model like this is non-convex, nonlinear, and again, hybrid. Still, there is yet another difficulty, how are gaits determined for a model like this?

Choosing the contact sequence is a problem of immense combinatorial complexity. For example, beginning in flight, the robot can place one of the four feet on the ground. From there, that foot can either lift off the ground, or any other can be placed on the ground. The combinations continue to grow immensely from there. Even for this problem that just considers the continous and discrete aspects of optimal motion, there is an immensely difficult task ahead.

To deal with these many issues, we chose an optimal control approach. That ensured that we didn't bias the results towards a particular motion by picking a particular control system. Within this optimization, we constrained the model to move at an average forward velocity. We enforced periodicity as a constraint. We enforced a number of additional constraints including ground clearance, limits on the motor velocity and torques, and realistic limits on joint positions. We did all of this while minimizing the COT. In our case we used the positive mechanical work performed by the motors, divided by the distance traveled. This cost is equal to the sum of the damping losses, collision losses, and negative work performed by the motors. We performed this optimization using two optimization schemes. In the first we used a modified version of the direct collocation framework proposed by Posa and Tedrake [98]. The direct collocation scheme, does not require the user to pre-define a contact sequence. It does that by solving the dynamic equations on a discrete grid in which impact forces are averaged over an extended time step. This removes the combinatorial contact problem, but the integrator in this method is not very accurate.

We therefore supplemented it with the multiple shooting optimization framework MUSCOD [17, 78, 30]. In that method you have to pre-define the contact sequence, but, the integrator is much more accurate. We utilized 40 shooting intervals, and the optimizer was responsible for enforcing continuity at the connection points of those shooting intervals. Generally, we would find an initial set of solutions and footfall sequences using Posa and Tedrake's method, and then confirm the results with the more accurate multiple shooting method.

In that process, we ended up looking at six different gaits. Four-beat walking, the traditional walking gait that quadrupeds perform, in which phases of triple stance alternate with phases of double stance. We also have two beat walking, which is like a grounded trotting gait, but with double hump ground reaction forces. This is a gait that we did not initially consider looking for, but was discovered by the direct collocation optimizer. We have tölting, a gait performed by Icelandic horses in which phases of double and single stance alternate. We have trotting, which, since our model is planar, is identical to pacing. These four are symmetrical gaits, for which we can simulate half of the stride and then mirror it. We also looked at the asymmetrical gaits: bounding and galloping. In this particular study, this is the traversal gallop favored by horses. In which there is a single air phase.

We then mapped the cost of transport on the y axis as a function of the average forward speed (Fig. 1.3). First off, we see that this robot clearly has an energetic benefit from switching gaits. At low speeds, the traditional quadrupedal walking gait is optimal, and at higher speeds, the robot should switch to trotting. At the highest speeds, galloping has similar cost to trotting. We also find that two-beat walking, while slightly higher in cost, at all speeds, had comparable cost to the more traditional four-beat walk, explaining why it might have been found naturally by our optimizer. Similarly, tölting is always slightly worse than trotting, but given its proximity, the results might explain why it appears naturally for some horses. Lastly we find that bounding, for this range of speeds, was never the most energetically favorable choice.

Given that these robotic models have no notion of a factor like preferred herd speed, or the resulting neurological adaptation that would go along with it, we can say that the energetic preference for different gaits at different speeds is mechanistic. That is, the dynamics that result from their robotic structure lead to energetics that favor particular gaits at particular speeds.

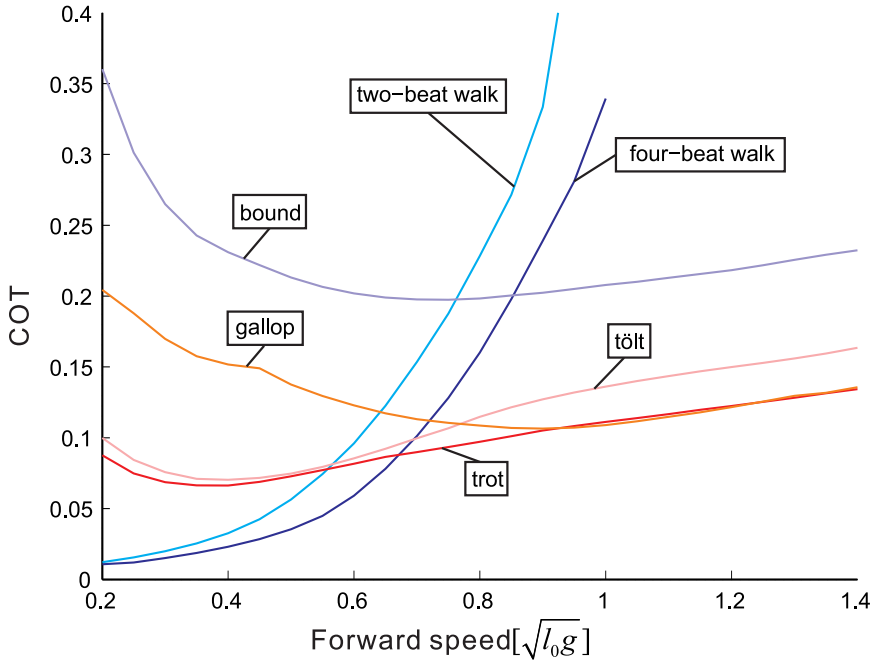

Figure 1.3: The cost of transport of the quadruped robot for different gaits with varying forward speed. These gaits were discovered using the multiple shooting implementation. Note that for slow velocities ($< 0.65\sqrt{l_o g}$), four-beat walking is the optimal motion. At intermediate speeds, trotting becomes optimal. Galloping and trotting have nearly identical cost values at high speeds ($> 0.9\sqrt{l_o g}$). Bounding is not optimal at any speed.

Simultaneous Optimization of Motion and Morphology

Our prior work [130], and work using similar techniques on more complex models [120], illustrates the difficulty in conducting an optimization on these highly nonlinear and non-convex systems, even when just optimizing for motion. Still, the most energetically economical robot must use a motion that is best suited for its parameters, which should be optimally chosen to minimize energetic losses. Additionally, multiple gaits should be exploited to allow economical motion across a wide range of velocities. The best robotic design must simultaneously be optimal in all aspects of motion and morphology. As detailed earlier in this section, the vast majority of existing work in this field seeks to improve upon each of these facets independently. There is, however, a growing body of work that explores these issues of motion and morphology simultaneously. For example, [56] optimized the length and position of segments as well as the motion in a single optimization of a sit-to-stand device to help elderly patients. In [88] limb lengths, positions, masses, and inertias were optimized simultaneously with the motion of a humanoid model to improve stability. Similarly,

[47, 40, 97, 24] work to optimize the motion and morphology of legged robots to a particular task. Additionally, a number of studies within the field of evolutionary robotics have conducted morphological optimizations. [119, 19, 90] had discrete morphological variations of creatures compete to satisfy a goal. In automatically creating discrete variations, and analyzing which variations were best able to complete the task, they were able to move towards the best design for that task. [97] used a genetic algorithm to simultaneously alter the controls and mass distribution of a biped to find stable locomotion. Still, to our knowledge there has been no methodology developed for conducting design comparisons while simultaneously optimizing for the continuous and discrete aspects of motion and morphology in legged robots.

1.3 Contributions

In this work, I seek to expand on these pioneering efforts by developing a methodology for evaluating the best choice in discrete design comparisons using the simultaneous optimization of motion and morphology. I developed and implemented that methodology throughout four projects.

In the first, I compared the two most common implementations of actuation and elasticity in legged robots. I asked if parallel or series elastic actuation is the more energetically economical choice for a one-dimensional hopping robot. I compared the two configurations for three cost functions: the positive work done by the motors, the thermal losses in the motors, and a combination of the two previous cost functions, the electrical work. I then mapped the optimal motion cost landscape as a function of configurable parameters in the hoppers [134]. In the best case, the series configuration was more economical for the positive motor work, the parallel configuration was better for thermal losses, and series was best for the electrical work.

In the second project, I took this work a step further and included the configurable parameters directly within the optimization [133]. Additionally, I included gear friction in the models. I again conducted the analysis for three cost functions, but this time, also looked at three transmission cases: frictionless, small rotary-to-linear transmission, and large rotary-to-linear transmission. I found, for the most realistic cost function, the electrical work, that series was the better choice when the majority of the transmission was handled by a low-friction rotary-to-linear transmission. Parallel was the better choice for a smaller low-friction rotary-to-linear transmission.

In the third project, I extended this analysis to a two-dimensional monoped moving at a forward velocity with either parallel or series elastic actuation at the hip

and leg [132]. Yet again, the analysis was carried out for the three cost functions discussed above. In general it was best to have a parallel elastic actuator at the hip, and a series elastic actuator at the leg. That configuration also had feasible optimal solutions at higher velocities.

In the final project, I looked at a discrete morphological comparison that incorporated the continuous and discrete aspects of motion. I asked if there is an energetic benefit to having an articulated spinal joint instead of a rigid spine joint in a quadrupedal legged robot [135]. I found that for asymmetrical gaits, the articulated spine led to significant energy savings at high speeds, primarily due to improved leg recirculation. Additionally, the articulated spine allowed for motion at higher speeds.

The combination of the above projects forms a methodology for the simultaneous optimization of both the discrete and continuous aspects of motion and morphology. The work presented in this dissertation not only develops this methodology, but also gives answers about specific design questions that are common in the field of modern legged robots, and, gives insight into why animals in nature move in the ways they do.

CHAPTER II

A Comparison of Series and Parallel Elasticity in a Monoped Hopper

2.1 Introduction

[1] Walking, running, and other modes of legged locomotion are almost exclusively based on movements that are periodic in nature and accompanied by repeated fluctuations of potential and kinetic energy. Ideally, the associated energetic fluctuations are contained within the system itself. Such systems can avoid unnecessary negative actuator work by choosing intelligent motion trajectories, and by passively storing and recovering excessive energy in compliant elements. Human in-place hopping, for example, can accommodate 70% of the fluctuations in kinetic and potential energy through energy storage in the Achilles tendon [79].

There is broad agreement that elastic elements are similarly useful in legged robotic systems [62] as they are in nature [6]. Springs are used in robots for two main purposes: at the hip to tune the leg swing dynamics to a desired frequency [128], and in the legs to mimic the behavior of a Spring Loaded Inverted Pendulum model (SLIP) which stores large amounts of energy during the stance phase of a running gait [15]. The efficacy of both approaches has been studied extensively using conceptual passive dynamic models [117, 39, 111]. Of course, real robots do require actuation to compensate for friction, negative actuator work, and collision losses, as well as to enable stabilizing feedback control. This actuation can be included in parallel or in series to the elastic element. So far, no consensus has been reached on which is the more energetically efficient of these two alternatives. Robotic implementations exist with both parallel elastic actuation (PEA) [67] and series elastic

[1] This chapter has been previously published in the 2015 IEEE International Conference on Robotics and Automation [134].

actuation (SEA) [46, 59, 113] (Fig. 2.1).

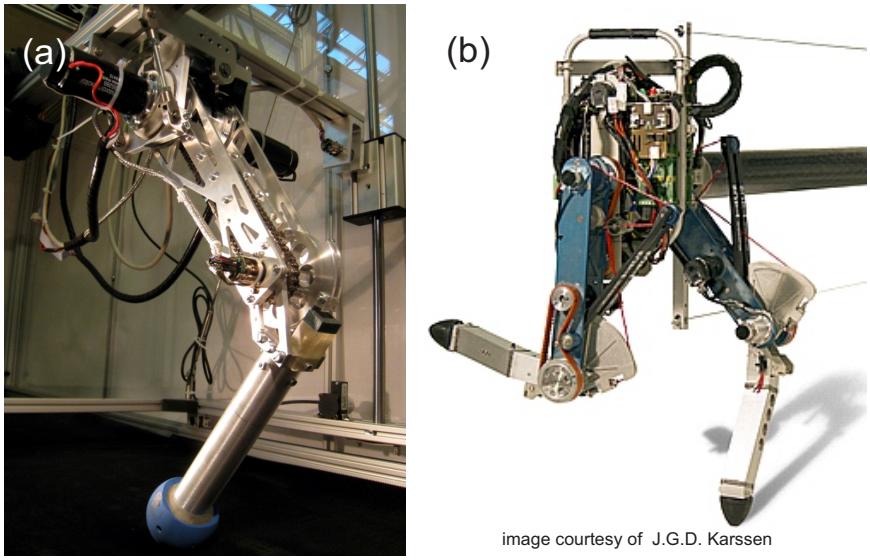

Figure 2.1: Both parallel and series elastic actuators have been implemented in legged robotics, but there is still no consensus about which is the more energetically efficient of the two. ScarlETH (a) makes use of series elastic actuators in the knee and hip joint [62]. Phides (b) uses a parallel elastic actuator in the knee [67]. Phides also contains a series elastic element and a clutch to prevent damage during collisions. Our work looks to gain a deeper understanding of the benefits of each through a detailed analysis on a conceptual monopod hopper.

The main argument in favor of series elastic actuation is the fact that in SEA, joint motion and actuator motion are fully decoupled. This decoupling implies that the actuator inertia does not add to the joint inertia and that gears and other components are fully protected from impacts. In PEA, on the other hand, the actuators have to produce only a part of the overall joint torques, as the torques created by the parallel springs act additively. This might greatly reduce the thermal losses associated with force creation; particularly for electrically driven systems. On the downside, the spring torques might counteract the actuator torques when moving a joint actively; for example, for leg retraction during swing.

At a closer look, the debate becomes more complicated: clutches, small serial elastic elements, and other additional mechanical components, can help overcome some of the aforementioned shortcomings [48]. The stiffness of the employed compliant elements will influence the overall energetics and must be chosen differently for SEA and PEA. Similarly, many effects, such as inertia and thermal losses, depend on the

selected transmission ratio, and choosing a better suited gear box can thus help alleviate their impact. Most importantly, a suitable adaptation of input and motion trajectories allows for the exploitation of the properties of each actuation concept and could thus have a huge impact on the overall power consumption. The actuator inertia in an SEA, for example, can be used to temporarily store kinetic energy [110], and the need for leg retraction with PEA can be reduced by a smart choice of motion trajectories. Due to their differing strengths and weaknesses, a SEA driven robot will hence look and move differently than a PEA driven robot. In other words, rather than asking if one *particular* robot with SEA is better than the same robot with PEA, we must ask whether the *most energetically economical* robot with SEA is better than the *most energetically economical* robot with PEA – given that both are moving in an optimal fashion.

To answer that question, we applied optimal control and parameter optimization to compare SEA and PEA in conceptual models of a monoped hopper, which can be regarded as the archetype of running robots. By choosing energetically optimal trajectories, and studying an optimal choice of spring stiffnesses and gear ratios, we show theoretical upper bounds on the energetic economy of each of the concepts. The conceptual models that we employ allow a broad generalization of the obtained results, while being detailed enough to produce realistic values of power consumption. Our work shows that a SEA hopper with optimal ideal transmission and stiffness values has comparable or better energetic efficiency than the optimal PEA robot when regarding positive actuator work, electrical losses, and positive electrical work. These results are in agreement with our theoretical predictions.

2.2 Methods

2.2.1 Model

As the basis of our study, we use the simple model of a vertical hopper [108]. It consists of a main body with mass m_1 and a foot segment with mass m_2. The motion of the hopper is restricted to a pure vertical movement. Its state is described by the position and velocity of the main body (given by y and $\dot{y}$) and the length of the leg (l and $\dot{l}$). To create realistic motions, it is assumed that l is constrained to be $0.5l_o < l < 1.15l_o$ (where l_o is the uncompressed leg length). The motion of the foot is coupled to the main body by a spring with stiffness k and damping ratio ζ (Fig. 2.2). Having damping in the springs and a foot with mass means that the system is not energetically conservative. As a result, positive net work must be performed by the

actuators over the course of a stride. This work is created by an electric DC motor that produces a torque of F_{mot} and has a reflected inertia of j_{mot}. This actuator is either connected in series with the spring (SEA) or in parallel to the spring (PEA).

In the SEA case, the spring is rigidly attached to the foot on one end, and attached to a servo-controlled DC motor on the other end. An additional pair of states (u and $\dot{u}$) describes the motion of this actuator. To create realistic behaviors, the actuator motion is constrained within $-0.15l_o < u < 0.15l_o$. For the SEA case, the generalized coordinate vector has three components: $\mathbf{q}_{SEA} = (y,\ l,\ u)^T$. Since the actuator is in series with the spring, the joint force, F, is equal to the force produced by the spring:

$$F = k\left(l_o + u - l\right) + b\left(\dot{u} - \dot{l}\right) \tag{2.1}$$

b is the damping coefficient of the spring, which is computed from the damping ratio ζ. The mass matrix for this system is given by

$$\mathbf{M}_{SEA} = \begin{bmatrix} m_1 + m_2 & -m_2 & 0 \\ -m_2 & m_2 & 0 \\ 0 & 0 & j_{mot} \end{bmatrix}. \tag{2.2}$$

The dynamics are driven by the generalized torques $\boldsymbol{\tau}_{SEA} = (0,\ F,\ F_{mot} - F)^T$.

For PEA, the spring is rigidly attached to both the foot and the main body. The actuator is mounted in parallel to this spring, such that the total joint force, F, is the sum of the spring force and the actuator force:

$$F = k\left(l_o - l\right) + b\dot{l} + F_{mot} \tag{2.3}$$

Since actuator motion and leg motion are coupled, the vector of generalized coordinates $\mathbf{q}_{PEA} = (y,\ l)^T$ is only two dimensional. The reflected actuator inertia j_{mot} acts along the coordinate of l, which leads to the following mass matrix for the PEA:

$$\mathbf{M}_{PEA} = \begin{bmatrix} m_1 + m_2 & -m_2 \\ -m_2 & m_2 + j_{mot} \end{bmatrix} \tag{2.4}$$

The dynamics are driven by the generalized torques $\boldsymbol{\tau}_{PEA} = (0,\ F)^T$.

In both variations, all states and parameters are normalized with respect to total mass m_o, uncompressed leg length l_o, and gravity g (Table 2.1).

During flight, the motion of the hopper is governed by the equations of motion $\mathbf{M}\ddot{\mathbf{q}} = \mathbf{h} + \boldsymbol{\tau}$. The differentiable force vector $\mathbf{h}$ includes only the gravitational terms and is given by $\mathbf{h}_{SEA} = (-(m_1 + m_2)g, m_2 g, 0)$ and $\mathbf{h}_{PEA} = (-(m_1 + m_2)g, m_2 g)$,

respectively.

For both models, the main body velocity and the leg retraction rate must be equal during ground contact ($\dot{y} = \dot{l}$). That leads to the modified EOMs of $\ddot{y} = \ddot{l} = \frac{F}{m_1} - g$ for SEA and $\ddot{y} = \ddot{l} = \frac{F}{m_1+j_{mot}} - \frac{m_1}{m_1+j_{mot}}g$ for PEA. This constraint implies that at the moment of touch-down, a collision brings the foot velocity $v_{foot} = \dot{y} + \dot{l}$ to zero. This collision is associated with energetic losses $E_{col.}$, which differ between SEA and PEA:

$$\begin{aligned} E_{SEA,col.} &= \frac{1}{2} m_2 v_{foot}^2 \\ E_{PEA,col.} &= \frac{1}{2}\left(m_2 + \frac{j_{mot} m_1}{m_1 + j_{mot}}\right) v_{foot}^2. \end{aligned} \tag{2.5}$$

For PEA, the actuator inertia contributes to the collision.

Since we are interested in the energetic efficiency of the two actuation concepts, we included a detailed motor model in our simulation. We modeled the actuators as geared DC-motors [76]. To simplify the analysis, we neglected the electrical dynamics due to the motor inductance as well as friction in the gears. For a given supply voltage U_o, the maximal input power of a DC motor is given by $P_{max} = \frac{(U_o)^2}{R}$, and its no-load-speed by $\dot{u}_{max} = \frac{U_o}{n k_T}$. In these equations n is the transmission ratio, k_T the motor constant, and R the armature resistance. Rather than explicitly defining U_o, n, k_T, and R, we used P_{max} and $\dot{u}_{max}$ to parametrize the motor. Therefore $\dot{u}_{max}$ is a single parameter that represents the gear box. With this, the electrical losses can be expressed as a function of the actuator force F_{mot}:

$$P_{loss} = F_{mot}^2 \frac{\dot{u}_{max}^2}{P_{max}} \tag{2.6}$$

This equation implies that thermal losses are proportional to the square of the no-load-speed $\dot{u}_{max}$ (and inversely proportional to n^2). The no-load-speed is an important free parameter in the optimization since its value has a direct impact on the thermal losses as well as on the reflected motor inertia j_{mot}. This inertia can be computed as

$$j_{mot} = \frac{j_{unsc.}}{\dot{u}_{max}^2} \tag{2.7}$$

It is based on an unscaled inertia $j_{unsc.}$ that is given by $j_{unsc.} = j_{rotor}\frac{U_o^2}{k_T^2}$ [110]. This reduces all important motor equations to the two parameters P_{max} and $j_{unsc.}$, which were based on an existing robotic hopper [62] (Table 2.1).

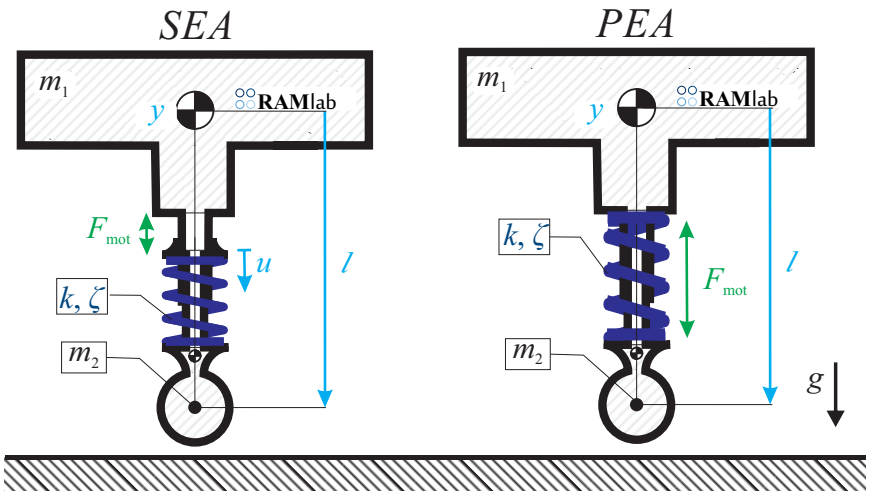

Figure 2.2: Using optimal control, this study investigated whether a legged robot is more efficient with series elastic actuation (SEA, left) or parallel elastic actuation (PEA, right). For different values of transmission ratios and spring stiffnesses, we identified optimal periodic motion trajectories in a numerical optimization framework. These nominal motions represent upper bounds on the energetic efficiency of each actuator variation and thus allow a fair comparison between the two concepts.

Table 2.1: Model parameters expressed with respect to total mass m_o, leg length l_o, and gravity g.

$m_1 = 0.95\ m_o$	$m_2 = 0.05\, m_o$	$\zeta = 0.2$
$P_{max} = 24\, m_o g\sqrt{g l_o}$	$j_{unsc.} = 0.6\, m_o g l_o$	

2.2.2 Cost Functions

To measure the energetic efficiency of each actuation variation, we used three cost functions: positive actuator work, electrical losses, and positive electrical work. All cost functions are expressed as an integral over a single hop, from time $t = 0$ until $t = T$.

2.2.2.1 Actuator Work

The positive actuator work refers to the positive mechanical work that is performed by the actuator. For the series elastic actuator, it is defined as:

$$c_{act} = \int_0^T max\left(F_{mot} \cdot \dot{u}, 0\right) dt \tag{2.8}$$

For the parallel elastic actuator, the actuator velocity is equal to the joint velocity. Therefore the positive actuator work is defined as:

$$c_{act} = \int_0^T max\left(F_{mot} \cdot \dot{l}, 0\right) dt \tag{2.9}$$

2.2.2.2 Electrical Losses

The electrical losses cost function expresses the thermal losses in the motor. For both the parallel and series cases it is given by:

$$c_{loss} = \frac{\dot{u}_{max}^2}{P_{max}} \int_0^T F_{mot}^2 dt \tag{2.10}$$

2.2.2.3 Electrical Work

Electrical work is the integral of the positive electrical power used by the actuator. It combines mechanical work and electrical losses. For the series case, the electrical work is equal to:

$$c_{el} = \int_0^T max\left(F_{mot}\dot{u} + F_{mot}^2 \frac{\dot{u}_{max}^2}{P_{max}}, 0\right) dt \tag{2.11}$$

and for the parallel case, it is equal to:

$$c_{el} = \int_0^T max\left(F_{mot}\dot{l} + F_{mot}^2 \frac{\dot{u}_{max}^2}{P_{max}}, 0\right) dt \tag{2.12}$$

2.2.3 Optimal Control

For these models and cost functions, energy efficient motions were generated via optimal control. To this end, we analyzed motions from apex transit to apex transit, and enforced periodic boundary conditions to simulate a continuous hopping motion. Hopping height was fixed to $1.3\,\mathrm{l_o}$. The motor force $F_{mot}(t)$ was parametrized by a piecewise linear representation, and both l and u were constrained to be within their admissible range of motion.

These assumptions and constraints were implemented in the multiple shooting optimization package MUSCOD [30] to obtain optimal force inputs and periodic states. A range of optimizations was conducted for each actuator type and cost function, while varying the spring stiffness in the range k = 10-100 $m_o g/l_o$ and actuator no-load-speed in the range $\dot{u}_{max}$ = 0.05-5.5 $\sqrt{l_o g}$. Within this parameter-grid, successful

optimizations were used as initial guesses for neighboring grid points, and optimizations were initiated multiple times. This process ensured that each parameter combination was tested multiple times with slightly different initial conditions and that local minima were avoided.

2.3 Theoretical Predictions

This section provides broad theoretical predictions for the comparison between PEA and SEA. For more detailed predictions and derivations, see Appendix A.

From an energetic point of view, the advantage of SEA is that the actuator inertia does not contribute to the collision losses, which reduces the need for active actuator work. The downside is that the full joint force F must be supported by the actuator, which drives up the thermal losses in the motor. Avoiding this is usually stated as the main benefit of PEA, in which the motor force acts only in addition to the spring force. Yet, both collision losses and thermal losses, depend on the chosen transmission. A larger transmission ratio decreases thermal losses, while driving up the reflected actuator inertia.

2.3.1 Positive Actuator Work

Minimizing the positive actuator work is equivalent to minimizing the sum of the collision losses, the negative actuator work, and the damping losses [110]. A variety of strategies can be used in an optimal motion to minimize these losses (Fig 2.3). These strategies require different motion profiles for SEA and PEA, and do not work equally well for both actuator concepts. This difference is caused by the way the two actuator concepts create net positive work. For SEA, the actuator force is dominated by the force needed to balance the spring force F. To perform net work, an active actuator motion $\dot{u}$ is performed against this force. In contrast, in PEA the actuator motion $\dot{u}$ is directly coupled to the leg motion and cannot be chosen freely. Work is consequently performed by a modulation of the motor force F_{mot}. Since this has only a small influence on the compression velocity of the leg, it limits strategies that seek to reduce damping losses in the spring. In a SEA, for example, the actuator remains at rest during the first half of stance and then retracts during the second half. This retraction reduces the expansion velocity of the spring and thus minimizes the damping losses, which grow with the square of the spring extension $P_{damp} = b\left(\dot{l} - \dot{u}\right)^2$. Since for a PEA the two motions are coupled, this strategy cannot be applied and the overall damping losses are larger.

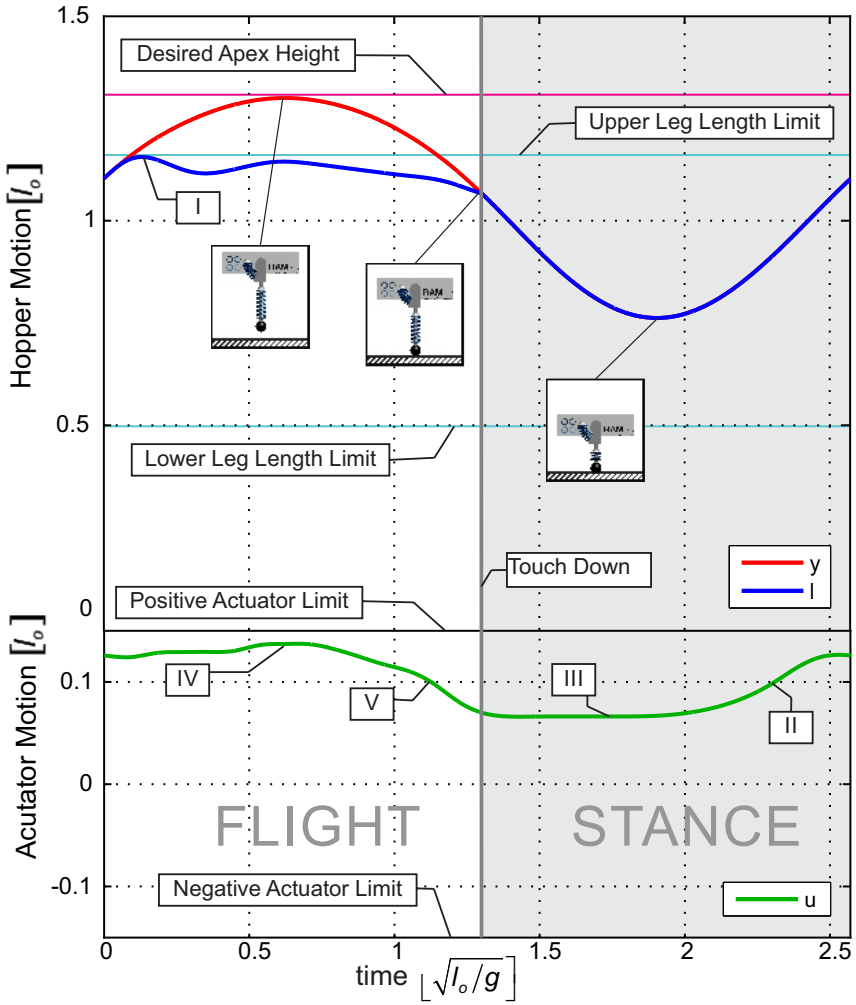

Figure 2.3: Shown are main body position (y, top), leg length (l, top), and actuator motion (u, bottom) of a 1D hopper. Positive mechanical work was minimized while constraining apex-transit to 1.3 m. The resulting motion extends the leg as much as possible to reduce effective hopping height (I), minimizes damping by moving the actuator at the end of stance (II), reduces negative work by keeping the actuator at rest during the first half of stance (III), maximizes vertical momentum by maximally extending the leg at apex transit (IV), and reduces collision losses by retracting shortly before touch-down (V).

The actuator losses can be expressed as:

$$c_{act,SEA} = C_{SEA} + E_{SEA,col} \tag{2.13}$$
$$c_{act,PEA} = C_{PEA} + E_{PEA,col}$$

where C_{SEA} and C_{PEA} are constants representing the sum of the negative actuator work and damping losses for each case, and $E_{SEA,col}$ and $E_{PEA,col}$ are the collision

losses as they are defined in eqn. (2.5).

PEA suffers from higher collision losses, as the reflected actuator inertia contributes to the collision. From eq. (2.5), we can directly quantify these additional losses as:

$$E_{PEA,col.} - E_{SEA,col.} = \frac{v_{foot}^2}{2} \left(\frac{j_{unsc.} m_1}{m_1 \dot{u}_{max}^2 + j_{unsc.}} \right). \tag{2.14}$$

These losses scale directly with the no-load-speed $\dot{u}_{max}$. The only way to compensate for this is by reducing the impact velocity of the foot. However, this will increase the negative actuator work and the retraction will pre-load the spring, which will lead to faster spring compression rate, and therefore increased damping losses. We therefore expect that the additional collision losses are directly reflected in the necessary positive actuator work.

2.3.2 Electrical Losses

Electrical losses are merely a function of motor force and only depend indirectly on the performed work. To understand the implications of this cost function, let us assume an energetically conservative motion, with a massless foot ($m_2 = 0$) and no damping in the springs ($b = 0$).

To sustain such a loss-less motion, a SEA simply has to hold the motor at a fixed position ($\dot{u} \equiv 0$) while in a PEA the motor does not create any force ($F_{mot} \equiv 0$). In the series actuation case, the optimal no-load-speed is thus $\dot{u}_{max} = 0$, which precludes any thermal loss as they are given by eq. (2.10). In the parallel elastic case, on the other hand, the optimal no-load-speed is $\dot{u}_{max} = \infty$, which prevents any collision losses within the actuator (as then the motor inertia is zero, as given by eq. (2.7)). This shows clearly, that different actuation concepts require different transmission ratios.

In a more realistic consideration, actuators must perform some net positive work to compensate for energy losses. This means that the SEA has to create motion against the spring force F and that the PEA must apply an active force as the leg is extending. Both requirements lead to a trade-off with respect to the transmission ratio.

For a SEA that trade-off stems from the motor force needed to accelerate the reflected inertia j_{mot} of the motor. Since this inertia is inversely proportional to $\dot{u}_{max}^2$, it prohibits a no-load-speed that is too close to 0. The electrical losses can be expanded to

$$c_{loss} = \frac{T}{P_{max}} \left((m_1 g \dot{u}_{max})^2 + \left(\frac{j_{unsc}}{\dot{u}_{max}} \right)^2 \sigma^2 \left(\ddot{u}_{act} \right) \right) \tag{2.15}$$

in which the first term accounts for the force required to compensate for gravity over the course of a hop and the second term accounts for the force required to create net positive work (see [108], Chapter 4 for a detailed derivation). $\sigma^2(\ddot{u}_{act})$ is the variance of the active actuator acceleration, which is a consequence of the need for positive net work and an active actuator motion. From this, we can identify an optimal transmission ratio as:

$$\dot{u}_{max} = \sqrt{\frac{j_{unsc.}\sigma(\ddot{u}_{act})}{m_1 g}} \tag{2.16}$$

For PEA, the trade-off arises because an infinitly large no-load-speed would lead to infinite thermal losses if the required motor force is not equal to 0. While $\dot{u}_{max}$ directly scales c_{loss} (eq. (2.10)), decreasing it introduces other unwanted effects. As shown before, collision losses depend on the reflected actuator inertia according to eq. (2.5) and increase for smaller $\dot{u}_{max}$. In addition, a substantial amount of kinetic energy is stored in the reflected rotor inertia at the instance of lift-off (when the leg is extending with maximal velocity). This stored kinetic energy scales with $j_{mot} = \frac{j_{unsc.}}{\dot{u}_{max}^2}$, and can lead to negative actuator work that is required to slow down and reverse the extension of the leg. All these effects depend on the chosen motion profile and allow for a large range of compensatory strategies. For example, the negative actuator work needed to slow down the leg extension during flight can be conducted in part via the leg spring and could be reused for leg retraction before touch-down. These strategies, in turn, create secondary effects, such as an increase of the damping losses. This makes a more detailed analysis of the optimal no-load-speed for PEA very difficult. Still, we would expect that an optimal no-load-speed can be found that trades off these requirements.

2.3.3 Electrical Work

Minimizing electrical work represents a trade-off between minimizing actuator work and electrical losses. We thus expect that the result for this cost function combines the characteristics of both previously discussed cases. In particular, we hypothesize, that electrical work has a clear optimum for the no-load-speed.

2.4 Numerical Results

Using optimal control, we minimized each cost function for both SEA and PEA. While spring stiffness was not considered as a factor in the analytical considerations presented in the previous section, we included it in the numerical analysis to investi-

gate potential differences between SEA and PEA.

As expected, SEA clearly outperformed PEA when considering positive actuator work as a cost function (Fig 2.4). The ability to reduce damping and collision losses favors the series elastic actuation concept. The losses showed a clear dependence on the chosen no-load-speed and increased for slower actuators with a higher reflected inertia. To compensate for this inertia, the optimizer discovered strategies that reduced the amount of energy lost in the collision. For example, by retracting the leg in order to decrease the relative velocity between the foot and the ground. Still, the general trend of the resulting cost-values matched the predictions based on collision losses, as the compensatory motion led to increased negative actuator work and damping losses.

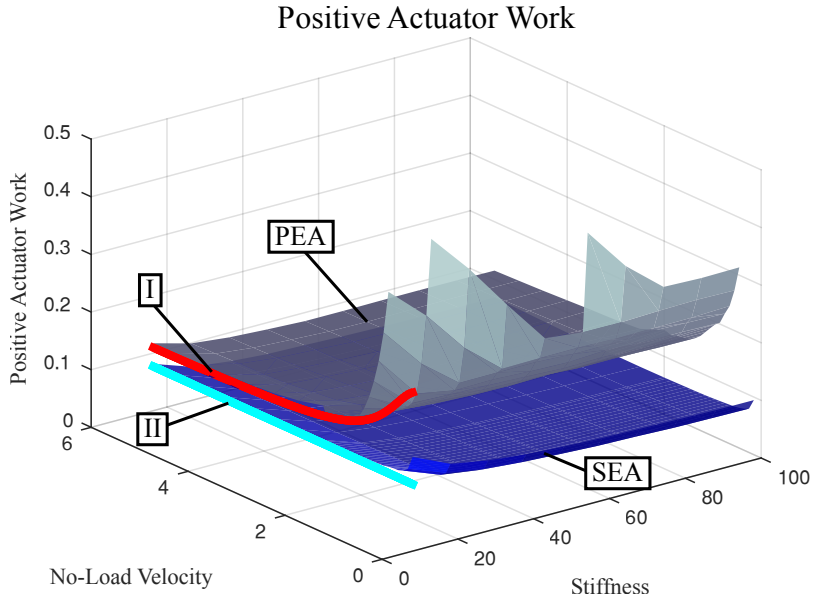

Figure 2.4: Optimal values of the *positive actuator work* of a continuous hopping motion are shown for varying parameter choices of leg spring stiffness and actuator no-load-speed. In this comparison, SEA always has a lower value for positive actuator work than PEA, independent of no-load-speed and stiffness. The increase in the cost value for PEA at small values of the no-load-speed is indicative of the increased collision losses that result from a higher reflected inertia. The shown predictions (PEA: I, SEA: II) are based on eqns. (2.13), with fitted values for $C_{SEA} = 0.10\, m_o g l_o$, $C_{PEA} = 0.13\, m_o g l_o$, and $v_{foot}^2 = 0.53\, l_o g$.

For electrical losses, we discovered a clear minimum for both PEA and SEA as a function of the no-load-speed (Fig. 2.5). The global minimum PEA value of $0.0059\, m_o g l_o$, occuring at a stiffness of $80\, m_o g / l_o$ and a maximal no-load-speed of

$0.35\sqrt{l_o g}$ is slightly lower than the minimum SEA value of $0.0136\, m_o g l_o$, occuring at a stiffness of $100\, m_o g / l_o$ and a maximal no-load-speed of $0.35\sqrt{l_o g}$. This is a surprising result. An often hypothesized advantage of using PEA is that the spring force and motor force act additively, which can greatly reduce the required motor force. And since the electrical losses depend explicitly on the square of the motor force F_{mot}^2, one would expect that a cost function based on electrical losses would strongly favor PEA. In practice, however, the thermal losses of both concepts can be made nearly 0 with the correct choice of $\dot{u}_{max}$.

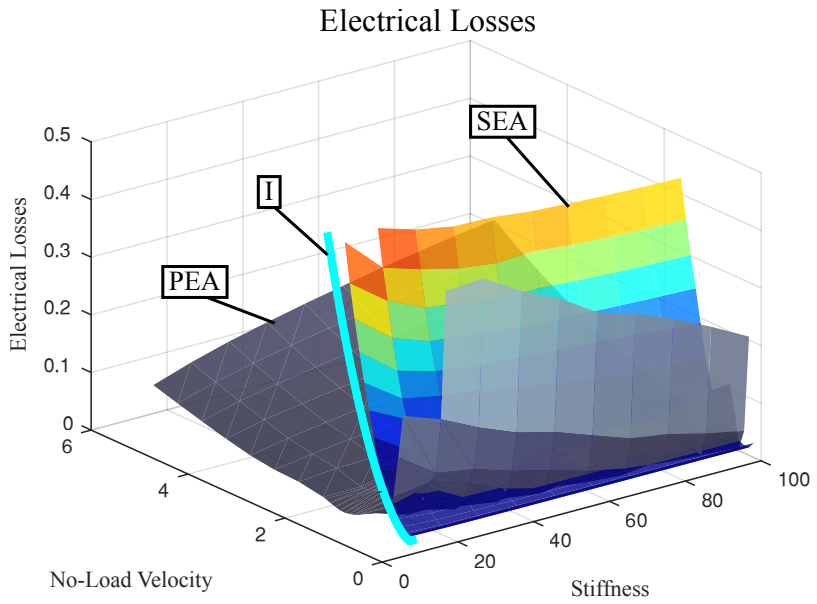

Figure 2.5: Optimal values of *electrical thermal losses* are shown for varying parameter choices of leg spring stiffness and actuator no-load-speed. The theoretical prediction of the SEA cost (I) from eq. (2.15) was fitted to the data in the figure ($T = 3.5$, $\sigma^2(\ddot{u}_{act}) = 0.005$). Overall, the optimal value for PEA is only slightly better than for SEA, despite the fact that the cost function is based on the integral of squared torques. To operate optimally, the two actuator concepts require particular transmission ratios (here represented by the actuator no-load-speed) and the cost can increase dramatically in the case of a sub-optimal transmission choice.

Electrical work as a cost function essentially combines the results of positive actuator power and electrical losses. Optimal transmission values can be clearly indentified for both PEA and SEA, and the optimal parameter choices are very similar to those found when optimizing electrical losses. Since this cost function considers actuator work, SEA is significantly more energetically efficient than PEA (Fig 2.6); provided the right transmission is chosen. This result is an indication that the fundamental

differences in collision and damping losses play a much larger role in differentiating PEA and SEA than the square of the motor force.

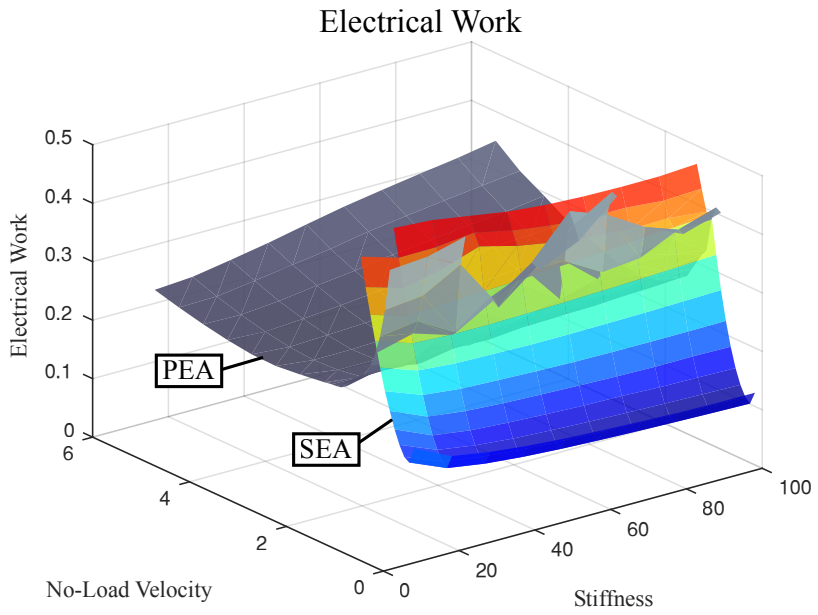

Figure 2.6: Optimal values of the *electrical actuator work* are shown for varying parameter choices of leg spring stiffness and actuator no-load-speed. Similar to electrical losses, we can identify clear minima with respect to the no-load-speed. Overall, the minimal value for SEA is significantly smaller than for PEA. This reflects that electrical work combines positive actuator work and electrical losses.

Apart from very low stiffness values, the spring stiffness did not have a significant influence on any of the cost functions studied. SEA and PEA were always equally sensitive to the selected spring stiffness, and no dependency between the chosen actuator concept and an optimal stiffness value were found. This observation largely confirmed previous results [108].

2.5 Conclusion

For a one-dimensional monoped hopper that is driven by a geared DC motor, our results show that with the correct choice of the transmission parameter, a hopper with SEA is more energetically efficient than one with PEA when looking at positive actuator work and electrical work. Electrical losses can be made to be nearly 0 for both actuators. This is largely attributed to the fact, that for a hopper with PEA, the motor inertia contributes to energetic losses due to the ground contact collisions.

Our optimizations showed that even for a force-squared cost function such as electrical losses, PEA is not able to overcome the increased collision and damping losses to be significantly more efficient than SEA.

The results, as they are presented in this chapter merit some further discussion. To be able to create theoretical predictions of the optimization outcomes (and thus ensure that the obtained solutions are not merely local minima or otherwise flawed results), we had to considerably simplify the model. Our analysis did, for example, not include the effects of gear-friction, or the need for active leg retraction as it is required in a multi-legged gait. We therefore believe that the value of this chapter is not in finding a definite answer to the question of which actuation concept is better. This answer will likely depend on a particular robotic implementation. Rather, we believe that the theoretical predictions and results help understand the fundamental processes that are involved in the energetics of robotic running and can thus guide a detailed system analysis if needed.

With a thorough understanding of the effect of stiffness and maximal no-load-speed on the monoped hopper, our next goal is to extend this work to more complex systems. By including morphological parameters directly in the optimization, we will be able to expand our method for comparing SEA and PEA to systems such as a planar monoped or biped.

CHAPTER III

Energy-Optimal Hopping in Parallel and Series Elastic 1D Monopeds

3.1 Introduction

[1] Springs play a fundamental role in legged locomotion. In nature, elastic elements are used for energy storage, as return springs, and to cushion impacts [7]. Model based analyses have shown that compliant legs can explain the dynamics of human walking and running [41], as well as a wide variety of quadrupedal gaits, including walking, trotting, tölting, and galloping [38, 37]. In all these cases, elastic energy storage enables the recycling of energy and improves energetic economy. [22] and [15] observed that during running gaits, animals conserve energy by having the body undergo an elastic bouncing motion. In human in-place hopping, for example, the majority of the energetic fluctuations are generated passively through elastic energy storage in muscles and tendons [79, 28]. Motivated by these biological benefits, elastic elements have been incorporated successfully in robotic simulations e.g. [8, 129] and in hardware prototypes e.g. [100, 59, 63, 118, 95].

In robotic hardware, the two primary ways of incorporating elasticity into legs are to place springs in parallel or in series with the actuation source (Figure 3.1). In a parallel elastic actuator (PEA) the motor contracts and extends the entire leg and spring. The spring force and motor force therefore act additively. The motor inertia moves with the joint and is not isolated from impacts. In a series elastic actuator (SEA) the motor moves the proximal end of the spring. The motor force must overcome the spring force. The motor inertia does not directly add to the joint motion and is isolated from impacts. Both types of actuator have been implemented in prototypes e.g. [67, 46]. Yet, to date, there is still no detailed understanding of

[1] This chapter has been previously published in the Journal of Mechanisms and Robotics [133].

the effect of each actuator type on the energetics and motion characteristics of legged systems. In particular, there is still disagreement about which actuator solution is more energetically economical.

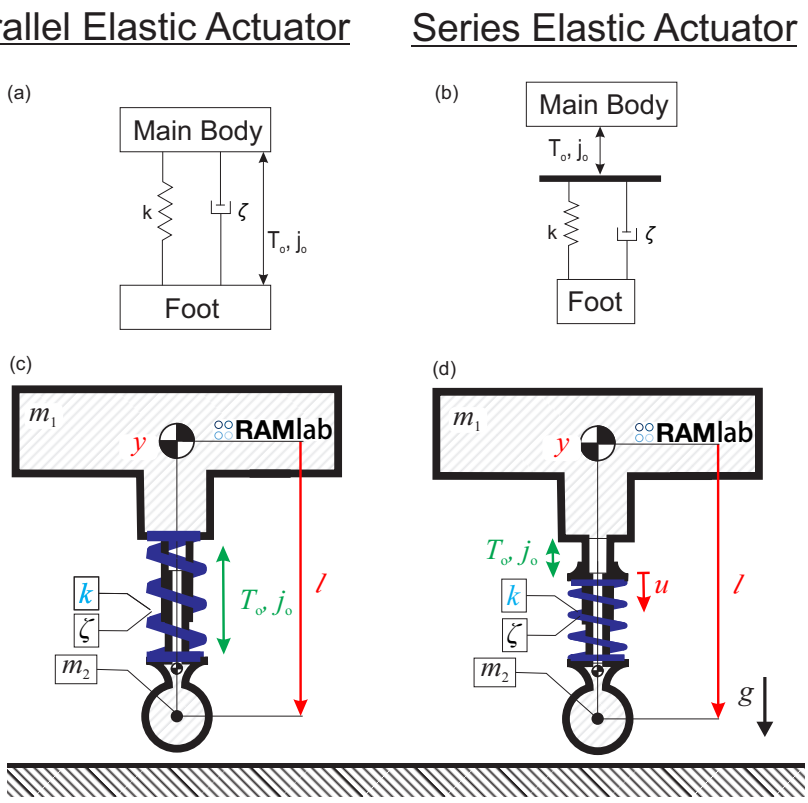

Figure 3.1: This study investigated energetically optimal hopping motions for a one-dimensional hopper with either parallel elastic actuation (PEA, shown as schematic in (a) and detailed model in (c)) or series elastic actuation (SEA, (b) and (d)). For PEA, the motor contracts and extends the entire spring. For SEA, the motor moves the proximal end of the spring. For both hoppers we simultaneously optimized motion trajectories, actuator inputs, and actuation parameters for three different cost functions: positive mechanical motor work, thermal electrical losses, and positive electrical work. The hoppers have DC motor models with transmissions and reflected rotor inertia j_o. The optimization included main body position y, leg length l, motor position u (only for SEA), motor force after the transmission T_o, spring stiffness k, and rotary gearbox ratio n_r (not shown).

There is a broad range of similar questions, that essentially try to determine the benefits of discrete design choices. Can a compliant ankle joint in a robot's leg improve efficiency? Is a quadrupedal robot faster with a spine that is rigid or deformable? Is a set of swinging arms useful for robotic locomotion? These questions are fundamentally difficult to answer. One cannot simply swap a particular feature

in a robotic implementation or robotic model and then compare the performances of the two different variations. This is because an optimal robot with one of the two variations will likely have to look and behave very differently than an optimal robot with the other. For example, a robot with PEA might require a different spring stiffness and a different transmission ratio than a robot with SEA, and the two actuator types might need very different ways to power their motion. If we keep the system parameters of the two robots identical or apply the same type of motion in both cases, we will implicitly bias the comparison to favor one variation over the other. After all, we are not interested in the question of whether a *certain* robot with a *certain* motion strategy and a *certain* choice of parameters performs better with one design variation or the other. We would like to know if the *best possible* robot, with the *best possible* set of parameters, and the *best possible* motion strategy can benefit from the design variation. To answer this question, we have to investigate optimal motion, optimal parameters, and optimal morphology at the same time. Due to the complexity of the problem, it is impossible to do this comparison by conducting an exhaustive search or an analytical evaluation. Instead, we propose to use trajectory optimization to find the best possible actuator inputs and motion trajectories while simultaneously optimizing the system parameters.

This approach extends upon existing morphological optimizations in legged robotics [88, 47, 40, 97]. These past studies optimize parameters to optimally adapt a model to a particular task, but do not use the technique to compare discrete designs. It also extends on existing discrete structural comparisons [21] by using trajectory optimization on a realistic motor model and including morphological parameters directly in the optimization. In particular, this technique has not been applied in previous studies comparing PEA and SEA. An initial comparison was conducted, for example, by [65], and found that PEA was more economical. [45] on the other hand, found SEA to be more economical for a model of a human ankle joint. The difference in the two studies likely stems from their comparisons of *particular* implementations of each actuator type, rather than the *best* implementation. Furthermore, the studies significantly simplified the problem. [65] only looks at a single cost function and a single set of parameters for actuator comparisons. [45] has similar simplifications, including ignoring the motor inertia and damping in the springs.

In this work, we performed a thorough comparison of PEA and SEA for the exemplary case study of in-place hopping. In a trajectory optimization framework, we considered inputs, motion trajectories, and system parameters simultaneously to understand their mutual effects and their full implications on the choice of PEA or SEA.

As a basis for our study, we used a model that, while simple enough to lead to general conclusions, has enough detail to model more realistic motions during hopping, such as leg dynamics during flight. In particular, our models incorporated feet with mass, detailed electric DC motor models, damping in the springs, and gearbox friction. In addition, we enforced realistic constraints on the possible parameter values, motion trajectories, and motor inputs. We considered two different cases of rotary-to-linear transmissions that represent common values in modern legged robotics. We contrasted these two types with the more theoretical scenario of a completely frictionless transmission. Within each of these three cases, we examined a variety of cost functions quantifying work and force-based efforts. We found that the optimal actuator type and motion was highly dependent on both the type of rotary to linear transmission as well as on the chosen cost function.

As hopping is highly relevant in legged locomotion, which often uses the template of a spring loaded inverted pendulum (SLIP) for bipedal [15] and multi-legged [16] locomotion, our results are relevant for both a fundamental understanding of the effect of elastic actuators on legged motion as well as for applied hardware design. In addition to answering the question of which actuator type is better in different situations, our study provides a detailed understanding of what optimal motions look like and can therefore be used to 'calibrate' trajectory optimization results in real hardware. To this end, the chapter represents a culmination of our previous efforts analyzing optimal actuation [134, 132, 110].

3.2 Theoretical Discussion

In the past, discussions about which actuation concept is better suited for legged robotics often argued that PEA is better when minimizing motor torque and SEA is better when minimizing mechanical work e.g. [68]. To illustrate this argument and to use it as a departure point for our own work, we can formalize this distinction in terms of two different cost functions: the positive mechanical motor work C_{mech} (where the work done by the motor is equal to $T_m\omega_m$) and the thermal electrical losses C_{therm} (which is proportional to T_m^2). In these expressions, T_m is the torque created by the motor, ω_m is the motor velocity. Since C_{therm} is only dependent on T_m, one could think that this cost function would indeed prefer PEA, where motor force and spring force act additively and the motor torque is thus reduced. SEA would be at a disadvantage, as its motor must actively provide the entire force acting on the leg. For C_{mech} the situation is reversed. For SEA, the motor and main body components

are well insulated from impacts, and the inertia of the motor does not add directly to the joint motion, potentially leading to reduced mechanical losses. PEA seems to be at a disadvantage, as the rotor inertia now factors into collisions.

Upon closer inspection, however, the situation is not so clearly delineated. For each actuator type, adaptations in the hardware and in the motion strategy can alleviate the respective disadvantages. To illustrate the effects of different parameters and motion strategies, let us examine the simplified case of (nearly) loss-less hopping. To this end, we consider a hopper model with no foot mass and no damping in the springs. This hopper is driven by a motor with a rotor inertia of j_m that is connected to the joint via a frictionless gearbox with transmission ratio n. For both the PEA and SEA version of this hopper, we can, in fact, find entirely lossless solutions for *both* cost functions. PEA can achieve $C_{\text{mech}} = 0$ by having the motor input no torque ($T_m = 0$) and therefore having the spring perform the hopping task passively. With this motion strategy, the only possible source of mechanical losses are collision losses in the rotor inertia:

$$E_{\text{p,mc}} = \frac{1}{2}\left(\frac{j_o m_1}{m_1 + j_o}\right) \cdot v_{\text{foot}}^2, \tag{3.1}$$

where m_1 is the main body mass and v_{foot} represents the velocity of the foot at touchdown [134]. The reflected rotor inertia of the motor j_o scales with the square of the transmission ratio n: where we assume that the transmission ratio converts rotary to linear motion, giving j_o units of mass. By setting $n = 0$ and thus $j_o = 0$, the collision losses can be completely removed, which leads to $C_{\text{mech}} = 0$. There are no disadvantages to this choice, since no torque is required from the motor. This strategy also achieves $C_{\text{therm}} = 0$, as $T_m = 0$. In contrast, SEA can yield $C_{\text{mech}} = 0$ by setting $\omega_m = 0$. This fixes the location of the proximal end of the spring, letting the spring perform the hopping task entirely passively. Since in SEA, the rotor inertia is decoupled from the motion, no losses occur and the motion is periodic. This solution, however, requires a non-zero force to keep the motor in place as the leg spring compresses. In order to achieve $C_{\text{therm}} = 0$, SEA must thus set the transmission n to infinity. Since $T_o = nT_m$, where T_o is the output torque after the gearbox, C_{therm} is proportional to $\frac{T_o^2}{n^2}$. Using $n = \infty$ yields $C_{\text{therm}} = 0$. Again, there are no disadvantages to this choice, since no motion is required from the motor.

Even though the model in this analysis is a contrived example, it shows two important issues. First, with the right choice of motion and parameters, PEA and SEA can achieve the same performance for *both* work-based and torque-based cost functions. No actuator type is better per se. Second, the two actuator types require

almost diametrically different strategies and parameters. PEA applies no force as the motor moves with the spring and utilizes a transmission ratio of $n = 0$. Choosing the opposite extreme of $n = \infty$ drives C_{therm} to infinity, as the collision losses in the motor become infinite. SEA keeps the motor at rest and requires a transmission ratio of $n = \infty$. If SEA were to choose the opposite extreme of $n = 0$ then C_{therm} would be driven to infinity, as it would take an infinite T_m to keep the motor still. It is clear that when trying to answer the question of which actuator type is better, we need to take into account that each actuator requires substantially different motion strategies and parameters.

The extreme values for n in this example are a consequence of the assumption that the hopping is otherwise lossless. As soon as we introduce damping and collision losses, these transmission values become extremely non-optimal. When the motors must move and apply torques to do positive mechanical work to replace the inevitable energetic losses, finite non-zero transmission values n are necessary. In particular, SEA can no longer have an infinite n, as the resulting infinite reflected rotor inertia would require an infinite T_m to move the motor to replenish losses, which will drive both cost functions to infinity. PEA can also no longer have $n = 0$, as it will take an infinite T_m to transmit force through the gearbox and add energy to the system. That infinite T_m will again drive both cost functions to infinity. The infinite costs at both extremes of n suggests that there exist optimal choices for n in between. For a simplified SEA hopper, for example, such an optimal value has been derived analytically in [110]. Similar types of dependencies likely exist for other parameters and must be resolved by including the parameters in an optimization formulation.

Furthermore, there exist a number of complex relationships between optimal parameter choices and motion strategies. For example, for an actuator with PEA, one strategy would be to let the leg oscillate freely during flight ($T_m \approx 0$), which minimizes T_m and thus C_{therm}. Moreover, this oscillation can be timed such that the foot has zero velocity at touchdown, leading to no collision losses even in the presence of a foot mass. This timing is achieved by tuning the natural frequency f of the leg spring

$$f = \sqrt{\frac{k}{m_2 + j_o}}, \tag{3.2}$$

which depends on the choice of stiffness k, transmission ratio n, and foot mass m_2. That is, through this natural dynamic oscillation, the choice of motion and of parameters are coupled. Such an exploitation of natural dynamics can happen in a variety of ways, and must thus be accounted for when trying to answer the question of which

actuator type is more economical.

The main takeaway of these considerations is that motion and optimal morphology are strongly coupled and will differ greatly between hoppers with PEA and SEA. In order to figure out which actuator type is better, we have to investigate optimal motion and optimal morphology at the same time, such that we can compare the *best* possible SEA robot to the *best* possible PEA robot. In addition to the examples mentioned above, this question is even further complicated by the presence of friction in the gearbox and limits on the motor force and joint motion. With torque inputs, motion trajectories, system parameters, and limits mutually affecting each other in such complex ways, numerical optimization is the only suitable tool to understand the full implications of the choice of PEA or SEA.

3.3 Methods

In this chapter we used trajectory optimization to find the most energetically economical motions and parameters for each actuator configuration and used these optimal results as a basis for comparison. In particular, we examined optimal, periodic, one-dimensional, in-place hopping, and studied a variety of cost functions in a model based approach. To this end, we established parametrized models of electrically driven PEA and SEA hoppers that included a dynamical model, a motor model, a detailed transmission model, and realistic limitations on all states and parameters. In this section, we outline these models, discuss our parameter choices, describe the cost functions, and detail our optimization approach. To minimize the number of free parameters in our analysis, all states and parameters were normalized with respect to total mass m_o, uncompressed leg length l_o, and gravity g.

3.3.1 Dynamical Model

Our study was based on the simple model of a hopper (Fig. 3.1). The hopper consisted of a main body with mass m_1 and a point foot segment with mass m_2. The motion of the hopper was restricted to a pure vertical movement; i.e., hopping in place. Its state was defined by the position and velocity of the main body (given by y and $\dot{y}$) and the length and contraction velocity of the leg (l and $\dot{l}$). The motion of the foot was coupled to the main body by a spring with stiffness k and damping ratio ζ. Having damping in the springs and a foot with mass meant that the system was energetically non-conservative. As a result, positive net work had to be performed over the course of a stride. This work was created by an electric DC motor with an

attached transmission that produced a torque of T_o and had a reflected inertia of j_o. The mass of the motor is included as part of m_1. This actuator was either connected in parallel to the spring (PEA) or in series with the spring (SEA). During flight, the motion of the hopper was governed by the equations of motion $\mathbf{M}\ddot{\mathbf{q}} = \mathbf{h} + \boldsymbol{\tau}$, with the mass matrix $\mathbf{M}$, the gravitational terms $\mathbf{h}$, and the generalized forces $\boldsymbol{\tau}$.

For PEA the motor was mounted in parallel to the spring, such that the leg force, F, was the sum of the force in the spring and the motor force:

$$F = k\left(\ell_o - \ell\right) - b\dot{\ell} + T_o. \tag{3.3}$$

The damping coefficient of the spring b was computed from the damping ratio ζ:

$$b = 2\zeta\sqrt{km_2}. \tag{3.4}$$

Since motor motion and leg motion were coupled, the vector of generalized coordinates $\mathbf{q}_{\text{PEA}} = (y,\ \ell)^T$ was only two dimensional. The reflected rotor inertia j_o acted along the coordinate of ℓ, which led to the following mass matrix for PEA:

$$\mathbf{M}_{PEA} = \begin{bmatrix} m_1 + m_2 & -m_2 \\ -m_2 & m_2 + j_o \end{bmatrix}. \tag{3.5}$$

The system was driven by the generalized forces $\boldsymbol{\tau}_{\text{PEA}} = (0,\ F)^T$. The differentiable force vector was given by $\mathbf{h}_{\text{PEA}} = (-(m_1 + m_2)g, m_2 g)^T$.

In the SEA case, the spring was rigidly attached to the foot on one end, and attached to the motor transmission on the other. An additional pair of states (u and $\dot{u}$) described the position of the proximal end of the spring (coordinate origins were defined such that for $u = 0$, and an uncompressed spring, the leg length ℓ was equal to the resting length ℓ_o). The generalized coordinate vector thus had three components: $\mathbf{q}_{\text{SEA}} = (y,\ \ell,\ u)^T$. Since the motor was in series with the spring, the leg force, F, was equal to the force produced by the spring:

$$F = k\left(u + \ell_o - \ell\right) + b\left(\dot{u} - \dot{\ell}\right). \tag{3.6}$$

The mass matrix for this system was given by:

$$\mathbf{M}_{\text{SEA}} = \begin{bmatrix} m_1 + m_2 & -m_2 & 0 \\ -m_2 & m_2 & 0 \\ 0 & 0 & j_o \end{bmatrix}. \tag{3.7}$$

The system was driven by the generalized forces $\boldsymbol{\tau}_{\text{SEA}} = (0,\ F,\ T_o - F)^T$. The differentiable force vector was given by $\mathbf{h}_{\text{SEA}} = (-(m_1 + m_2)g, m_2 g, 0)^T$.

For both models, the main body velocity and the leg retraction rate were equal during ground contact ($\dot{y} = \dot{\ell}$). That led to the modified EOMs of $\ddot{y} = \ddot{\ell} = \frac{F}{m_1 + j_o} - \frac{m_1}{m_1 + j_o} g$ for PEA and $\ddot{y} = \ddot{\ell} = \frac{F}{m_1} - g$ for SEA. This constraint implies that at the moment of touch-down, a collision brought the foot velocity $v_{\text{foot}} = \dot{y} + \dot{\ell}$ to zero.

3.3.2 Motor and Transmission Model

Since we were interested in the realistic trade-offs between thermal losses and mechanical work within each of the actuation concepts, we included a model of an electric DC motor in our simulation [76]. To simplify the analysis, we neglected the electrical dynamics due to the winding inductance. The motor torque is related linearly to the electrical motor current i via the motor torque constant k_T ($T_m = i k_T$). The thermal losses in the motor are given by:

$$P_{\text{therm}} = i^2 R = \frac{T_m^2}{k_T^2} R = \frac{T_m^2}{k_T k_b} R = \frac{T_m^2}{K}, \tag{3.8}$$

where R is the armature resistance, k_b is the motor speed constant, and $K$is the speed torque gradient of the motor. Here we made use of the fact that in SI units, $k_T = k_b$.

The motor rotor had an inertia of j_m and was modeled to be connected to a transmission system. This transmission had two roles. First, it amplified the motor torque ($T_o = n T_m$) while reducing the output speed ($\omega_o = \frac{1}{n}\omega_m$). Second, it converted the rotational motion of the motor to a linear motion that allowed the hopper's leg to extend and contract. We defined the overall transmission as the combination of a rotary gearbox with transmission ratio n_r (a unitless quantity), and a rotary to linear transmission with transmission ratio n_ℓ (with normalized units of $\frac{\text{rad}}{\ell_o}$). The overall transmission ratio n was given by the product of $n_r n_\ell$. For simplicity, we neglected the inertia associated with the transmission, assuming that the inertia of the actuator is dominated by the reflected inertia of the rotor:

$$j_o = (n_r n_\ell)^2 j_m. \tag{3.9}$$

We considered two representative values used for converting rotary to linear motion in modern legged robotics: a large value of $n_\ell = 200 \frac{\text{rad}}{\ell_o}$ and a small value of $n_\ell = 2 \frac{\text{rad}}{\ell_o}$.

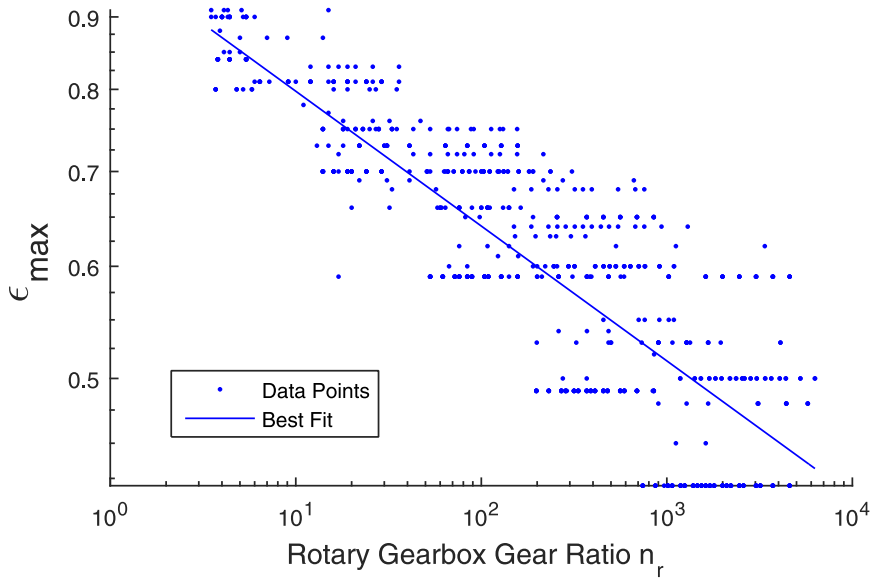

Figure 3.2: The logarithmic regression of the maximum torque conversion efficiency of the rotary gearbox ϵ_{max} as a function of the rotary gearbox gear ratio n_r. The regression was based on 809 gearboxes [82].

These values for n_ℓ were chosen because they are roughly representative of the transmission given by a ball screw [124] and a knee joint bent at approximately forty-five degrees respectively. For both cases, for simplicity, we considered n_ℓ to be a frictionless transmission. This is evident for the knee joint and good approximation for the ball screw, which can have an efficiency of torque conversion of 90% and higher [124]. The only source of transmission friction was thus in the rotary gearbox n_r. This was an important consideration. A particular choice of n_ℓ may be able to better avoid n_r frictional losses. We modeled these n_r losses as being created by a planetary gearbox with dry friction. The torque output after the transmission is therefore given by:

$$T_o = n_\ell \left(n_r T_m - \text{sign}(\omega_m) T_f \right), \tag{3.10}$$

where T_m is the torque output by the motor, ω_m is the motor speed, and T_f is the coulomb frictional torque of the gearbox. We calculated T_f in Eqn. (3.10) from the maximum gearbox torque conversion efficiency ϵ_{max}:

$$\epsilon_{\text{max}} = \frac{T_{\text{o,max}}}{T_{\text{o,max}} + n_\ell T_f} \tag{3.11}$$

where $T_{\text{o,max}}$ is the maximum continuous output torque. Substituting into Eqn. (3.10)

and rearranging yields:

$$T_f = T_{\text{o,max}} \frac{(1 - \epsilon_{\text{max}})}{n_\ell \epsilon_{\text{max}}}. \tag{3.12}$$

For comparison, we included a third case in our analysis which assumed a completely frictionless transmission system (with $\epsilon_{max} = 1$). This was done to understand which transmission choices would be optimal in the absence of any penalty associated with larger gearbox friction. Since in this frictionless case, there is no difference between n_ℓ and n_r, we simply set $n_\ell = 1$.

3.3.3 Model Parameters

We found all necessary motor parameters by applying logarithmic regression to data from 132 Maxon motors in the RE and EC series [82]. We found that:

$$K \approx 0.00567\,(m_m)^{1.80}\,1/\text{Nms} \tag{3.13}$$

$$j_{\text{rot}} \approx 2.85 \times 10^{-05}\,(m_m)^{1.72}\,\text{Kgm}^2 \tag{3.14}$$

$$T_{\text{m,max}} \approx 0.570\,(m_m)^{1.20}\,\text{Nm} \tag{3.15}$$

$$\omega_{\text{m,max}} \approx 1350\,(m_m)^{-0.182}\,1/\text{s}, \tag{3.16}$$

where m_m is the mass of the motor in kg, $T_{\text{m,max}}$ is the maximum motor torque [2], and $\omega_{m,max}$ is the maximum permissible speed of the motor. Note that the values in these equations are not yet normalized.

We modeled the maximal efficiency to scale exponentially with the gear ratio n_r by the exponent γ. This decision was motivated by the observation that gear ratio scales approximately exponentially with stage number, which in turns scales approximately linearly with efficiency [82]. Our efficiency estimate was based on a logarithmic regression over 809 gearboxes from a major motor and gearbox manufacturer [82]. The results of the regression are shown in Fig. 3.2b. We found that:

$$\epsilon_{\text{max}} \approx 0.993\,(n_r)^{-0.0952} \approx 1\,(n_r)^{-0.0952} = n_r^\gamma, \tag{3.17}$$

where the final approximation ensured that the efficiency was 100% when there was no gearbox ($n_r = 1$).

We assumed that the gearbox was appropriately chosen to be able to handle the maximum motor torque. As a result, we calculated the maximum continuous output

[2]This value is twice the maximum continuous torque the motor can provide. It is the maximum value suggested through personal communication with Maxon Motor

Table 3.1: Model parameters and bounds expressed with respect to total mass m_o, leg length l_o, and gravity g.

$m_1 = 0.95\, m_o$	$u_{\min} = \text{-}0.15\, \ell_0$	$n_{\text{r,min}} = 1$
$m_2 = 0.05\, m_o$	$u_{\max} = 0.15\, \ell_0$	$n_{\text{r,max}} = 6285$
$\zeta = 0.2$	$k_{\min} = 0.0001\, m_o g/\ell_o$	$\ell_{\min} = 0.5\, \ell_0$
$\ell_{\max} = 1.15\, \ell_0$	$k_{\max} = 1000\, m_o g/\ell_o$	$K = 2.3 \times 10^{-04}\, 1/m_o\sqrt{g\ell_o}$
$j_{\text{rot}} = 1.48 \times 10^{-05}\, m_o \ell_o^2$	$T_{\text{m,max}} = 0.0157\, m_o g \ell_o$	$\omega_{\text{m,max}} = 748\,\text{rad}\sqrt{g/\ell_o}$

torque after the transmission, $T_{\text{o,max}}$, by:

$$T_{\text{o,max}} = n_r n_\ell T_{\text{m,max}} \tag{3.18}$$

All parameters and their limits are reported in Table 3.1. They are based off of our previous hardware [62], as done in [110]. In particular, we chose a value of $m_m = 0.6\,\text{kg}$, $m_o = 5\,\text{kg}$, and $\ell_o = 0.4\,\text{m}$.

3.3.4 Cost Functions

To measure the energetic efficiency of each actuation variation, we used three cost functions: positive mechanical motor work, thermal electrical losses, and positive electrical work. All cost functions are expressed as an integral over a single hop, from time $t = 0$ until $t = T$.

3.3.4.1 Positive Mechanical Motor Work

The positive mechanical motor work refers to the positive mechanical work that is performed by the motor. In a periodic motion, it is equivalent to the sum of the damping losses, collision losses, negative motor work, and frictional losses in the gearbox. The positive motor work is defined as:

$$C_{\text{mech}} = \int_0^T \max\left(T_m \omega_m, 0\right) dt. \tag{3.19}$$

3.3.4.2 Thermal Electrical Losses

The thermal electrical losses cost function expresses the i^2R losses in the motor windings. It is given by:

$$C_{\text{therm}} = \int_0^T \frac{T_m^2}{K} dt. \tag{3.20}$$

3.3.4.3 Positive Electrical Work

Positive electrical work is the integral of the positive electrical power used by the motor. It combines mechanical work and thermal losses. The positive electrical work is equal to:

$$C_{\text{el}} = \int_0^T \max\left(T_m\omega_m + \frac{T_m^2}{K}, 0\right) dt, \tag{3.21}$$

As in [110] we assumed that the robot was unable to recover negative electrical work and store it. Negative motor work could be used, however, to compensate for thermal losses. This cost function provides a close approximation of the total energy discharge from a battery that would be required to power the motors.

3.3.5 Trajectory Optimization

For these models and cost functions, energy efficient motions were generated via trajectory optimization using a multiple shooting approach. To this end, we analyzed motions from apex transit to apex transit, and enforced periodic boundary conditions to simulate a continuous hopping motion. The optimization problem can be formulated mathematically as:

$$\min_{T,T_m,\mathbf{q},\dot{\mathbf{q}},k,n_r} C\left(\mathbf{q},\dot{\mathbf{q}},T_m\right) \tag{3.22}$$

subject to:

$$\begin{aligned}
&\mathbf{M}\ddot{\mathbf{q}} = \mathbf{h} + \boldsymbol{\tau} \qquad (3.23)\\
&\mathbf{q}(0) = \mathbf{q}(T)\\
&y(T) = 1.3\ell_0\\
&u_{\min} < u(t) < u_{\max}\\
&\ell_{\min} < \ell(t) < \ell_{\max}\\
&-T_{m,\max} < T_m(t) < T_{m,\max}\\
&-\omega_{m,\max} < \omega_m(t) < \omega_{m,\max}\\
&k_{\min} < k < k_{\max}\\
&n_{r,\min} < n_r < n_{r,\max}
\end{aligned}$$

A hopping height of $y(T) = 1.3\ell_0$ was chosen to ensure that the hoppers had a flight phase. All bounds are given in Table 3.1. The motor torque $T_m(t)$ was parametrized as a piecewise linear function. The above optimization problem was implemented in the optimization package MUSCOD, which utilizes a fourth/fifth-order Runge-Ketta-Fehlberg numerical integration algorithm [17, 78, 30]. We tried multiple initial conditions, all leading to the same results.

Note that the gearbox gear ratio n_r and the spring stiffness k were free parameters in the optimization. System properties that were unrelated to the actuator configuration were left fixed. These parameters included the masses (m_1 and m_2) and the damping ratio ζ.

In order to obtain a system that behaved better numerically we approximated discontinuities in the cost functions (as has been done, for example, by [123]). In particular, we smoothed the $\max(0, x)$ function using the equation:

$$\max(0, x) \approx \sigma \log\left(1 + e^{\frac{x}{\sigma}}\right) \tag{3.24}$$

with $\sigma = 0.001$. We also smoothed the function $\text{sign}(\omega_m)$ using the equation:

$$\text{sign}(\omega_m) \approx \frac{2}{1 + e^{-\alpha\omega_m}} - 1, \tag{3.25}$$

with $\alpha = 100$.

3.4 Optimal Configurations, Motions, and Parameters

As a result of the optimization-based motion generation and parameter identification, we found that the ideal actuator type was both dependent on the choice of rotary to linear transmission and on the selected cost function. For positive electrical work, which combines mechanical motor work with thermal losses and reflects a realistic trade-off between these two contributions, we found that SEA was the optimal actuator type for an ideal, frictionless transmission as well as for the $n_\ell = 200\frac{\text{rad}}{\ell_o}$ case. For a hopper with $n_\ell = 2\frac{\text{rad}}{\ell_o}$, PEA was the optimal actuator type (Fig. 3.3). In the following, we elaborate on the optimal actuator type for each configuration and detail the resulting motion profiles and parameter choices for each case.

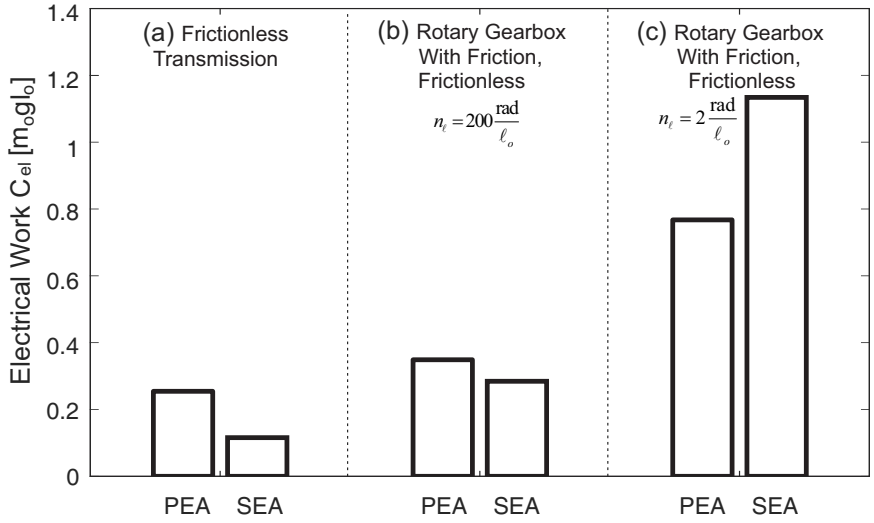

Figure 3.3: The optimal positive electrical work values at a hopping height of h = $1.3\,\ell_o$. Three cases are shown: a theoretical entirely frictionless transmission, a rotary to linear transmission of $n_\ell = 200\frac{\text{rad}}{\ell_o}$ with a rotary gearbox with friction, and a rotary to linear transmission of $n_\ell = 2\frac{\text{rad}}{\ell_o}$ with a rotary gearbox with friction. SEA is the most energetically economical choice for both the frictionless transmission and $n_\ell = 200\frac{\text{rad}}{\ell_o}$ cases. PEA is better for the $n_\ell = 2\frac{\text{rad}}{\ell_o}$ case.

3.4.1 Frictionless Transmission

For a completely frictionless transmission, the energetically optimal actuator type depended on the cost function (Fig. 3.4). For positive mechanical motor work C_{mech}, the SEA hopper was 67% more energetically economical than PEA ($.070\,m_o g\ell_o$ vs. $.14\,m_o g\ell_o$). For both actuator types, energy was primarily lost to damping, accounting for 85% of C_{mech} for SEA and 96% for PEA. In terms of thermal electrical losses C_{therm},

the PEA hopper was 72% more economical than SEA ($.017\, m_o g \ell_o$ vs. $.036\, m_o g \ell_o$). For the electrical work C_{el} the SEA hopper was 75% more energetically economical than PEA ($.12\, m_o g \ell_o$ vs. $.25\, m_o g \ell_o$). For both actuator types, the C_{el} cost was primarily caused by damping and thermal losses in the spring and motor. Negative mechanical motor work was negligible, indicating a preference for following the natural dynamics of the system and exploiting passive storage of excess energy.

When optimizing for C_{mech} and C_{therm} individually, the results can largely be explained by the inherent advantages of each actuator type. SEA's advantage when optimizing for C_{mech} stemmed from the fact that SEA can directly influence the relative rate of spring motion and therefore decrease damping losses. For example, during the second half of stance, the actuator u is pushed downwards to inject energy but also to reduce the extension rate of the spring (as discussed in [108]). Such a strategy is not possible for PEA during stance where the spring motion is inherently coupled to the main body motion. PEA can reduce damping losses during flight, however, by holding the leg at its maximum length. This strategy reduces the effective hopping height and avoids oscillations with their associated damping losses in the air. Additionally, the foot is released slightly before touchdown to have its relative velocity with the ground be approximately zero (i.e. the leg velocity $\dot{\ell}$ approximately matched the main body velocity $\dot{y}$), minimizing collision losses (we will refer to this as the *clamping strategy*). As for minimizing C_{therm}, the main advantage of PEA stemmed from the fact that PEA did not need to support the weight of the robot, which reduced the required motor forces. Furthermore, the parameters for spring stiffness and gear ratio were tuned precisely such that when the leg oscillated nearly freely during flight (without any large peaks in the motor torque T_m) the leg velocity, $\dot{\ell}$ approximately matched the main body velocity at touchdown (we will refer to this as the *oscillation strategy*), which again minimized collision losses (Fig. 3.5).

What is surprising, is that the rather small margins for each of these two cost functions turned into a large benefit for SEA in the combined cost function of positive electrical work C_{el}. This clear advantage of SEA can be explained by the fact that the optimal motion profiles for C_{mech} and C_{therm} were very similar (Fig. 3.5). The motor trajectory held the leg length nearly constantly at its maximum extension during flight and injected energy into the system during stance. It was therefore easy for SEA to find a strategy that could keep both C_{mech} and C_{therm} small at the same time when optimizing for C_{el}. The total C_{el} effort is merely a sum of the individual cost functions (Fig. 3.4). For PEA, in contrast, the motion trajectory differed significantly depending on the chosen cost function. For C_{mech}, the motion of the leg was similar

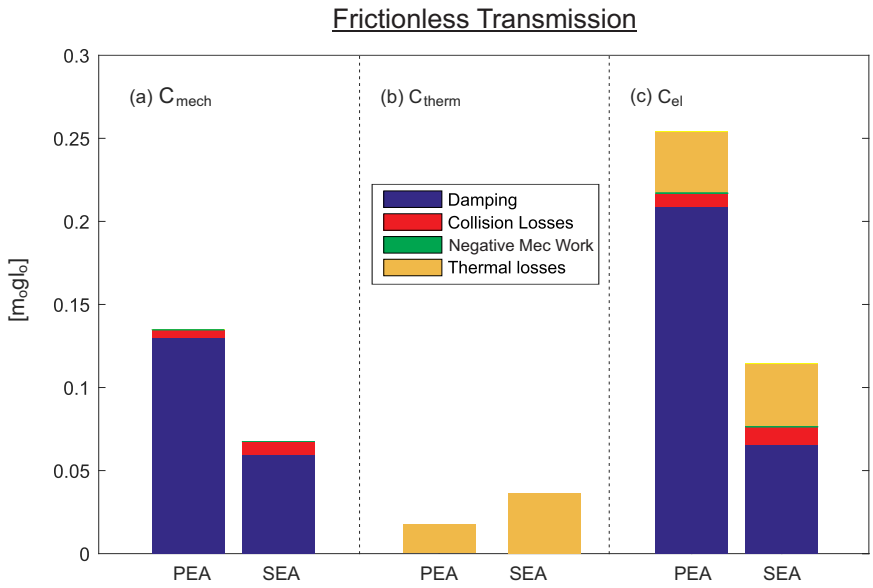

Figure 3.4: An energetic breakdown is shown for the three cost functions in the case of a frictionless transmission. For both the positive mechanical motor work and the positive electrical work, SEA is the energetically optimal actuator type. For thermal losses, PEA is the optimal actuator type. The majority of the losses for both C_{mech} and C_{el} arise from damping losses. For SEA, the C_{el} cost is approximately the sum of its C_{mech} and C_{therm} losses, as it utilizes approximately the same motion strategy for all cost functions. For PEA, however, the C_{el} losses are much larger than the combination of the other two cost functions. This increase occurs because PEA utilizes very different strategies when optimizing for either C_{mech} or C_{therm}. Therefore it must trade-off between two very different strategies in the combined cost function C_{el}.

to SEA, utilizing the *clamping strategy*; whereas for C_{therm}, the optimal motion is the *oscillation strategy*. For the combined cost function C_{el}, PEA therefore had to resolve a severe trade-off between two very different actuation strategies. As a result, for C_{el}, PEA had both higher mechanical work (primarily driven by an increase in damping losses) and higher thermal losses than for either C_{mech} or C_{therm}.

The above flight motion strategies indicate an important difference between our modeling and previous modeling efforts. The presence of foot mass and actuator inertia in our model allows us to present these optimal actuation strategies during the flight phase. Those strategies differ, for example, from those presented in [122, 8, 106] which, due to their massless foot, only look at forces during the stance phase. Furthermore, having massless feet, and no damping, as the above papers do, allows for entirely lossless hopping strategies. For example, [8] states that for a SEA "it is possible to find a running gait that requires no work from the telescopic actuators,

Table 3.2: Optimal stiffness and transmission values for the frictionless transmission. Here n is the overall transmission ratio ($n = n_r n_\ell$).

Cost Function	**Actuator Type**	**k** ($m_o g/\ell_o$)	**n** (rad/ℓ_o)
Positive Motor Work C_{mech}	PEA	27.5	41.0
Positive Motor Work, C_{mech}	SEA	192	789
Thermal Losses, C_{therm}	PEA	21.5	193
Thermal Losses, C_{therm}	SEA	37.8	703
Positive Electrical Work, C_{el}	PEA	7.80	103
Positive Electrical Work, C_{el}	SEA	186	797

for any combination of speed and stride length." For PEA, the same can be said. Without collision losses or damping, the spring can passively store and replace all of the energy during hopping. Having both cases be entirely lossless would make a comparison of the two types of actuators impossible, and therefore justifies the added complexity of our model.

For all cost functions, the optimal PEA hopper had a significantly lower transmission ratio $n = n_r n_l$ than SEA (Table 3.2). Smaller values for n are better for PEA, because the reflected rotor inertia directly adds to the collision losses (Eqn. (3.1)). Since the spring force and motor torque act additively for PEA, the output torques from the motor are much smaller than for SEA, and there is thus no large penalty for using a smaller gearbox. Along the same lines of reasoning, SEA required a larger n to reduce the effective motor torque T_m and the associated thermal losses. Since leg motion and actuator motion were decoupled, there was no penalty for the resulting larger reflected rotor inertia.

For both actuation types, n was much smaller for the positive motor work cost function C_{mech} than for the other two cost functions. This result reflects again the fundamental differences that arise when considering C_{therm}. For C_{therm}, minimizing motor torques plays a more important role. Increasing n leads to smaller required T_m. This consideration is not important for C_{mech}, which is independent of n.

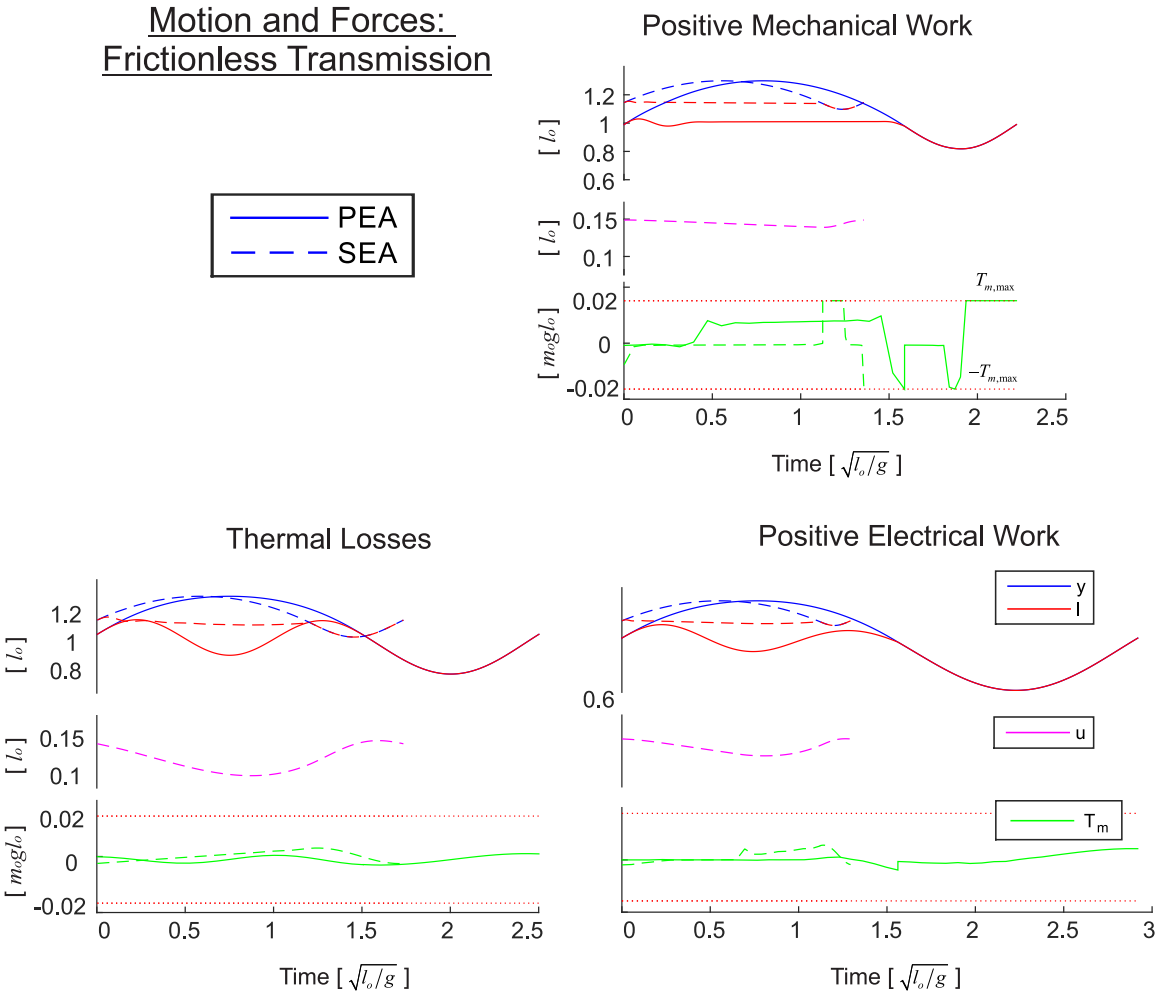

Figure 3.5: Optimal motions and actuator inputs for the frictionless transmission. Shown are the results for optimizations based on positive mechanical motor work, thermal losses, and electrical work. The leg motion for SEA (dashed line) is very similar for all cost functions. In contrast, for PEA (solid line), the leg motion is drastically different when optimized for positive mechanical motor work as compared to thermal losses. As a result, when positive mechanical motor work and thermal losses are combined into a single cost function, the electrical work, PEA must trade-off between two very different motion strategies.

3.4.2 Rotary Gearbox With Friction, Large Rotary to Linear Transmission

Introducing friction in the transmission led to a new trade-off: in addition to creating a larger reflected rotor inertia, larger transmission ratios were now additionally penalized by larger friction values. For a rotary to linear transmission value of $n_\ell = 200\frac{\text{rad}}{\ell_o}$, this trade-off is not particularly grave.

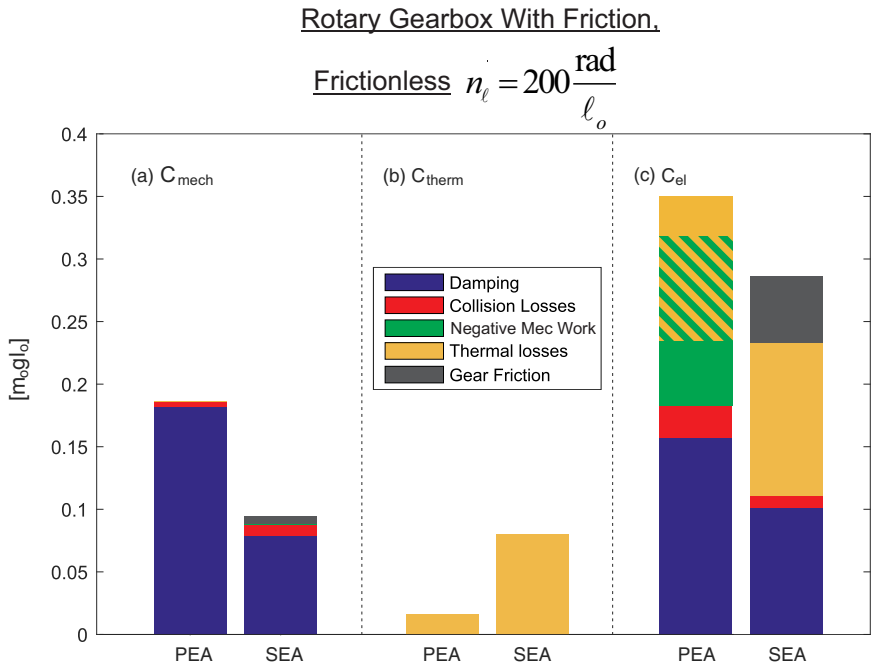

Figure 3.6: Shown is the energetic breakdown for the three cost functions in the case of a rotary gearbox with friction and $n_\ell = 200\frac{\text{rad}}{\ell_o}$. Similar to the frictionless transmission case, for both C_{mech} and C_{el}, SEA was the energetically optimal actuator type. For C_{therm}, PEA was the optimal actuator type. The majority of the losses for C_{mech} arose from damping losses. For C_{el}, thermal losses played a large role. For PEA, negative mechanical motor work compensated for a large proportion of the thermal losses (the cross-hatched region, indicating that though both losses occurred, they only were counted once). SEA has significantly higher thermal losses when optimizing for C_{el} than C_{therm}. It could decrease these thermal losses by increasing n_r, but it would come at the cost of increased gear friction losses. Gear friction was only a significant source of losses for SEA.

As a result, the energetically optimal actuator type was cost function dependent in the same way as for the frictionless transmission (Fig. 3.6). For C_{mech}, the SEA hopper was 65% more energetically economical than PEA ($.096\, m_o g \ell_o$ vs. $.19\, m_o g \ell_o$). For both actuators, energy was still primarily lost to damping, accounting for 84% of C_{mech} for SEA and 97% for PEA. Frictional losses in the gearbox were relatively low, as both actuators chose small optimal n_r values, which therefore had high efficiencies (Table 3.3). For SEA, the optimizer chose an overall transmission ratio of $n = 256\,\frac{\text{rad}}{\ell_0}$ while PEA had $n = 200\,\frac{\text{rad}}{\ell_0}$ (i.e., no rotary gearbox at all). As a result, for SEA, the frictional losses accounted only for 7% of the SEA losses and for none of the PEA losses. For C_{therm}, the PEA hopper was 131% more energetically economical than SEA ($.017\, m_o g \ell_o$ vs. $.080\, m_o g \ell_o$). For C_{el} , the SEA hopper was 20% more

Table 3.3: Optimal stiffness and transmission values for the rotary gearbox with friction, $n_\ell = 200\frac{\text{rad}}{\ell_o}$ case. Here n is the overall transmission ratio ($n = n_r n_\ell$).

Cost Function	**Actuator Type**	**k** ($m_o g/\ell_o$)	**n** (rad/ℓ_o)
Positive Motor Work, C_{mech}	PEA	16.4	200
Positive Motor Work, C_{mech}	SEA	23.3	256
Thermal Losses, C_{therm}	PEA	22.9	200
Thermal Losses, C_{therm}	SEA	25.6	492
Positive Electrical Work, C_{el}	PEA	5.93	200
Positive Electrical Work, C_{el}	SEA	23.4	500

energetically economical than PEA ($.28\, m_o g\ell_o$ vs. $.35\, m_o g\ell_o$).

The results for the three cost functions followed the same general trend as in the completely frictionless transmission. The results held largely because of the advantage SEA obtains from utilizing a highly efficient rotary to linear transmission with a large transmission ratio. With the rotary to linear transmission doing most of the reduction ($n_l = 200\,\frac{\text{rad}}{\ell_0}$), only small values for n_r are necessary and there is a very small penalty for SEA to choose a large transmission ratio $n = n_l n_r$ (Eq. (3.17)). Therefore, the SEA costs showed only a slight increase due to gear friction. PEA, however, favored smaller transmission ratios for C_{mech} and C_{el}. Here PEA attempted to have as low a transmission ratio as possible, choosing to have $n_r = 1$ for all cost functions. Still, with $n_l = 200\,\frac{\text{rad}}{\ell_0}$, it was forced to have a minimum transmission ratio that was larger than its optimal choice for the frictionless transmission. This non-optimal choice of n drives up PEA costs for C_{mech} and C_{el} much higher than the slight gear friction for SEA, maintaining the trends from the frictionless transmission while increasing costs. In particular, for PEA, negative mechanical motor work became a significant portion of the C_{el} losses, likely to avoid excess collisional losses from the larger transmission (Eqn. (3.1)). For C_{therm}, the PEA cost and transmission ratio are nearly identical to the frictionless transmission.

For both PEA and SEA, the optimal motion was nearly identical to the frictionless transmission for C_{mech} and C_{therm} (Fig. 3.7). For C_{el} there was again a trade-off between the *oscillation strategy* and the *clamping strategy*. The optimal C_{el} motion, however, changed. Whereas for the frictionless case, PEA chose the *oscillation strat-*

egy, here it chose the *clamping strategy*. The consequences of the choice to suppress the natural oscillatory motion of the spring can be seen in the largely increased negative mechanical motor work for C_{el}.

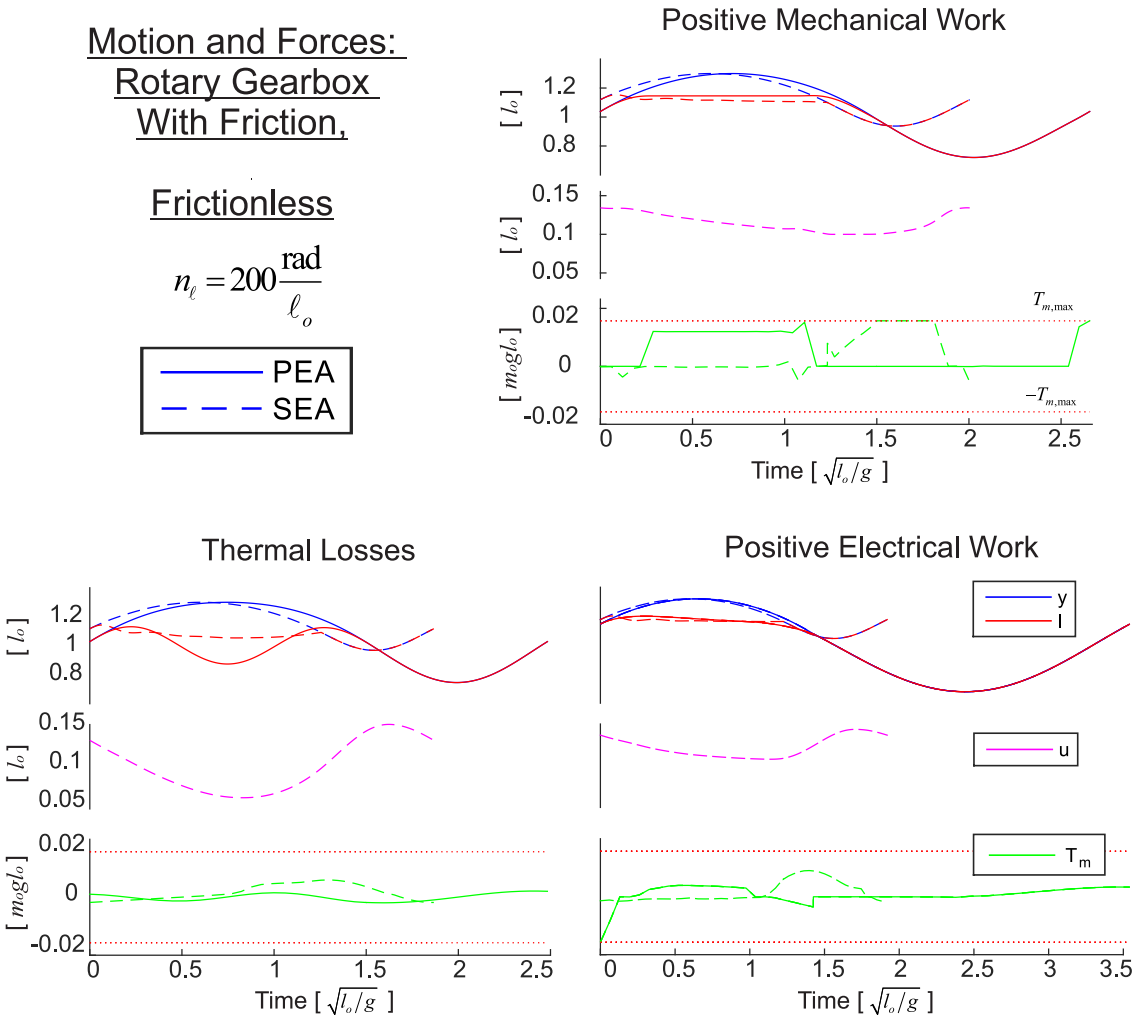

Figure 3.7: Optimal motions and actuator inputs for the rotary gear box with friction and frictionless $n_\ell = 200 \frac{\text{rad}}{\ell_o}$ case. Shown are the results for positive mechanical motor work (a), thermal losses (b), and electrical work (c). The most notable difference from the frictionless motion, was that for PEA electrical work, it was no longer optimal to have the leg oscillate during flight. Instead, PEA and SEA adopted similar strategies during flight, holding their legs near maximum extension.

3.4.3 Rotary Gearbox With Friction, Small Rotary to Linear Transmission

The rotary to linear transmission value of $n_\ell = 2\frac{\text{rad}}{\ell_o}$ in this case is relatively small. This case will therefore require substantially larger n_r values, which in turn will create larger friction losses.

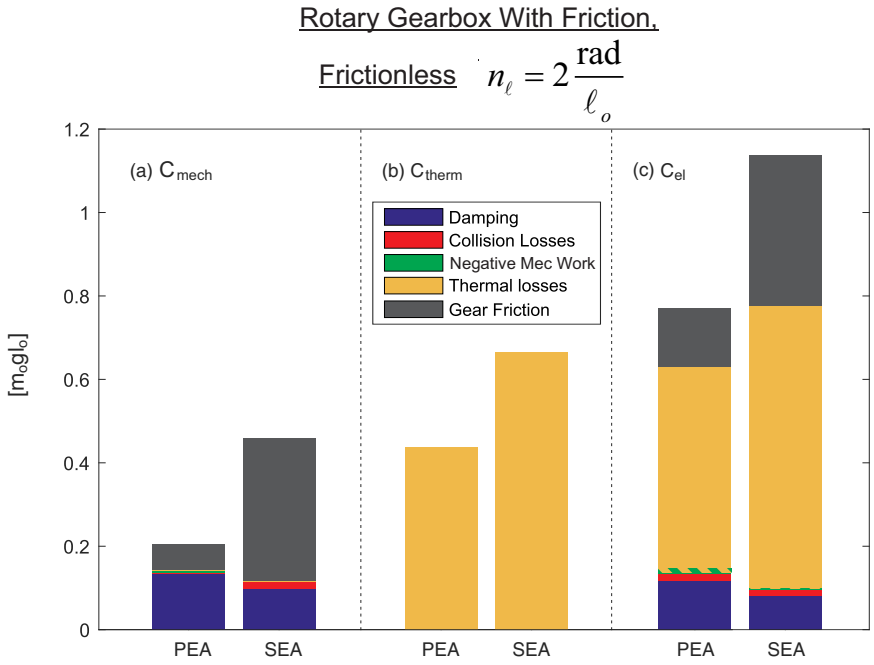

Figure 3.8: The figure shows the energetic breakdown for the three cost functions in the case of a rotary gearbox with friction with $n_\ell = 2\frac{\text{rad}}{\ell_o}$. PEA was now optimal for all cost functions. The majority of the losses for C_{mech} arose from frictional and damping losses. For C_{el}, thermal losses and gear friction dominated the losses.

This clearly benefited PEA, which was the energetically optimal actuator type for all cost functions in this case (Fig. 3.8). For C_{mech}, the PEA hopper was 77% more energetically economical than SEA ($.21\, m_o g \ell_o$ vs. $.46\, m_o g \ell_o$). For PEA, energy was primarily lost to damping, accounting for 65% of the losses. The frictional losses in the gearbox accounted for 30% of losses. For SEA, the trend was reversed: 75% was lost to gearbox friction, whereas 21% was lost to damping. For C_{therm}, the PEA hopper was 41% more energetically economical than SEA ($.44\, m_o g \ell_o$ vs. $.67\, m_o g \ell_o$). For C_{el}, the PEA hopper was 39% more energetically economical than SEA ($.77\, m_o g \ell_o$ vs. $1.1\, m_o g \ell_o$). For both actuators, the losses were dominated by thermal losses and gear friction (Fig. 3.8).

In contrast to the previous cases, there was now a significant penalty for SEA

Table 3.4: Optimal stiffness and transmission values for the rotary gearbox with friction, frictionless $n_\ell = 2\frac{\text{rad}}{\ell_o}$ case. Here n is the overall transmission ratio ($n = n_r n_\ell$).

Cost Function	**Actuator Type**	**k** ($m_o g/\ell_o$)	**n** (rad/ℓ_o)
Positive Motor Work, C_{mech}	PEA	19.8	27.0
Positive Motor Work, C_{mech}	SEA	41.8	306
Thermal Losses, C_{therm}	PEA	31.2	90
Thermal Losses, C_{therm}	SEA	91.8	406
Positive Electrical Work, C_{el}	PEA	34.4	63.0
Positive Electrical Work, C_{el}	SEA	119	388

to choose a large n, as it directly led to a large n_r and meant that there were significant frictional losses (Eq. (3.17)). PEA, with its smaller optimal rotary gearbox transmission n_r therefore suffered far lower frictional losses (Table 3.4).

The optimal motion for both PEA and SEA was now nearly identical for all three cost functions (Fig. 3.9). For all cost functions, both hoppers used the *clamping strategy*. There was no longer any oscillatory behavior by the PEA hopper. This lack of oscillatory behavior likely results from the presence of significant rotary gearbox friction. PEA could no longer choose as small of an n_r value as in the previous two cases, meaning that gear friction induced losses whenever the leg moved. Therefore, the optimizer chose to clutch the leg for all cost functions, avoiding unnecessary leg oscillation and removing any trade-off for C_{el}. C_{el} represented primarily the sum of C_{mech} and C_{therm}.

3.5 Discussion & Conclusion

In this study, we employed numerical optimization to compare optimal hopping motions of series and parallel elastic actuated hoppers. To make the comparison between the two actuation concepts as fair as possible, we compared the *best possible* hopper with SEA to the *best possible* hopper with PEA. To this end, we optimized actuator forces, motion trajectories, and system parameters simultaneously. The analysis was performed for three different cost functions: positive mechanical motor work C_{mech}, electrical thermal losses C_{therm}, and positive electrical work C_{el}. We studied

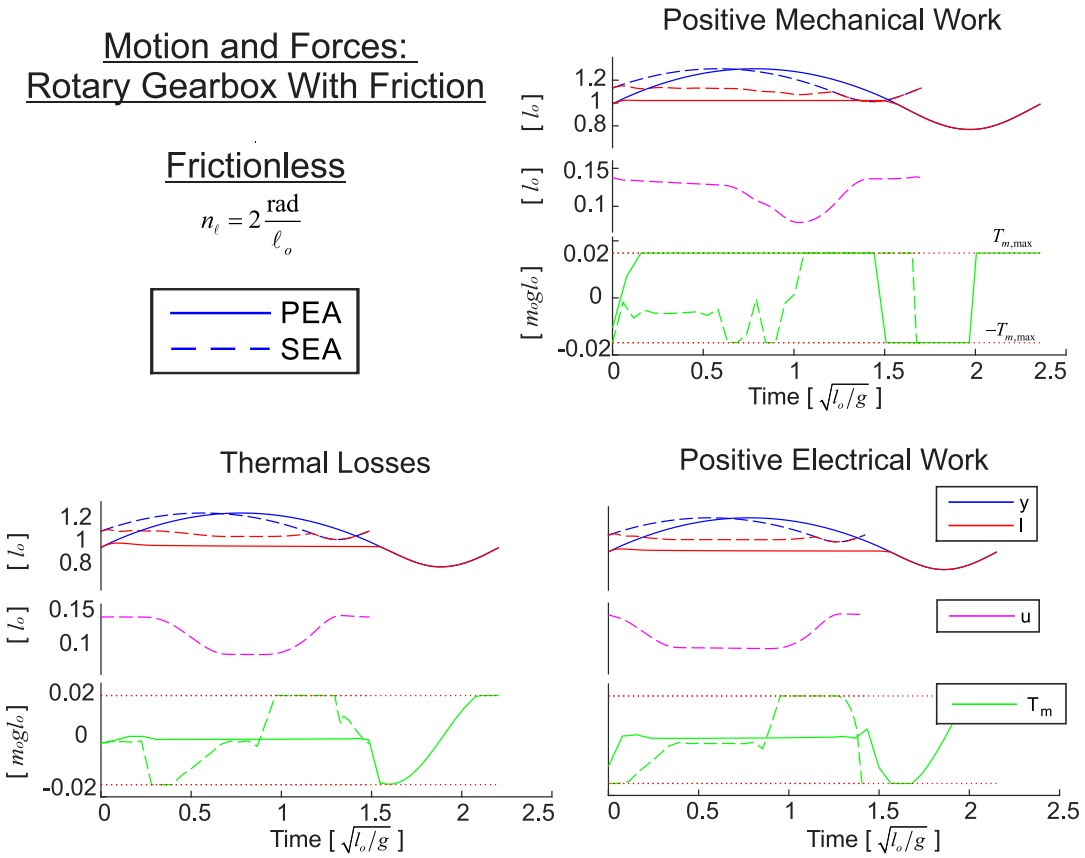

Figure 3.9: Optimal motions and actuator inputs for the rotary gear box with friction and frictionless $n_\ell = 2\frac{\text{rad}}{\ell_o}$ case. The motion here was very similar for both PEA and SEA for all three cost functions. Both hoppers extended their legs to near maximum extension during flight and held them there until touchdown.

hopping for two representative cases of rotary to linear transmission. In addition, we compared these results to an idealized case without friction in the transmission. Optimizing system parameters such as the rotary gearbox ratio and the stiffness of the springs was crucial. The different actuator types did require very different parameter values to perform optimally.

Given that C_{el} is the most complete cost function, we would conclude that for electrically driven hoppers, SEA is the most energetically economic actuator solution when the majority of the transmission ratio is accommodated for by a very high efficiency rotary to linear transmission, such as a prismatic ball screw. For a hopper with a smaller transmission (such as a robot hopping with a bent knee), however, PEA performed better. These optimal choices are primarily a consequence of the fact that SEA requires larger overall transmission ratios than PEA, as could be seen

clearly when looking at the frictionless transmission. When the transmission ratios are achieved in an efficient way, SEA is the better actuator type. If they are subject to friction losses, PEA becomes the better actuator type.

Throughout our analysis, it became evident, that each configuration had a unique optimal motion profile and a set of parameters that differed greatly between the two actuation concepts. This clearly illustrated the necessity of our optimization approach. From a conceptual point of view, this simultaneous optimization of motion and morphology extends the paradigm of system-based design to include the future motion of the robotic system already at the design stage. We strongly believe, that such a combined and simultaneous optimization of robot and motion will be at the core of future robotic design. This technique is slowly making its way into robotics, for example in the optimization of an assistive device for sit-to-stand motions [56], to create stable running motions in a human-like robot [88], and to optimize limb lengths for particular tasks [47]. Here, we extended its principle to make a discrete design comparison between two fundamentally different morphologies. In the future, this approach can potentially be applied to more complex models and robots to achieve truly optimal performance during the design phase.

There are further important considerations for the actuator problem that must be explored before implementation in hardware. For PEA, the motor inertia is not isolated from collisions, which can lead to significant energetic losses. Therefore, it is imperative that the foot velocity is near-zero at touchdown. PEA achieves this by utilizing the *oscillation strategy* and *clamping strategy*, which let the spring passively retract the foot and minimize foot velocity with minimal energetic effect. Overall, we would argue that these optimal hopping strategies for PEA are more sensitive to timing issues and would be harder to implement in hardware. These strategies require a precise tuning of the spring stiffness, rotor inertia, and foot mass to achieve the correct spring natural frequency. However, small deviations from the optimal parameter values (e.g., caused by modelling errors or disturbances in the motion) can get in the way of this phase matching and might result in large collision losses.

In the present study, to avoid biasing the results towards either actuation configuration, we did not constrain the hopping frequency. The primary constraint on the hopping motion was that the hopper had to reach a height of $y = 1.3\ell_0$. This constraint ensured that the hoppers had both a stance phase and a flight phase. Timing was not considered, however, in finding the energetically optimal motion. From the motion plots, it is clear that SEA has significantly shorter optimal hopping periods, suggesting a potential advantage over PEA. In our prior work, the effect of frequency

was implicitly included by enforcing an average velocity during 2-dimensional motion [132] and was found to have little effect on the energetics at most speeds. Still, future studies could consider exploring hopping at a fixed frequency to see additional sensitivity effects.

There are additional mechanical and sensing complexities that must be taken into account when implementing either actuator type in hardware. For example, in PEA, the gearbox is not isolated from collisions. To prevent unnecessary damage to the gears, PEA would likely need an additional mechanism that softens these collisions. Furthermore, the spring could be disengaged to allow for easier leg retraction during swing. [67], for example, implements a clutch that disengages the spring during flight, and a small series elastic element that protects the gearbox. SEA would need additional components as well. Since SEA moves the proximal end of the spring, which in turn changes the leg length, it would need additional sensors to measure the location of each. More moving parts for SEA further means that additional bearings and mechanical components are necessary in practice.

Despite the simplicity of our models compared to a final hardware implementation, the motion strategies shown here can provide templates for further optimizations with more complex models and gaits. Given that hopping can be considered the archetype of legged locomotion [104, 72], one would expect that similar motion patterns will be found in active running and walking gaits of multi-legged robots. They can thus be used to systematically initialize optimizations, or be employed as a tool to check the viability of more complex optimization results. This could enable roboticists to detect and avoid local minima that do not represent the global optimum in their optimizations. Finally, the actuation strategies that we observed in the optimal solutions provide an interesting departure point for further hardware development. For example, the *clamping strategy* that the optimizer discovered for PEA, where the leg was held fixed during the flight phase, could be implemented more efficiently with an actual clutch rather than with a DC motor.

The results presented in this work have been developed for the particular case of 1D hopping with electrically driven actuators. Certain parameters, such as the mass of the motors, are based off of our previous hardware [62]. The obtained motions, parameter choices, and cost values are specific to this choice of problem. From the work presented here, it is clear that even for this particular problem, the optimal actuation type is case dependent. It is impossible to state conclusively whether in general SEA or PEA is the better actuation concept for legged robots. Naturally, the cases presented in this work only represent a sample of a wide range of possible hopper

configurations, and focus on energetics. There likely is a gradual transition from hoppers which would benefit from SEA to hoppers which should use PEA as friction in the transmission becomes more important. That is, ball screws are available with a wide variety of transmissions, knees can be operated at many different angles, and hybrids of the two transmission systems even exist [102]. Each of these transmission types can benefit a particular actuator. Additionally, more complexity has been introduced by robotic prototypes that utilize both SEA and PEA within a single design [67]. Future studies should take into account the vast variety of possible configurations.

The highly complex dependence on actuation type, parameters, and motion profile emphasizes the necessity of optimization to explore design issues. Still, it is important here to state that the methods we use are local, and so we are unable to guarantee their global optimality. In hopes of escaping local minima, all of the results presented in this chapter represent optima that have been tested from a variety of different initial conditions.

Given that our evaluation took into account different cost functions that penalized force and work independently, our results can still be considered fairly general. Furthermore, this chapter should also be understood as an introduction of a systematic methodology that enables a fair comparison of different robot morphologies. In a sense, the comparison of PEA and SEA is just an application of this method. In the future, this methodology can and should be extended to include other models as well as more complex motions. Moreover, the methodology can be utilized to look at other cost functions to maximize performance metrics other than energetics, such as maximizing hopping height.

Overall, the presented work gives a deeper understanding of the optimal motion for both SEA and PEA driven hopping motions. Understanding this underlying optimal motion can help designers ensure that they are not losing energy by unintentionally fighting the natural dynamics of a particular type of actuator. This understanding also gives insight into the coupling of morphology and motion. By using trajectory optimization, we can see how the choice of transmission ratio and stiffness change for a particular implementation and how these parameters and the resulting motion mutually influence each other. Recognizing these relationships opens the possibility to make robots more efficient, faster, and more robust.

CHAPTER IV

Optimal Configuration of Series and Parallel Elasticity in a 2D Monoped

4.1 Introduction

[1] The way that a legged system is built and the way that it moves are fundamentally connected. This connection is readily apparent when a legged robot moves in a way that maximizes its energetic economy. Model based studies have shown that robots moving in this way take advantage of their *natural dynamics* [38, 41] (the intrinsic morphologically based motions that result from the interplay of gravity, inertia, and elasticity in the springs). For these models, springs play a key role in explaining the dynamics of legged systems.

Motivated by nature [84, 7] and the passive dynamic results above, we include elasticity in our models. To understand the energetic considerations of a particular morphology, we also incorporate actuators. In doing so, we now alter the passive structure of the robot, and consequently, alter the way in which the legged system moves efficiently. The optimal motion is further complicated by the fact that we have many different choices on how to implement the actuators, and, that different motor and spring parameters are ideal for each case. The two most common implementations are to place the springs either in series (Series Elastic Actuator, SEA) or in parallel (Parallel Elastic Actuator, PEA) with the motor. The primary advantage of SEA is that the motor inertia is coupled by a spring to the joint inertia. As a result, the motor is well isolated from impacts, and the motor inertia does not interfere with the joint motion. The primary advantage for PEA is that the motor force and the parallel spring force act additively, which can decrease the force requirements on the

[1] This chapter has been previously published in the 2016 IEEE International Conference on Robotics and Automation [132]

motor.

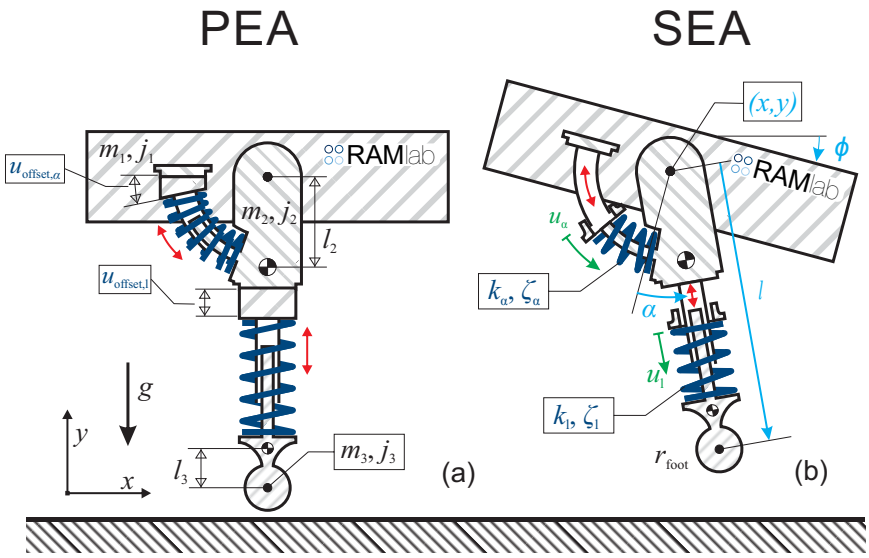

Figure 4.1: In this chapter we use optimal control to find the most energetically economical configuration of actuators on a two-dimensional monoped. We compare four configurations, a parallel elastic actuator (PEA) at both the hip and the leg (shown on the left), a series elastic actuator (SEA) at both locations (shown on the right), a SEA at the hip and PEA at the leg, and a PEA at the hip and an SEA at the leg. In the optimization, we simultaneously optimize for the motion and morphology of each configuration to ensure that we compare the best possible version of each monoped. Our models have mass in the legs and feet, damping, and realistic DC electric motor models. We additionally include realistic constraints on the leg length, motor force, and motor velocity.

In this chapter we seek to find the optimal configuration of SEA and PEA in a two-dimensional monoped. While in the past we have worked with one-dimensional monopedal hopping [134], moving to a second dimension greatly increases the complexity of the problem. Both the hip and the leg can have either PEA or SEA, leading to four possible actuator configurations. The two-dimensional monoped moves with a forward velocity, which leads to much more complex motions that require careful coordination between the hip and leg. The parameter space over which to optimize morphology is greatly expanded by the addition of a second motor and spring. Lastly, and perhaps most importantly, we are optimizing for the motion and parameters of actuators that have very different roles in legged locomotion. The hip actuator coordinates the leg swing dynamics, while the leg springs mimics the behavior of a spring loaded inverted pendulum (SLIP) [75].

We seek motions that minimize the cost of transport (COT) (the amount of en-

ergy divided by the distance traveled [35, 126]), for three separate cost functions: the positive motor work, electrical losses, and the positive electrical work. Utilizing our prior results [134] and previous model-based studies [110], we hypothesize that the optimal configuration will be cost function dependent. For the positive motor work and positive electrical work costs of transport (COT), we predict that the optimal configuration will have a series leg, as a SEA was energetically optimal for the one-dimensional hopper. For the electrical losses COT, we predict that the optimal configuration will have a parallel leg, as PEA was slightly more economical for in-place hopping. For all three cost functions, we hypothesize that the two-dimensional monoped will favor a parallel hip. This prediction is motivated by [42], who found periodic walking gaits on flat ground with no energy input. As there is no active input in their bipedal model, the hip spring acts entirely to time the swing leg dynamics passively. A PEA with no torque applied mimics this situation. Therefore, we predict that with an optimal stiffness, the parallel spring should largely account for leg swing timing.

By systematically testing these hypotheses, we show the possibility of using optimization to make design choices on a realistic robot model performing a realistic task. While our work on the one-dimensional hopper [134] showed how optimization can be used to compare two distinct legged robot morphologies, the task was intentionally simplified to allow us to ensure our methodology worked. The two-dimensional motion optimized for here represents the motion that each leg of a biped undergoes during running, with all the complexities of swing-leg coordination. Furthermore, the choice of actuator is an open question in hardware and simulation. ScarlETH has SEA in both the hip and the knee [62]. MABEL also makes use of SEA [46] while Phides utilizes PEA [69]. In prosthetics, the effect of parallel and series elasticity has also been studied on an ankle joint [45]. In simulation, [65] compare PEA and SEA for stationary hopping and conclude that PEA is more energetically efficient for typical robotic properties and motions. This work, however, only looks at the electrical losses, ignores losses during flight, ignores collision losses, and does not include a detailed electric motor model. With this present work, we include these missing aspects and we show how our previous methodology can be extended to compare different configurations of SEA and PEA in order choose the most energetically economical structure.

To make our optimization procedure relevant for actual hardware design choices, we use realistic models. These models have mass in the feet and upper leg, realistic DC electric motor models, and damping in the springs. The models have realistic

constraints on torques, velocities, leg lengths, and all parameter values. In these optimizations we include the stiffness and motor parameters as free variables. In this way we ensure that the optimizer is allowed to choose the best morphology for a particular actuator configuration. We show that the optimal configuration depends on the velocity as well as the cost function. The optimal configuration is primarily driven by damping losses and negative actuator work, with collisions playing a comparatively small role.

4.2 Methods

4.2.1 Model

The 2D monoped models in this study (Fig. 4.1) are similar to our previous models [110, 130]. In this section we extend the equations of motion to include PEA. Each model includes three rigid bodies: the main body, upper limb, and lower limb. The main body has a mass of m_1 and an inertia of j_1, with the hip joint located at the center of mass (COM). It has three degree of freedoms: its horizontal and vertical position x, y and orientation ϕ. The upper limb segment connects to the main body via a rotational hip joint. It has a mass of m_2 and an inertia of j_2. Its COM is located at a distance l_2 from the hip joint. The lower limb segment, which moves relative to the upper limb through a prismatic knee joint, has mass m_3 and inertia j_3. The COM is located a distance l_3 away from the center of the foot. The remaining model states are the angle of the leg, α, and the length of the leg, l, which is measured from the COM of the main body to the center of the foot.

In contrast to our previous work [110], in this model both the hip joint and knee joint can either have PEA or SEA to control the desired motion. These models are therefore the two-dimensional extension of our previous work on one-dimensional hoppers [134]. If PEA is chosen for the hip joint, the rotational hip spring is rigidly attached to the upper leg segment at one end and to the main body at the other end with an offset angle $u_{offset,\alpha}$ (this spring pre-compression is introduced to keep the comparison between SEA and PEA fair). The hip torque is the sum of the torque produced by the spring and the motor:

$$T_P = k_\alpha(\alpha_o + u_{offset,\alpha} - \alpha) + b_\alpha \dot{\alpha} + T_{mot} \tag{4.1}$$

Where α_o is the rest angle of the hip spring. Similarly, for the knee joint:

$$F_P = k_l(l_o + u_{offset,l} - l) + b_l\dot{l} + F_{mot} \tag{4.2}$$

Where l_o is the rest length of the leg spring.

For SEA, the motor force is equal to the force produced by the spring. Here the hip spring is connected directly to the hip motor on one end, and connected to the upper limb at the other end. The motor position of the hip, u_α, is introduced as an additional generalized coordinate. Similarly, for the leg, the motor position u_l is an additional generalized coordinate. These displacements are driven by the motor torques τ_α and τ_l. The joint forces for the hip and knee joints become:

$$T_S = k_\alpha(\alpha_o + u_\alpha - \alpha) + b_\alpha(\dot{u_\alpha} - \dot{\alpha}) = T_{mot} \tag{4.3}$$

$$F_S = k_l(l_o + u_l - l) + b_l(\dot{u_l} - \dot{l}) = F_{mot} \tag{4.4}$$

The damping coefficients b_l and b_α are obtained from desired damping ratios ζ_l and ζ_α. Based on the selection of the actuators, four different configurations are tested in the following section for optimal performance (PEA-hip and PEA-leg, PEA-hip and SEA-leg, SEA-hip and PEA-leg, SEA-hip and SEA-leg). The number of generalized coordinates for the model depends on the particular configuration being chosen.

To keep the following analysis general, all states and parameters are normalized with respect to the total mass m_o, gravity g, and relaxed leg length l_o. The values of all of the parameters we use in this study and their bounds are shown in Table 4.1 (these are roughly obtained from previous hardware [62]).

4.2.2 System Dynamics

As described before, the total number of generalized coordinates depends on the type of actuator chosen for each joint. For example, if PEA is chosen for the hip and SEA for the knee joint, the generalized coordinates are $\mathbf{q} = [x, y, \phi, \alpha, l, u_l]^T$ and the generalized forces are $\boldsymbol{\tau} = [0, 0, 0, T_P, F_S, \tau_l - F_S]^T$. The continuous dynamics of the model are governed by the equations of motion (EOM) which are stated in the canonical form [109]:

$$\mathbf{M}(\mathbf{q})\ddot{\mathbf{q}} + \mathbf{h}(\mathbf{q},\ \dot{\mathbf{q}}) = \boldsymbol{\tau} + \mathbf{J}^T(\mathbf{q})\boldsymbol{\lambda}, \tag{4.5}$$

where $\mathbf{M}(\mathbf{q})$ is the mass matrix and $\mathbf{h}(\mathbf{q},\ \dot{\mathbf{q}})$ represents the Coriolis, centrifugal, and gravitational terms. The contact Jacobian $\mathbf{J}$ maps the vector of contact forces λ

Table 4.1: Model parameters and limits expressed with respect to the total mass m_o, leg length l_o, and gravity g. All values are based roughly on past prototypes [62].

$m_1 = 0.7\, m_o$	$j_1 = 0.4\, m_o l_o^2$	$l_{min} = 0.5\, l_o$
$m_2 = 0.2\, m_o$	$j_2 = 0.004\, m_o l_o^2$	$l_{max} = 1.15\, l_o$
$m_3 = 0.1\, m_o$	$j_3 = 0.004\, m_o l_o^2$	$u_{min,l}$ = -0.15 l_o
$k_{min,l} = 0.0001\, m_o g/l_o$	$l_o = 1\, l_o$	$u_{max,l} = 0.15\, l_o$
$k_{max,l} = 1000\, m_o g/l_o$	$l_2 = 0.25\, l_o$	$u_{min,\alpha} = -\pi/4$
$k_{min,\alpha} = 0.0001\, m_o g/l_o$	$l_3 = 0.25\, l_o$	$u_{max,\alpha} = \pi/4$
$k_{max,\alpha} = 1000\, m_o g/l_o$	$P_{max,\alpha} = 9.4\, m_o g\sqrt{g l_o}$	$j_{unsc,l} = 0.251\, m_o g l_o$
$r_{foot} = 0.05\, l_o$	$P_{max,l} = 9.4\, m_o g\sqrt{g l_o}$	$j_{unsc,\alpha} = 0.251\, m_o g l_o$
$c_{lim,\alpha} = 0.091$	$\zeta_\alpha = 0.2$	$\bar{\dot{u}}_{min,l} = 0.0001\sqrt{l_o g}$
$c_{lim,l} = 0.091$	$\zeta_l = 0.2$	$\bar{\dot{u}}_{max,l} = 10\sqrt{l_o g}$
$\bar{\dot{u}}_{min,\alpha} = 0.0001\sqrt{l_o g}$	$\bar{\dot{u}}_{max,\alpha} = 10\sqrt{l_o g}$	

into the generalized coordinate space. The portions of the mass matrix for PEA and SEA configurations corresponding to the generalized coordinates $\mathbf{q} = [x, y, \phi, \alpha, l]$ are identical except for one key difference. For a PEA at the hip, we must add the reflected motor inertia $j_{mot,\alpha}$ to the term corresponding to (α, α) (in this case M(4,4)), where $j_{mot,\alpha}$ is given by:

$$j_{mot,\alpha} = \frac{j_{unsc,\alpha}}{\bar{\dot{u}}_\alpha^2}. \tag{4.6}$$

In the above equation $j_{unsc,\alpha}$ is the unscaled inertia and $\bar{\dot{u}}_\alpha$ is the no-load speed of the motor. To avoid repetition, we refer the reader to our previous work [134] for details on these terms. Similarly, for a PEA at the leg, we must add the reflected motor inertia $j_{mot,l}$ to the term corresponding to (l, l) (in this case M(5,5)), where $j_{mot,l}$ is obtained by replacing α with l in Eqn. (4.6).

4.2.3 Cost Functions

To compare the efficiency of different combinations of the two actuator types for a 2D monoped hopping over a range of forward velocities, three cost functions are utilized to quantify the cost of transport. For each optimization we fix the average forward hopping speed $\dot{x}_d$ and quantify the cost of transport. All of the cost functions can then be expressed as an integral over the stride time ($t = 0$ until $t = T$). The COT is obtained by dividing the energy consumption in one stride by the total weight of the model and the distance it traveled over the duration T of that stride.

4.2.3.1 Positive Motor Work

By minimizing the positive motor work, we minimize the sum of the total energetic losses in the contact collisions, viscous damping in the springs, and negative motor work [110]. For the SEA, the total motor work for a single stride is given by:

$$\begin{aligned} c_{mot,l,SEA} &= \int_0^T max\left(F_{mot} \cdot \dot{u_l}, 0\right) dt \\ c_{mot,\alpha,SEA} &= \int_0^T max\left(T_{mot} \cdot \dot{u_\alpha}, 0\right) dt, \end{aligned} \tag{4.7}$$

In the case of the PEA, the actuator velocities are the same as the joint velocities. At any moment, the joint power is equal to the generalized joint force multiplying the joint velocities. Therefore the positive motor work ($c_{mot,l,PEA}$, $c_{mot,\alpha,PEA}$) can be calculated by replacing $\dot{u_l}$ and $\dot{u_\alpha}$ with $\dot{l}$ and $\dot{\alpha}$ respectively.

For all actuation configurations, the final cost function for one stride is the summation of the positive motor work at both the hip and knee joint.

4.2.3.2 Electrical Losses

The electrical losses represent the thermal losses in the motor. For both the parallel and series cases, the thermal losses in a single stride can be quantified as:

$$c_{loss} = \int_0^T \left(\frac{\bar{\dot{u}}_l^2}{P_{max,l}} F_{mot}^2 + \frac{\bar{\dot{u}}_\alpha^2}{P_{max,\alpha}} T_{mot}^2 \right) dt \tag{4.8}$$

where $P_{max,l}$ and $P_{max,\alpha}$ represent the maximal motor power in the leg and hip motors respectively.

4.2.3.3 Electrical Work

We can also combine the two previous cost functions and balance the trade-off between motor work and thermal losses by using a more sophisticated cost function, the positive electrical work. This cost function is unique in that it allows negative work in one motor to be used to perform positive work or compensate for losses in another. For the series hip series leg case, the cost function is:

$$c_{el,SEA,SEA} = \int_0^T max\left(F_{mot} \cdot \dot{u_l} + T_{mot} \cdot \dot{u_\alpha} + \frac{\bar{\dot{u}}_l^2}{P_{max,l}} F_{mot}^2 + \frac{\bar{\dot{u}}_\alpha^2}{P_{max,\alpha}} T_{mot}^2, 0 \right) dt \tag{4.9}$$

For a parallel hip, $\dot{u_\alpha}$ is replaced with $\dot{\alpha}$. For a parallel leg, $\dot{u_l}$ is replaced with $\dot{l}$.

4.2.4 Optimization

We use optimal control to find energetically economical motions for each of the three cost functions (expressed as COT). In these optimizations we enforced periodic boundary conditions in order to obtain a continuous hopping motion. The motion obtained represents the ideal energetic cost, obtained during uninterrupted locomotion without outside disturbances. The results are therefore the upper bound on energetic economy. They do not take into account the additional energetic cost associated with stabilizing feedback.

We obtain optimal motor input by conducting velocity parameter studies using the multiple shooting optimization package MUSCOD [30]. MUSCOD provides a continuous piecewise linear motor input profile that minimizes the chosen cost function. For each point in these parameter studies, we fix the velocity, but leave morphological parameters as free variables. We include the hip and leg stiffness (k_α, k_l), the no load speeds of the hip and leg motors $(\bar{\dot{u}}_\alpha, \bar{\dot{u}}_l)$, the apex height of the main body, and for PEA, the hip and leg motor offset $(u_{offset,l}, u_{offset,\alpha})$ directly in the optimization. The bounds on these parameters (given in Table 4.1) ensure that their values are realistic. The optimal motion is then obtained by integration of the equations of motion (Eqn. (4.5)). The above procedure is repeated for each actuator configuration and each cost function.

To ensure that the motions also remained realistic, we implemented constraints on the motion and motor input. The leg length was constrained to be $0.5l_o \leq l \leq 1.15l_o$. For SEA, the leg motor position was constrained to $-0.15l_o \leq u_l \leq 0.15l_o$. Additionally, the hip motor position was constrained to $-\pi/4 \leq u_\alpha \leq \pi/4$. For the motors we utilize the thermal loss conversion factor c_{lim}, which limits the available motor power to avoid overheating. For the SEA leg motor we have:

$$|F_{mot}| \leq c_{lim,l} \frac{P_{max,l}}{\bar{\dot{u}}_l}, \tag{4.10}$$

and

$$|\dot{u}_l| \leq \bar{\dot{u}}_l \left(1 - c_{lim,l}\right). \tag{4.11}$$

A detailed derivation of these equations can be found in Chapter 4.1.4 of [108]. For the SEA hip motor, l is replaced by α. For PEA, $\dot{u}_l$ is replaced by $\dot{l}$ and $\dot{u}_\alpha$ is replaced by $\dot{\alpha}$.

4.3 Results

We found that the optimal actuator configuration is both velocity dependent, and dependent on the cost function.

For the positive motor work COT, the optimal configuration was parallel for the hip and series for the leg (Fig. 4.2,a). That configuration has similar COT values to the other configurations at low velocities ($v < 0.325\sqrt{l_o g}$), but excels as velocity increases. For intermediate velocities, the monopeds with serial legs outperform those with parallel legs significantly. At a velocity of $v = 1.025\sqrt{l_o g}$ the serial leg monopeds have roughly the same COT (0.197). The monoped with a serial hip and parallel leg has a cost that is 13.86% higher, and the parallel hip parallel leg configuration has a cost that is 31.68% higher. At high velocities ($v > 1.125\sqrt{l_o g}$), the monopeds with series legs diverge in COT value, with the parallel hip and series leg becoming significantly more economical. At a velocity of $v = 1.425\sqrt{l_o g}$), the last solution found by the optimizer for the serial hip and serial leg, the monoped has a cost that is 38.72% higher than the parallel hip and series leg monoped. The optimizer found solutions for the PEA hip and SEA leg configuration at larger velocities (up to $v = 1.825\sqrt{l_o g}$) than the other configurations. The second highest velocity solution was found for PEA leg and PEA hip ($v = 1.525\sqrt{l_o g}$). The optimality of the series leg and parallel hip configuration stems primarily from low damping losses and negative motor work, with collisions playing a small role (Fig. 4.3,b). Fig. 4.3 also shows that both of the series leg configurations have significantly lower damping losses than the parallel leg configurations at high velocities.

For the electrical losses COT, the optimal configuration is again a PEA at the hip and a SEA at the leg (Fig. 4.2,b). As for the positive motor work, at low velocities ($v < 0.325\sqrt{l_o g}$), all of the configurations have nearly the same cost. At the last feasible solution for the parallel hip and parallel leg configuration ($v = 0.825\sqrt{l_o g}$), the monoped has a cost that is 153% higher than the parallel hip and series leg configuration. Additionally, the latter configuration had the most solutions found by the optimizer, with solutions found up to a velocity of $v = 1.825\sqrt{l_o g}$. The second highest velocity solution was found for the series leg and series hip monoped at $v = 1.425\sqrt{l_o g}$.

For the electrical work COT, there is no clear choice for the best configuration (Fig. 4.2,c). At low velocities, the series hip and parallel leg configuration is optimal, while at high velocities both the parallel hip series leg and series hip series leg monopeds are optimal (with both obtaining nearly the same cost).

4.4 Discussion & Conclusion

In this chapter, we apply optimal control to find the most energetically economical configuration of parallel and series elasticity on a two-dimensional monoped. In this process, we simultaneously optimize for motion and morphology. Not only do we compare the four different configurations of SEAs and PEAs, but we also optimize the springs, motor parameters, and motor offsets for each configuration. In addition, we enforce realistic constraints on leg length as well as motor force and velocity. We can therefore confidently say that we are comparing a realistic version of the best possible case for each configuration. Using these techniques, we have shown that for the positive motor work COT and the electrical losses COT, having a parallel hip and a series leg is the optimal configuration. For the positive electrical work, there is no consensus on the optimal choice.

While our optimal configuration prediction for the positive motor work COT was correct, our hypothesis proved incorrect for the other two COT. For electrical losses, this is not particularly surprising. For in-place hopping, the difference in optimal electrical losses for a serial leg compared to a parallel leg is small relative to the other cost functions [134]. It is therefore conceivable that the additional constraints and free parameters implemented here could lead to a shift in the optimal leg spring choice. For the positive electrical work, however, the result is entirely unexpected. The positive electrical work represents a combination of the positive motor work and the electrical losses. As the parallel hip and series leg is optimal for both positive motor work and electrical losses, it would seem that it should also be optimal for the positive electrical work. The discrepancy can likely be attributed to the fact that the cost function allows the negative work in one motor to be used to perform positive work or compensate for losses in the other. As this quality is not present for the positive motor work, the positive electrical work does not accurately represent a combination of the other two cost functions.

For both the electrical losses and the positive motor work COT, the optimizer was able to find solutions at higher velocities than the other configurations. At higher velocities there are increased motor torques and velocities, as well as increased leg contraction and extension. The limiting factors to finding solutions therefore become the motor and leg length constraints. That fact implies that the series leg parallel hip configuration is best able to choose motion strategies that avoid these constraints. As for the one-dimensional hopper [134], this is a surprising result. The main advantage of PEA is that the spring and motor torques act additively (Eqns. 4.2,4.1). It would

seem that therefore the PEA hip and the PEA leg would have a lower electrical loss COT, particularly at higher velocities where torques are much larger. Despite this, the PEA hip and SEA leg configuration has lower costs at nearly all velocities.

For the positive motor work, the series leg configurations have lower damping losses at higher speeds (Fig. 4.3). At first, it would seem that these losses are accounted for by the monoped's ability to use the motor position to decrease the rate of leg extension and compression(as in [134] for the one-dimensional hopper). At a closer look, however, the situation is more complex. The rapid increase in damping losses for the parallel leg configurations is driven by an increase in damping losses at the hip at high velocities. The damping loss increase occurs simply because at higher velocities, the leg is required to swing faster. The fact the the increase is steeper for the PEA leg configurations implies that there is an inherent coupling that occurs between actuators when there is a PEA at the leg. That is, the PEA at the leg is very sensitive to the timing of the leg oscillation. The choice of leg spring and leg motor mass therefore inherently sets a timing which the hip spring must adhere to. This coordination evidently leads to non-ideal hip motion, driving up hip costs. The series leg series hip configuration has lower damping losses than the series leg and parallel hip configuration at high velocities. Despite this, the lower negative motor work at high velocities required for the latter configuration drives down its overall cost.

In this work, we simultaneously consider a wide variety of parameters and constraints in a single optimization. This wide-ranging study comes at the expense of a detailed understanding of the fundamental effects of these design choices. As changing the parameters simultaneously influences the *natural dynamics* of the system, as well as the constraints, it is nearly impossible to extricate the effect of any one change on the system. For example, changing the no load speed in the hip motor will change the reflected motor inertia (Eqn. 4.6), which will in turn affect the motor dynamics for both PEA and SEA, collision losses for PEAs, and the ability to store energy in the motor for SEAs. Additionally, changing the no load speed changes the torque and velocity limits of the motors (Eqns. 4.10,4.11), directly affecting the constraints and limiting the possible motion. Every parameter changes the natural dynamics while simultaneously curtailing them (either by affecting the robots interaction with the constraints or the constraints directly).

While a fundamental understanding of the effect of PEA and SEA on two-dimensional legged locomotion is valuable and necessary, it was not our goal here. Instead, we showed that a complex and realistic design question for future hardware can be answered using optimal control. Despite the interplay of complicated motion and mor-

phology, our optimization methodology was able to give insight into the best design choices.

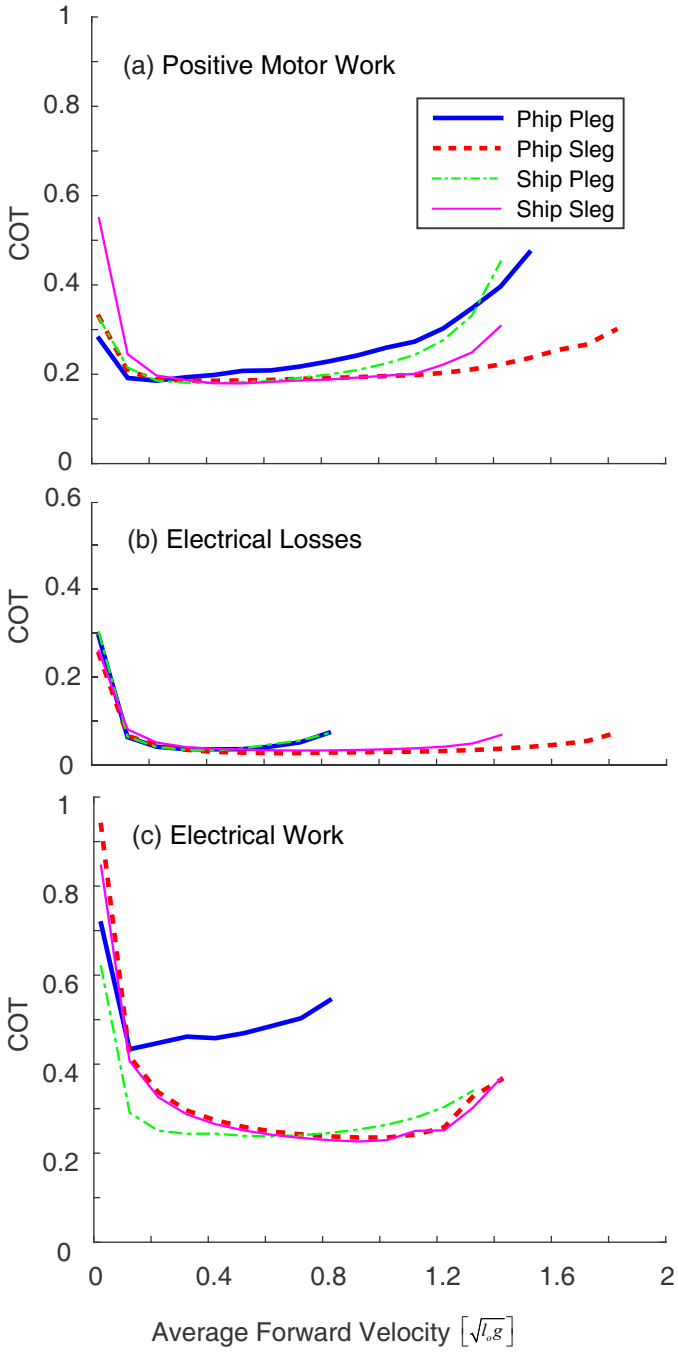

Figure 4.2: A comparison of cost values for each actuator configuration. For the positive motor work and electrical loss COTs, the parallel hip and series leg configuration is energetically optimal. This configuration has the lowest cost throughout much of the velocity range. It also has the most solutions, indicating that it is able to meet realistic motor constraints at the most velocities. For the positive electrical work COT, there is no clear consensus on the optimal configuration. Series hip and parallel leg is optimal at low velocities, and both series hip series leg and parallel hip series leg are optimal at high velocities.

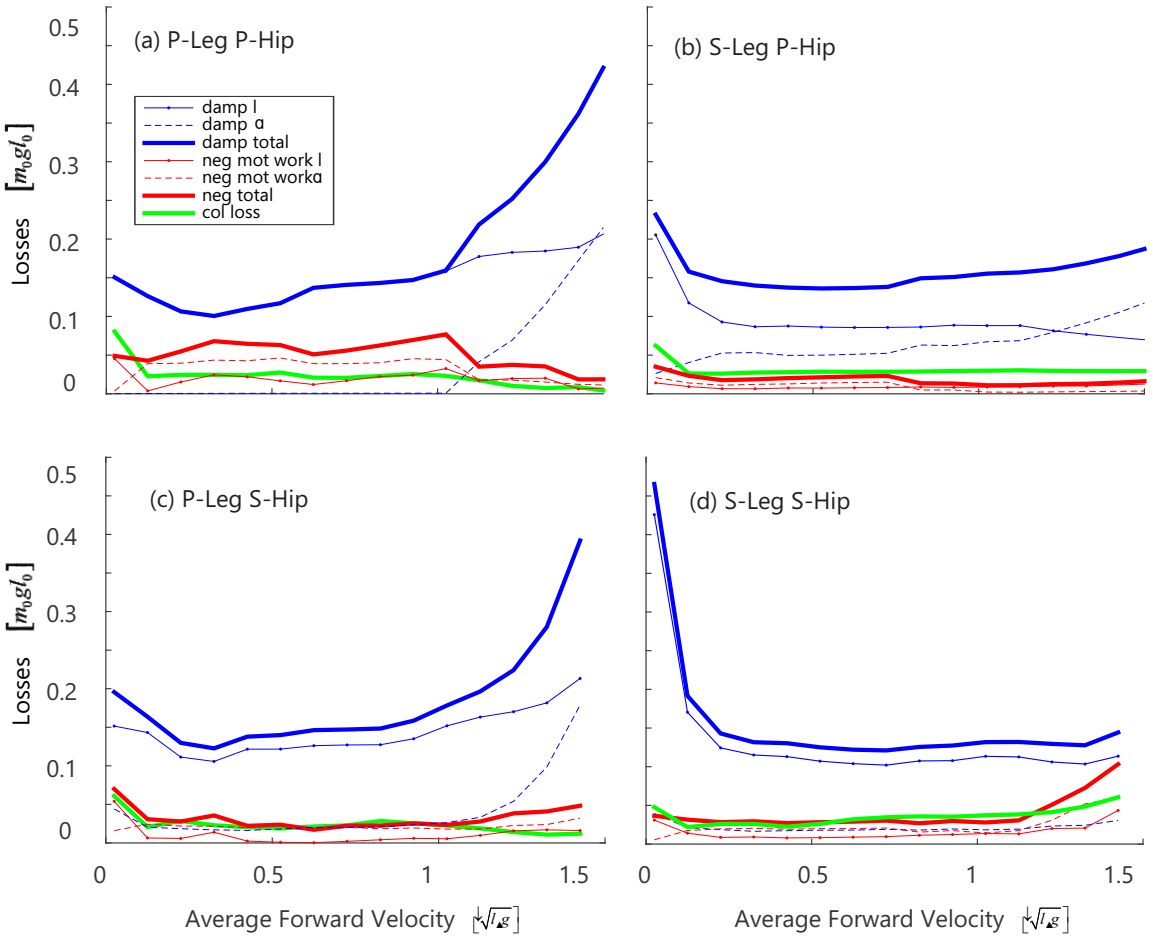

Figure 4.3: The sources of losses for the positive motor work COT of all actuator configurations. The losses can come from damping in the leg and hip springs, negative motor work in the leg and hip motors, and collision losses. The losses primarily come from damping. Collision losses are generally small in comparison. The influence of negative motor work varies among the configurations.

CHAPTER V

Spine Morphology and Energetics: How Principles From Nature Apply to Robotics

5.1 Introduction

[1] Being able to move in an energetically economical fashion is an important requirement for robots and animals alike [57, 126, 29, 105, 25, 123, 8, 130]. In nature, energy in the form of food can be a scarce resource. Especially for cursorial animals, this creates a strong incentive to locomote in an efficient manner. Similar constraints apply to robots. Once they have been deployed for a mission in the field, autonomous robots typically do not have many opportunities to recharge their batteries. At the same time, such robots – and in particular legged robots – have only a limited capacity to carry batteries and other fuel sources. To achieve truly autonomous operation, conserving energy is imperative.

It has been shown that legged animals can achieve this economical motion partly by moving in ways that are effectively tuned to their natural mechanical dynamics [79, 28, 38, 22]. That is, animals and humans take advantage of movement that arises through the passive interplay of gravity, ground contact forces, the elasticity in their muscles and tendons, and the mechanical inertia in their body segments. Using these natural dynamic motions allows them to store and recover mechanical energy and reduce the active work done by their muscles. Animals exploit, for example, the mechanical dynamics of an inverted pendulum as they walk with relatively straight legs [22]. When humans switch to running, they utilize the compliance in their tendons and muscles to store energy elastically while using a motion that exploits the mechanical dynamics of a spring loaded inverted pendulum [15]. Over the past years, these concepts have been steadily adapted into the world of legged robotics [108], and

[1] This chapter has been previously published in Bioinspiration & Biomimetics [135]

a number of robotic prototypes have been built that seek to take advantage of similar natural mechanical dynamics to achieve economical locomotion [58, 107, 46, 83, 13].

This exploitation of the natural mechanical dynamics has interesting implications for the design of robotic systems. The desire to move economically inherently couples the motion of a legged system to its morphology: the mechanical dynamics that a legged system exhibits are a direct consequence of the way it is built and these dynamics, in turn, dominate the way that an animal or robot should move in order to be economical. In this chapter, we investigate a particular aspect of morphology and its potential usefulness in robotics: the articulation in the spine of quadrupeds.

In nature, the advantages of an articulated spine seem to be closely coupled to the choice of gait. At lower speeds, quadrupedal mammals generally utilize symmetrical gaits, in which the legs on the left side perform exactly the same motion as the legs on the right, just 180° out of phase. At higher speeds, they tend to transition to asymmetrical gaits, in which the two sides of the animal perform different motions and/or the phase shift differs from 180° [5]. Animals primarily utilize the articulation in their spine for these high speed asymmetrical gaits [3], whereas less spine motion can be observed in the symmetrical gaits [5]. This is an important observation and any investigation of the usefulness of an articulated spine in legged robots should thus incorporate the question of gait as a key factor in its analysis.

It has been argued that, with an asymmetrical gait, an articulated spine provides a number of dynamical benefits for animals with regard to *leg recirculation*, *elastic energy storage*, and *stride length*. In particular, [50] pointed out that the articulation in the spine allows for faster recirculation of the legs. That is, the spinal rotation that is added in series to the flexion and extension of the hip and shoulder joints, enables a faster motion of the legs during swing. He further hypothesized that these additional degrees of freedom allow for longer stride lengths, attributing to a cheetah's high maximum speed [51]. [5] built upon Hildebrand's hypothesis when examining various models of quadrupedal animals and suggested that muscles and tendons in the articulation of the spine might act as additional elastic elements to store and release energy.

A number of studies have tried to assess the potential benefits of an articulated spine by performing comparative studies among quadrupedal models. [136], for example, developed a pneumatic-driven robotic quadruped with a rigid, passive, and active spine configuration. Using a step-function control pattern to achieve a bounding gait, they found that when the spinal motions are synchronized with leg movements, the extension and flexion of the active spine allows the robot to reach higher speeds. [66]

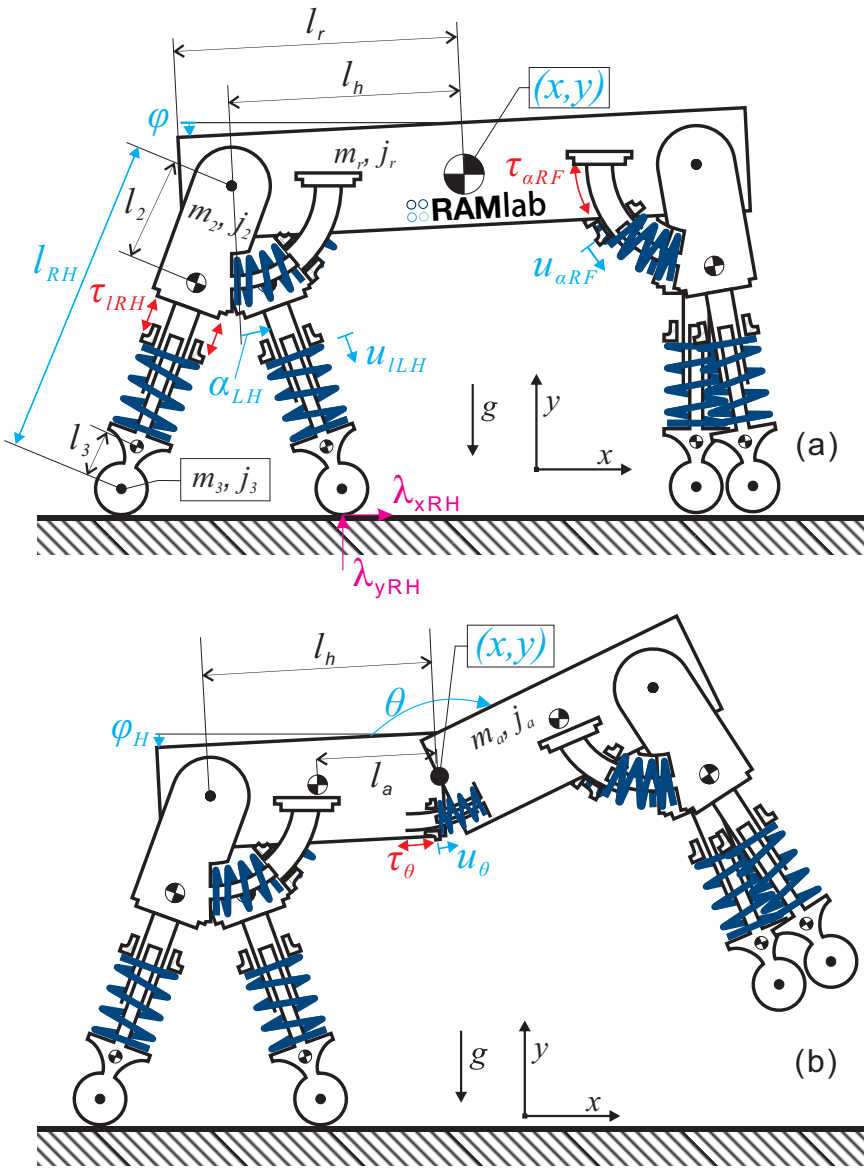

Figure 5.1: In this work, we investigate the benefits of an articulated spine for the use in quadrupedal robots. We base our comparison on two physics based models: one with a rigid main body (a) and one with an articulated main body (b). Both model instances have four distinct legs and incorporate complexities such as mass and inertia in all body segments, detailed motor models with limits on available torque and speed, as well as series elastic actuators. To ensure that we are making a fair comparison, we use optimal control to find the most energetically economical joint trajectories, actuator inputs, and footfall timing for each model across a broad range of gaits and locomotion velocities.

used a central pattern generator controller to obtain bounding gaits for a robotic simulation comparing rigid, passive articulated, and active articulated spinal config-

urations. They found that bounding with a series elastic actuated spine performed better than an articulated passive spine and rigid spine in terms of bounding power consumption. [49] compared two 2-dimensional quadrupedal bounding models, one with an articulated spine modeled as 6 rigid segments and one with a rigid spine modeled as 5 rigid segments. With these models, Haueisen analyzed the effects of speed and stride frequency on the energy requirements of both models for the bounding gait. She found that, during bounding, the articulated model utilized its articulated spinal joint in similar ways to that observed in nature and also found energetic benefits at higher speeds. Using optimal control, [21] found that, at sufficiently high speeds, an articulated model of a bounding quadruped was more economical than a rigid model. All of these prior comparative simulation studies considered simplified quadrupedal models that represented a two-legged planar bounding robot. The comparison of the two morphologies has also been explored for bounding in hardware [70], where, in contrast to the above studies, they did not observe an energetic improvement for the flexible spine.

To extend these comparison studies beyond bounding, in this work, our model incorporates four independent legs. This design choice allows us to explore the effect of an articulated spine over the full range of quadrupedal gaits found in nature. This is an important extension, as bounding rarely appears as the gait of choice [4], while other gaits such as walking, trotting, tölting, and galloping are employed by a significant number of quadrupeds of all sizes [11]. Furthermore, our prior work has shown that bounding was never the most economical gait for robots [130]. In addition to the four legs, our model incorporates complexities such as feet with mass, inertia in the legs and torso, detailed motor models with realistic limitations on torque and speed, as well as series elastic springs with damping that generate the rich natural mechanical dynamics necessary for efficient locomotion. These complexities allow for physically realistic motions across a wide range of velocities and gaits.

Utilizing this model, in this chapter we investigate whether and how the benefits of an articulated spine translate from nature into the world of robotics. We consider the choice of gait and investigate the three mechanical mechanisms stated above. Our tool of choice for this investigation is physics based simulation which we use to compare two model instances – one with and one without an articulated spine. The coupling of motion and morphology poses a particular challenge in this context: in order to optimally exploit their respective natural dynamics, each of the two morphologies will require distinctly different actuation patterns and joint movements to move forward in an economical fashion. Using the same control strategy for both morphologies

would implicitly bias the comparison to favor one or the other. To overcome this issue, we let a numerical optimizer find the best possible joint trajectories, actuator inputs, and footfall timing to minimize the energetic cost of locomotion. By doing this individually for each morphology, we effectively remove the question of control from the comparison. This approach reduces the investigation of the benefits of an articulated spine solely to the mechanical differences between the two model instances. In the process, we create a causal relationship between morphology and performance. In addition to understanding the potential benefits of an articulated spine for robots, this approach also allows us to add new insight into the hypotheses put forth by Hildebrand and Alexander [50, 51, 5].

The dimensions and parameters of our model are roughly based off the quadrupedal robot, Starl*ETH* [61, 112], and are similar to the models used in our previous studies on robotic gait selection [130, 129]. We created two model instances: one with a rigid main body and one with an articulated main body composed of two rigid segments connected by a rotational joint (Fig. 5.1). Similar to our previous work [130], we used optimal control to generate an energy cost landscape as a function of speed, using positive mechanical motor work normalized per distance traveled as the cost function. This was done for both model instances across a broad range of different gaits to allow for a fair comparison of the two morphological instances.

5.2 Methods

In this study, we compare two different instances of a physics-based model of a quadrupedal legged robot: one with a rigid spine (Fig. 5.1a) and one with an articulated spine (Fig. 5.1b). We employ optimal control to identify the most economical motion for each of the two instances across a wide range of locomotion speeds and gaits, generating a lower bound on the energetic cost of locomotion. As the model and optimization methods used in this study are similar to the ones used in our previous work [130], we restate them only briefly while focusing on the aspects most critical to the comparison of the rigid vs. articulated spine.

5.2.1 Model

The model is planar and consists of a main body and four individual legs with index $i \in \{LH, LF, RF, RH\}$ (labeled as left L, right R, hind H, and front F). Its geometrical dimensions are shown in Figure 5.1. The individual segments of the model all have distributed masses with associated inertias. Each leg consists of an upper

(m_2, j_2) and lower (m_3, j_3) segment that are connected with a prismatic joint that yields a variable leg length of l_i. The upper leg segments are attached to a main body at hip/shoulder joints (with joint angles α_i) at a distance l_r from the center of mass (COM). The main body is either a single rigid segment with mass m_r and inertia j_r or – in the case of the articulated spine – consists of two identical segments of half the size with mass $m_a = \frac{1}{2}m_r$ and inertia $j_a = \frac{1}{8}j_r$. These two segments are connected with a rotational joint with joint angle θ. The COM of each segment is a distance l_a from this rotational joint. The position of the center of the main body is given by horizontal and vertical positions x and y, and by the orientation of the main body φ. For the articulated model, we use the orientation of the hind segment φ_H for the same purpose.

There are three different joint types with index $p \in \{l, \alpha, \theta\}$ for leg extension, hip rotation, and spine rotation. All actuators are modelled as Series Elastic Actuators (SEAs) [100], as they were used in our existing robotic hardware [63, 62]. Comparable to ligaments in nature, the series springs give the robot the opportunity to elastically store and release energy in all joints. Each joint is therefore modelled to consist of a spring with stiffness k_p and damping coefficient b_p that connects to the joint at its distal end while its proximal end is connected to an electrical DC motor and gearbox with reflected inertia $j_{\mathrm{ref},p}$. For leg extension, this gearbox also converts the motor rotation into a linear motion.

For clarity, we will omit the indices i and p in the following description of the actuators. The position of an actuator (after the gearbox) is given by u and its speed by $\dot{u}$. The torque after the gearbox is given by T

In the SEAs, the joint torques/forces F are ultimately produced by the springs according to:

$$\begin{aligned} \mathbf{F}_l &= k_l \left(l_o + \mathbf{u}_l - \mathbf{l}\right) + b_l \left(\dot{\mathbf{u}}_l - \dot{\mathbf{l}}\right) && (5.1) \\ \mathbf{F}_\alpha &= k_\alpha \left(\mathbf{u}_\alpha - \boldsymbol{\alpha}\right) + b_\alpha \left(\dot{\mathbf{u}}_\alpha - \dot{\boldsymbol{\alpha}}\right) && (5.2) \\ F_\theta &= k_\theta \left(u_\theta - \theta\right) + b_\theta \left(\dot{u}_\theta - \dot{\theta}\right). \end{aligned}$$

With this, the generalized coordinate vector is given by

$$\mathbf{q} = \left(x,\ y,\ \varphi,\ \boldsymbol{\alpha},\ \mathbf{l},\ \mathbf{u}_\alpha,\ \mathbf{u}_l\right)^T \tag{5.3}$$

for the rigid model and by

$$\mathbf{q} = \left(x,\ y,\ \varphi_H,\ \theta,\ \boldsymbol{\alpha},\ \mathbf{l},\ \mathbf{u}_\alpha,\ \mathbf{u}_l,\ u_\theta\right)^T \tag{5.4}$$

Table 5.1: List of all model parameters. Values are expressed with respect to total mass m_o, leg length l_o, and gravity g.

Common Properties:

$m_2 = 0.05\ m_o$	$m_3 = 0.025\ m_o$	$j_2 = 0.001\, m_o l_o^2$
$b_l = 0.14\, m_o\sqrt{g/l_o}$	$j_{\mathrm{ref},l} = 1.796\, m_o$	$b_\alpha = 0.09\, m_o\sqrt{g/l_o}$
$l_2 = 0.25\ l_o$	$j_{\mathrm{ref},\alpha} = 0.449\, m_o l_o^2$	$r_{foot} = 0.05\ l_o$
$l_3 = 0.25\ l_o$	$k_\alpha = 2.5\, m_o g l_o/\mathrm{rad}$	$u_{\mathrm{max},\alpha} = 0.79\,\mathrm{rad}$
$T_{\mathrm{max},l} = 1.360\, m_o g$	$T_{\mathrm{max},\alpha} = 0.680\, m_o g l_o$	$\dot{u}_{\mathrm{max},\alpha} = 8.49\,\mathrm{rad}\sqrt{g/l_o}$
$j_3 = 0.001\, m_o l_o^2$	$l_h = 0.75\ l_o$	$k_l = 5.0\, m_o g/l_o$
$u_{\mathrm{max},l} = 0.15\,\mathrm{l_o}$	$\dot{u}_{\mathrm{max},l} = 4.24\,\sqrt{g l_o}$	

Rigid Model:

$m_r = 0.7\ m_o$	$j_r = 0.2\ m_o l_o^2$	$l_r = 0.93$

Articulated Model:

$m_a = 0.35\ m_o$	$j_a = 0.025\ m_o l_o^2$	$u_{max,\theta} = 1.57\,\mathrm{rad}$
$T_{\mathrm{max},\theta} = 0.680\, m_o g l_o$	$b_\theta = 0.24\, m_o\sqrt{g/l_o}$	$\dot{u}_{\mathrm{max},\theta} = 8.49\,\mathrm{rad}\sqrt{g/l_o}$
$j_{\mathrm{ref},\theta} = 0.449\, m_o l_o^2$	$k_\theta = 5\ m_o g l_o/\mathrm{rad}$	$l_a = 0.5 l_r$

for the articulated model. The vector of generalized torques is given by

$$\boldsymbol{\tau} = (0,\ 0,\ 0,\ \mathbf{F}_\alpha,\ \mathbf{F}_l, \mathbf{T}_\alpha - \mathbf{F}_\alpha,\ \mathbf{T}_l - \mathbf{F}_l)^T \tag{5.5}$$

and

$$\boldsymbol{\tau} = (0,\ 0,\ 0,\ F_\theta,\ \mathbf{F}_\alpha,\ \mathbf{F}_l,\ \mathbf{T}_\alpha - \mathbf{F}_\alpha,\ \mathbf{T}_l - \mathbf{F}_l,\ T_\theta - F_\theta)^T \tag{5.6}$$

, respectively.

All model parameters are provided in Table 5.1. The parameters used, including mass, inertia, length, and spring stiffness, are based on our existing hardware [62]. This also holds for the motor/gearbox parameters, such as the reflected inertia j_{ref}, the maximum output torque T_{max} limitation, and the speed limitation $\dot{u}_{\mathrm{max}}$. To reduce the number of free parameters, all values have been normalized with respect to total mass m_o, uncompressed leg length l_o, and gravity g.

The equations of motion (EOMs) for this model are stated in a floating base description using additional contact constraints (as described in detail in [108]). They

are expressed as a differential algebraic equation:

$$\mathbf{M}(\mathbf{q})\,\ddot{\mathbf{q}} = \mathbf{h}(\mathbf{q},\dot{\mathbf{q}}) + \boldsymbol{\tau} + \mathbf{J}_c^T(\mathbf{q})\,\boldsymbol{\lambda} \tag{5.7}$$

$$\boldsymbol{\phi}_c(\mathbf{q}) = \mathbf{0}, \tag{5.8}$$

with the mass matrix $\mathbf{M}$, the differentiable force vector $\mathbf{h}$, and the generalized torque vector $\boldsymbol{\tau}$. The algebraic function $\boldsymbol{\phi}_c(\mathbf{q})$ encodes the currently active contact constraints. It ensures that all the feet that are in contact with the ground do not slide or penetrate into the ground. The partial derivative of this function yields the contact Jacobian $\mathbf{J}_c = \partial\boldsymbol{\phi}_c/\partial\mathbf{q}$ whose transpose maps a vector of contact forces $\boldsymbol{\lambda}$ into the generalized coordinate space.

The sequence of footfalls that happens during locomotion breaks the simulation into individual phases (with index c) and each phase uses a different contact constraint function $\boldsymbol{\phi}_c$. At the end of each phase c (at time t_c) a specific number of feet must get in contact with the ground or leave the ground in order to transition into the next phase $c+1$. This requirement is encoded by an event function $\boldsymbol{\psi}_c$ that is evaluated at time t_c:

$$\boldsymbol{\psi}_c(t_c) = \mathbf{0}. \tag{5.9}$$

Furthermore, at the end of each phase, a collision might happen and velocities change instantaneously to match the new contact constraints $\boldsymbol{\phi}_{c+1}$. This instantaneous change in speed can be computed from:

$$\mathbf{M}\left(\dot{\mathbf{q}}^+(t_c) - \dot{\mathbf{q}}^-(t_c)\right) = \mathbf{J}_{c+1}^T\boldsymbol{\Lambda}_c \tag{5.10}$$

$$\mathbf{J}_{c+1}\dot{\mathbf{q}}^+(t_c) = \mathbf{0} \tag{5.11}$$

with $\boldsymbol{\Lambda}_c$ being the vector of impulses associated with the collision. Matlab functions to calculate $\boldsymbol{\phi}_c$, $\mathbf{M}$, $\mathbf{J}_c$, and $\mathbf{h}$ from Eqns. (5.7) and (5.8) are supplied in the supplemental files.

By prescribing a particular sequence of functions $\boldsymbol{\phi}_c$ and $\boldsymbol{\psi}_c$, we determine the gait of the model. The timing of events $\mathbf{t} \in \{t_o,\ ,\cdots,\ t_c,\ \cdots,\ t_{end}\}$ is left open. With this, we enforced eight different footfall patterns which can be broadly classified into a set of symmetrical and asymmetrical gaits (footfall patterns shown in Fig. 5.2). Symmetrical gaits are those "in which the left and right feet of each pair have equal duty factors and relative phases differing by 0.5" [4]. Equivalently, for these gaits, we only simulate half the stride and mirror it to obtain the second half. Asymmetrical gaits are those that do not meet these criteria. The symmetrical gaits we investigate

are four-beat walking, two-beat walking, tölting, and trotting. The asymmetrical gaits we investigate are bounding, grounded bounding, galloping, and gallop bounding. The majority of these gaits were chosen based off of our previous work [130]. Grounded bounding and gallop bounding were included because at high speeds, the optimizer chose phase durations within bounding and galloping that approached these gaits.

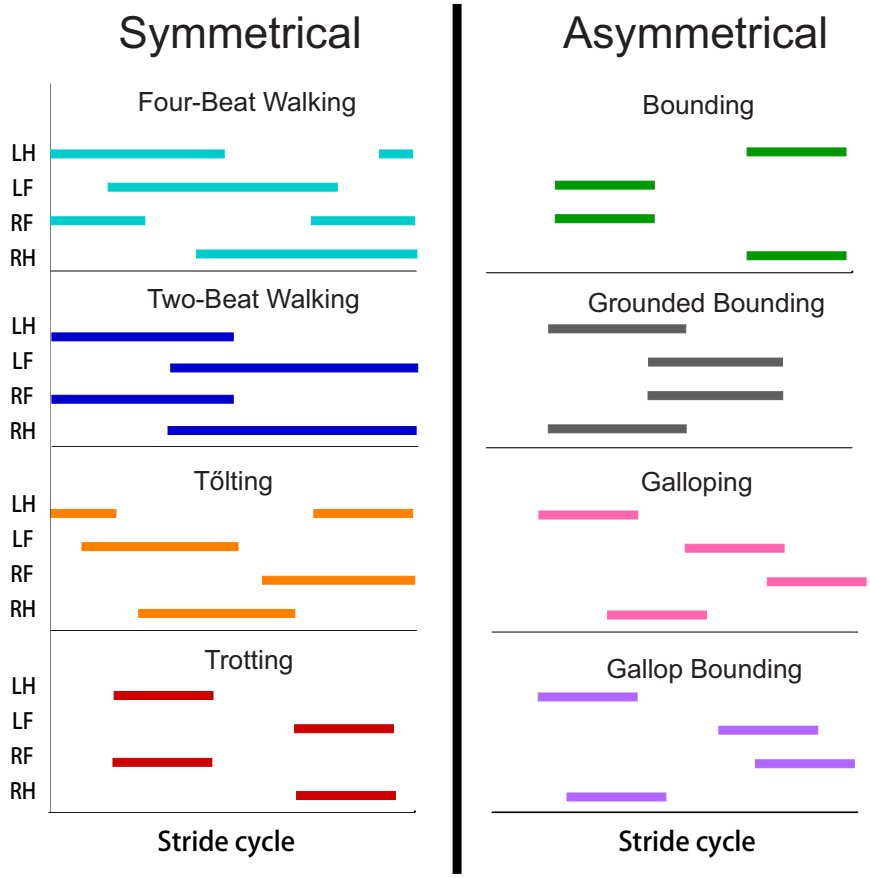

Figure 5.2: We explored four symmetrical and four asymmetrical gaits, whose footfall patterns are shown in this figure. The colored bars indicate when each leg is in stance (LH: left hind, LF: left front, RF: right front, RH: right hind). While the footfall sequence was fixed, the duration of each phase of the gait, as well as the total stride duration was chosen by the optimizer. The terms two-beat walking, grounded bounding, and gallop bounding were devised by the authors to clearly distinguish these gaits from trotting, bounding, and galloping. Since the models are planar, left and right legs are interchangeable, and some gaits could thus be omitted in our analysis. Pacing, for example, would be indistinguishable from trotting and was hence not considered.

5.2.2 Optimization

To compare the energetic economy of both model instances we considered the positive motor work cost of transport (COT). To this end, the positive motor work is computed as the integral of positive mechanical power summed over all motors over the duration of the stride and normalized by total mass and distance traveled:

$$\mathrm{COT} = \frac{\int_{t_0}^{t_{end}} \sum_{i,p} \max\left(T_{i,p} \cdot \dot{u}_{i,p}, 0\right) dt}{m_o g \left(x(t_{end}) - x(t_0)\right)}. \tag{5.12}$$

To improve the numerical behavior, we approximated the discontinuity in the cost function by smoothing the max(value, 0) function using the equation:

$$\max(s, 0) \approx \sigma \log\left(1 + e^{\frac{s}{\sigma}}\right) \tag{5.13}$$

with $\sigma = 1e - 5$.

With this, we can set up the search for the optimal motion to be a constrained optimization problem, in which we identify optimal joint trajectories $\mathbf{q}(t)$, torque inputs $\mathbf{T}(t)$, and event times $\mathbf{t}$:

$$\min \quad \mathrm{COT}\left(\mathbf{q}(t), \mathbf{T}(t), \mathbf{t}\right) \tag{5.14}$$

subject to the following constraints:

- The trajectories $\mathbf{q}(t)$ and $\mathbf{T}(t)$ comply with the dynamics defined in eqs. (5.7) & (5.8).
- For each phase c, it holds:
  - $t_c > t_{c-1}$.
  - The event is triggered at the end of the phase according to eq. (5.9).
  - Velocities $\dot{\mathbf{q}}$ change at the end of each phase as defined by eq. (5.10) & (5.11).
- The motion is periodic; i.e., $\mathbf{q}(t_o) = \mathbf{q}(t_{end})$ and $\dot{\mathbf{q}}(t_o) = \dot{\mathbf{q}}(t_{end})$
- Motor torques, speed, and positions are within the given limits for all joints i and p:
  - $-T_{\max,p} < T_{i,p}(t) < T_{\max,p}$.
  - $-\dot{u}_{\max,p} < \dot{u}_{i,p}(t) < \dot{u}_{\max,p}$.
  - $-u_{\max,p} < u_{i,p}(t) < u_{\max,p}$.

Table 5.2: Change in spinal angle at a speed of $1.0\sqrt{l_o g}$.

Gait	$\Delta\theta$
Four-Beat Walking	8.04 °
Two-Beat Walking	4.14 °
Tölting	7.83 °
Trotting	5.20 °
Bounding	51.5 °
Grounded Bounding	56.4 °
Galloping	22.4 °
Gallop-Bounding	112.7 °

- Vertical foot positions are non-negative, $\mathbf{y}_{foot} \geq \mathbf{0}$.

This constrained optimization problem was solved through a multiple shooting optimization framework (MUSCOD) ([30]) with methods illustrated and detailed in [130]. We examined locomotion velocities between 0.025 $\sqrt{l_0 g}$ and 4.5 $\sqrt{l_0 g}$. For each gait, we conducted an initial optimization at an initial speed and iteratively conducted optimizations at neighboring velocities in a branching method until the full range of velocities was covered or no solutions could be found. In this process, we used previously obtained solutions as the initial conditions of the neighboring velocities. At each particular speed, the solution with the lowest cost was taken as the optimal motion and re-used for re-initialization. This procedure was repeated from a variety of initial seeds to avoid local optima.

5.3 Results

On average, the optimization of a single gait at a particular speed converged in about 5 minutes on one core of a 2.40 GHz processor. The time it took to process a given gait over the entire range of velocities varied largely. Depending on how well neighboring data points could be used for seeding new runs and on how many data points were recomputed, it took between 2 (trotting) and 28 (gallop-bounding) days to process a gait with the chosen speed resolution.

We found that the articulation in the spine has been used primarily in the asymmetrical gaits. The optimal solutions for the bounding and galloping gaits had large joint motion in the spine, while the spinal joint underwent relatively small deflections over the course of a stride for symmetrical gaits (Table 5.2). An exemplary motion (galloping at $2.9\sqrt{l_o g}$) is shown for both model instances in Figure 5.3. More repre-

Table 5.3: Speed range.

Gait	**Lowest Speed**($\sqrt{l_o g}$) Min Speed in Search: 0.025		**Highest Speed**($\sqrt{l_o g}$) Max Speed in Search: 4.500	
	Rigid	Articulated	Rigid	Articulated
Four-Beat Walking	0.025	0.081	1.644	1.925
Two-Beat Walking	0.025	0.025	1.413	1.569
Tölting	0.025	0.025	3.394	3.556
Trotting	0.025	0.025	3.294	3.306
Bounding	0.031	0.025	2.994	4.500
Grounded Bounding	0.075	0.131	4.156	4.500
Galloping	0.094	0.106	3.338	4.500
Gallop Bounding	0.106	0.338	3.469	4.500

sentative motions for each gait and model can be found in the supplementary videos. The resulting cost landscapes are shown in Fig. 5.4. Table 5.3 lists the minimal and

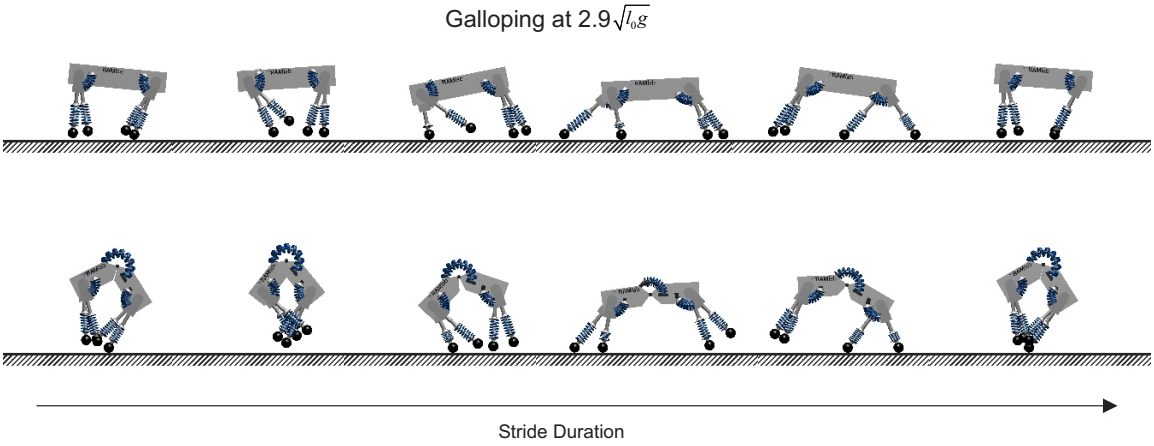

Figure 5.3: Video stills of an animation of a full stride of galloping at a speed of $2.9\sqrt{l_o g}$. It is evident that the spinal joint is being used heavily in the articulated model (bottom sequence).

maximal speeds for which a solution for each gait was found for each model instance. Table 5.4 lists the average changes in energetic cost and stride length between the two model instances. These averages were computed over the range of speeds at which solutions were found for both model instances and tested for statistical significance.

Among the symmetrical gaits, only four-beat walking showed a significant difference ($p < 0.05$) between the rigid and articulated models in terms of energetics. Walking with an articulated spine increased energy consumption by 31.8 %. All other symmetrical gaits had comparable energetic costs between the rigid and articulated models. Maximal speeds were constrained by the available torque and force capability

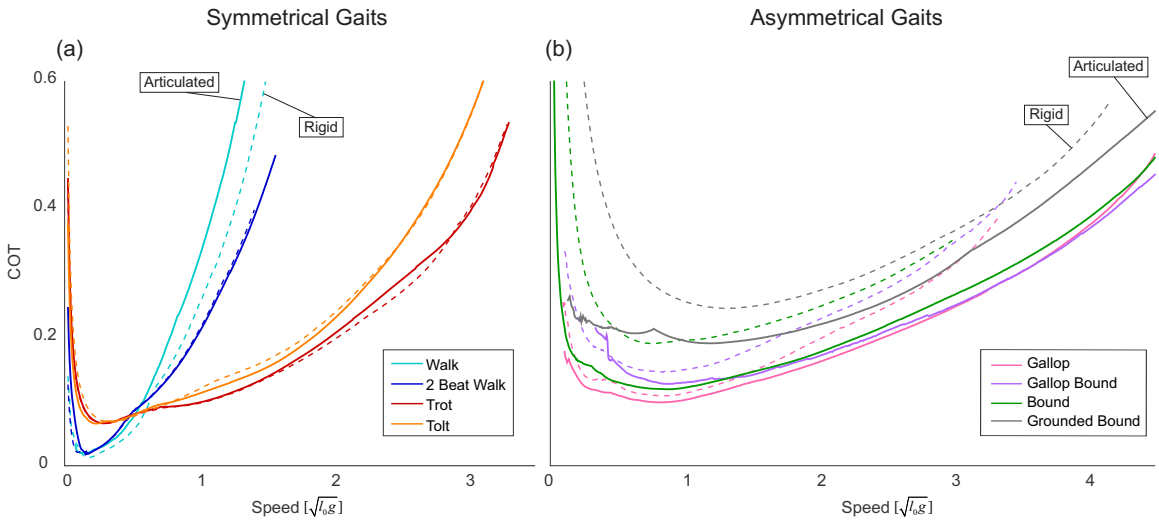

Figure 5.4: The positive mechanical work cost of transport is shown as a function of forward speed for all gaits that we explored. Solutions for the rigid spine model are presented as dotted lines, and solutions for the articulated spine model as solid lines. For symmetrical gaits, the two models have similar costs (a). For asymmetrical gaits, the articulated model instance has improved energetics and solutions extending to higher speeds.

in the motors. For all symmetrical gaits, the highest speed at which solutions were found was slightly higher for the model instance with the articulated spine.

The benefit of the articulated spine was clearly visible for the asymmetrical gaits, in which the articulation led to improved energetic economy and higher maximal speeds. Table 5.4 shows that the articulated model was significantly more economical than the rigid model for all asymmetrical gaits. Furthermore, for all asymmetrical gaits on the articulated model, we found solutions all the way to the upper bound of the speed range that we investigated (Table 5.3). For the rigid model, in contrast, the maximal speed was constrained to lower values ($<4.2\sqrt{l_o g}$) for all gaits, as the motors ran into torque limits. These torque limits were usually reached by the leg extension motors during the stance phase and by the hip motors during the swing phase preempting a particular leg's stance phase. Motor speed limits were generally not reached.

Confirming the results from our previous work [130], the combined cost landscapes showed that minimizing energy cost required switching from gait to gait as speed varies (Fig. 5.5). This choice of gait was slightly different for the two model instances. The rigid instance went from four-beat walking at low speeds, to trotting at intermediate speeds, to galloping at high speeds, to grounded bounding at the highest

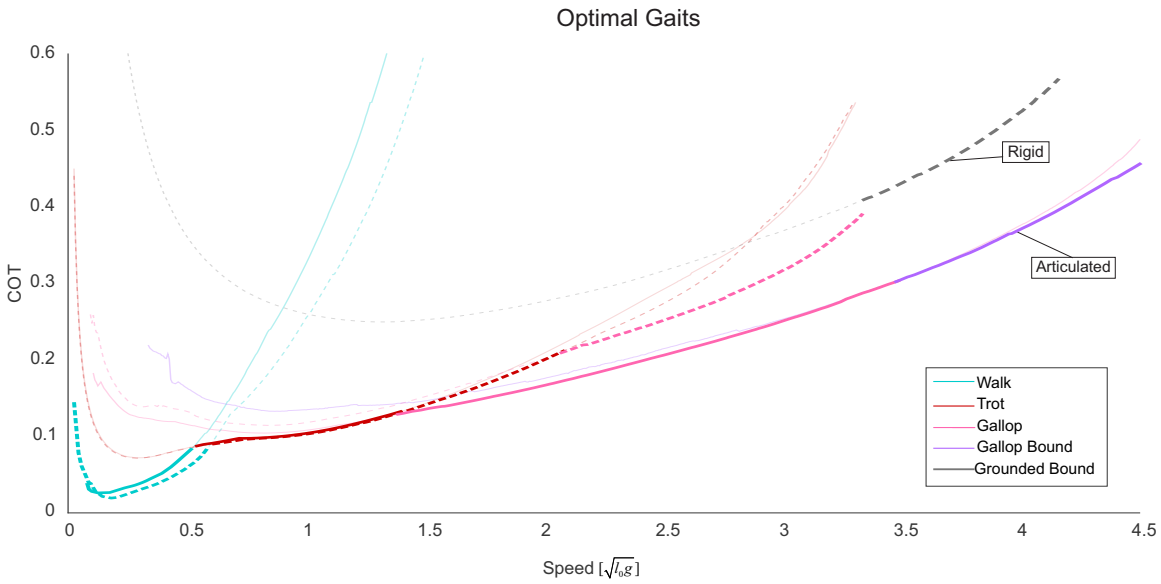

Figure 5.5: The optimal gait choice for each model instance is shown as a function of forward speed. Rigid solutions are presented as dotted lines, and articulated solutions are shown as solid lines. For clarity, the most economical gait choice at each speed is highlighted. At low speeds, where walking and trotting are the most energetically favorable gaits, the two model instances have similar costs. At higher speeds, where galloping, gallop-bounding, and grounded bounding are the most energetically favorable gaits, the articulated model instance has a much lower COT.

speeds. The articulated instance had the same gait sequence at low, intermediate, and high speeds, but transitioned to gallop bounding at the highest speeds. The biggest difference between the two model instances was observed for the transition speed between trotting and galloping. In particular, the results of the rigid (articulated) model instance indicated a transition from four-beat walking to trotting at a speed of $0.60\sqrt{l_o g}$ ($0.53\sqrt{l_o g}$) and from trotting to galloping at a speed of $2.05\sqrt{l_o g}$ ($1.28\sqrt{l_o g}$). The rigid instance transitioned from galloping to grounded bounding at a speed of $3.34\sqrt{l_o g}$ and the articulated instance transitioned from galloping to gallop bounding at a speed of $3.63\sqrt{l_o g}$.

To further investigate the source of the energetic improvements, we focused on the energetic breakdown for galloping (Fig. 5.6). Similar results were observed for the other asymmetrical gaits. At a speed of $3.34\sqrt{l_o g}$, the maximum speed at which we were able to find a rigid galloping solution, the rigid model had a mechanical COT of 0.390 and the articulated model had a COT of 0.284 (Note that the COT, which represents the energy consumed divided by the robot weight and distance traveled (Sec. 5.2.2), is a unitless quantity). For both models, collisions were the smallest

Table 5.4: Difference in COT and difference in stride-length for each investigated gait. p-values are based on a two-sample t-test.

Gait	**Mean COT Diff.**		**Mean Stride Length Diff.**	
	From Rigid	p-value	l_o From Rigid	p-value
Four-Beat Walking	0.078	< 0.001	0.257	< 0.001
Two-Beat Walking	0.001	0.895	-0.007	0.862
Tölting	-0.012	0.320	0.157	0.072
Trotting	0.004	0.578	0.110	0.386
Bounding	-0.106	< 0.001	0.464	< 0.001
Grounded Bounding	-0.034	< 0.001	0.316	< 0.001
Gallop Bounding	-0.054	< 0.001	1.413	< 0.001

source of losses. At this speed, collision losses accounted for 0.041 of the losses for the rigid model, and for 0.034 of the losses for the articulated model. Damping losses contributed approximately equally to the COT for both models: 0.187 for the rigid model and 0.182 for the articulated model. With these losses being similar, the difference in energetic cost was thus driven primarily by negative motor work. Starting at a speed of around $1.5\sqrt{l_o g}$, the negative motor work in the rigid model instance increased relative to the articulated model instance, coinciding directly with the worsened energetic economy of rigid galloping. At a speed of $3.34\sqrt{l_o g}$, for the rigid model, negative work accounted for a partial COT of 0.162 and for the articulated model for a partial COT of 0.068.

The primary source of this increased negative motor work were the hip motors used in *leg recirculation* (Fig. 5.7). At a speed of $3.34\sqrt{l_o g}$, the hips performed 0.154 of the total negative motor work for the rigid model, while only performing 0.033 of the total negative motor work for the articulated model. At that same speed, the legs performed 0.008 of the total negative motor work for the rigid instance and 0.007 of the total negative motor work for the articulated instance. For the articulated model, the motor at the spine performed 0.028 of the total negative work.

For asymmetrical gaits, the articulated model used the spinal joint to perform significant amounts of positive work. Table 5.5 shows the breakdown of positive work performed by the spinal joint for each asymmetrical gait at its maximum speed. It shows the total positive work done by the spinal joint, the portion done actively by the motor, the portion performed passively by the spring, and the portion done by the reflected motor inertia. Note that because the quadrupedal model is not energetically conservative, the value for the joint is less than the sum of the motor, spring, and inertia contributions. The spring performs a relatively small proportion of the positive

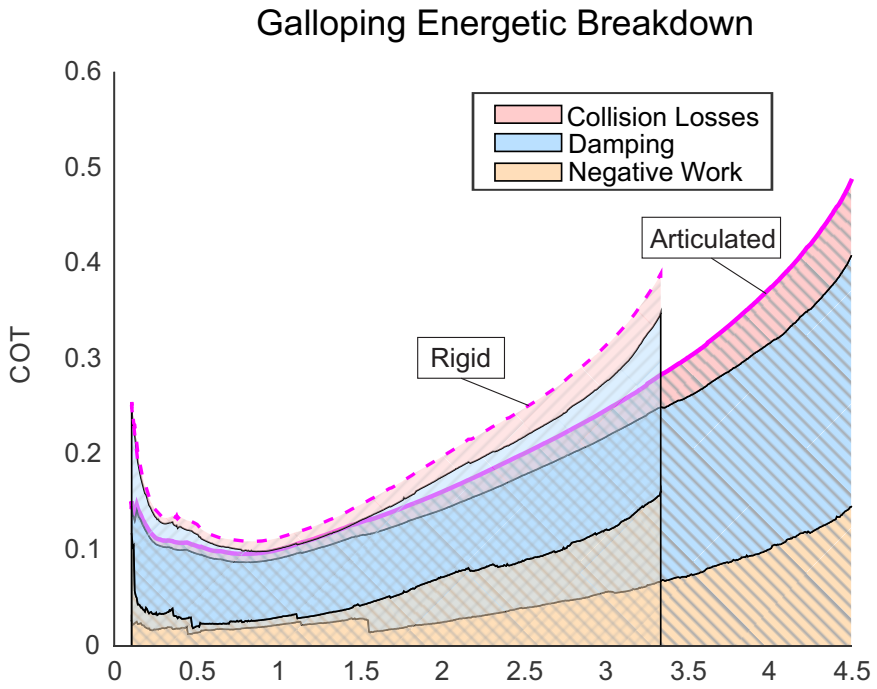

Figure 5.6: Breakdown of energy losses during galloping as a function of speed. For both model instances, collision losses play only a minor role. Damping losses are comparable for the two instances. The primary difference is an increase in negative work by the rigid model instance relative to the articulated model instance, beginning at a speed of around $1.5\sqrt{l_o g}$.

work compared to the motor and inertia. It is not used to store large amounts of energy. This lack of energy storage is true across all speeds. Galloping is shown as an exemplary case in Figure 5.8. The joint produces a much larger amount of positive work than it absorbs negative work.

Among the symmetrical gaits, only four-beat walking showed a significant difference ($p < 0.05$) between the rigid and articulated models in terms of *stride length*. Walking with an articulated spine increased step length by 10.4 %. All other symmetrical gaits had comparable stride lengths between the rigid and articulated models. For all asymmetrical gaits the articulated model employed significantly longer stride lengths than the rigid model (Table 5.4).

5.4 Discussion & Conclusion

In this paper, we explored the energetic benefits of including an articulated spine in the torso of a quadrupedal robot. We compared the positive mechanical work COT for two model instances – one with and one without an articulated spine – across

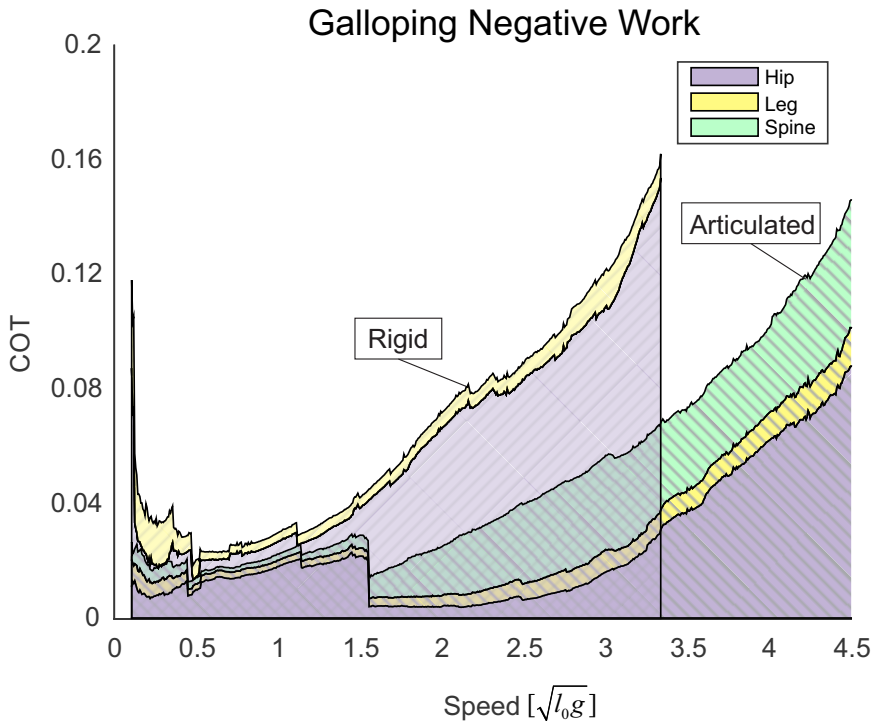

Figure 5.7: Breakdown of negative motor work during galloping as a function of speed. The negative work performed by the leg motors is comparable for both model instances. At high speeds, the motors at the hips perform much more negative work for the rigid model instance, driving up the overall costs. The articulated model's spinal motor performs additional negative work, but the overall total is still considerably lower than the rigid instance at high speeds

multiple gaits and a wide range of locomotion velocities. Using optimal control, we determined the best possible joint trajectories, actuator inputs, and footfall timing to minimize this COT individually for each gait, speed, and model instance. This was done to allow an adaptation of the motion to the respective morphology and to remove the question of control from the comparison. The model that we used built upon the large body of prior work comparing rigid and articulated spines by implementing a number of realistic characteristics, including series elastic actuation, an actuator model with limits on available torques and speeds, and most importantly, four independent legs that allowed us to explore the full range of quadrupedal gaits found in nature.

At higher locomotion velocities ($>1.28\sqrt{l_o g}$), our comparison revealed large energetic improvements for the articulated spine. In this speed range, asymmetrical gaits (in particular grounded bounding, galloping and gallop bounding) were the most efficient way of locomoting. For the four asymmetrical gaits that we explored, the

Table 5.5: Positive work done at the spinal joint at a speed of 4.5 $\sqrt{l_o g}$ is broken into contributions by motor, series spring, and rotor inertia. All power values have units of $(m_o g l_o)$

.

Gait	Joint	Motor	Spring	Inertia
Bounding	0.93	1.14	0.11	0.34
Grounded Bounding	0.66	0.93	0.11	0.30
Galloping	0.80	1.00	0.095	0.32
Gallop Bounding	0.77	1.10	0.095	0.40

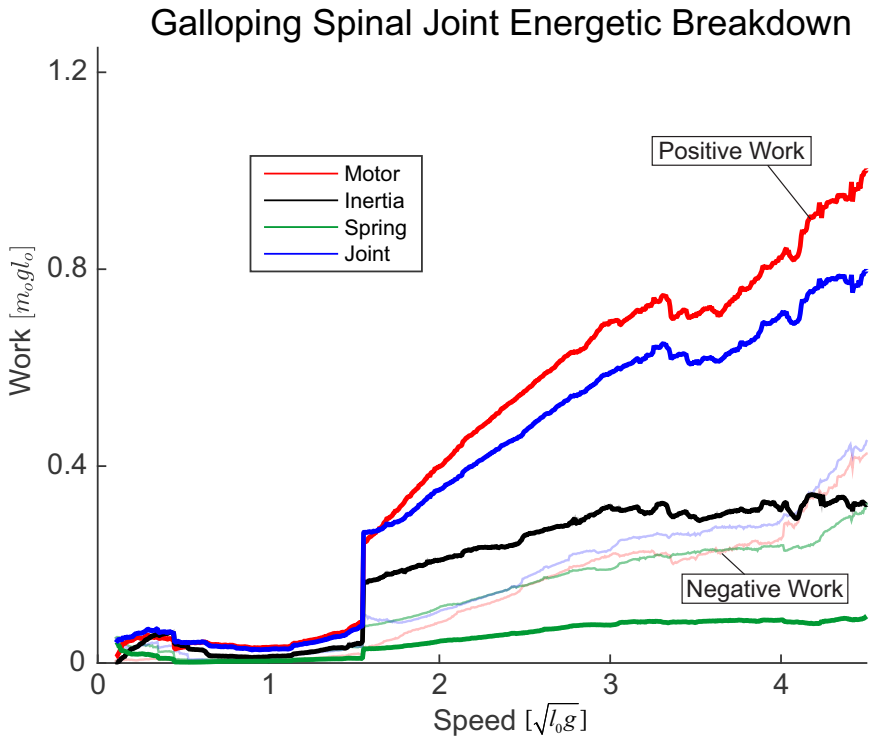

Figure 5.8: Breakdown of the work performed by the spinal joint during galloping as a function of speed. The positive work is shown as darkly colored lines. The negative work is shown as transparent lines. The joint performs much more positive work than negative work. The spring performs relatively little positive work at all speeds.

average savings (within the speed range in which solutions were found for both model instances) were between 17.3% (galloping) and 38.0% (bounding). Furthermore, for the model with the articulated spine, we were able to find solutions at much higher speeds than for the model with the rigid spine, whose maximal speed was limited by the torque limits in the actuators. At lower speeds, symmetrical gaits, in particular four-beat walking and trotting, were optimal. In this speed range, the articulated

spine had no positive effect. For symmetrical gaits, the cost values were nearly identical for all gaits. The only exception was four-beat walking with an articulated spine, which was, on average 31.8% more energetically costly than four-beat walking with a rigid spine. Comparing the most economical gaits at each speed, the articulated spine reduced the positive mechanical COT on average by 20.5 % across the entire range of velocities.

The benefits of the articulated spine have clearly been a function of the choice of gait. Improvements have primarily been observed for asymmetrical gaits. For symmetrical gaits, the energetic economy was similar for both models. In fact, these symmetrical gaits tend to not use the articulation in the spine and the angle of the spinal joint underwent relatively small changes over the course of a stride (Table 5.2). This is not particularly surprising, since for the symmetrical gaits, the legs of a pair move in opposite directions. That is, any rotation of the spine would only aid one of these legs, while hindering the other. Consequently, the optimizer choose almost no motion in the spine for symmetrical gaits. The same reasoning was put forth by [5]. He stated that animal energy storage in the longissimus aponeurosis ligament of the spine would not be useful for symmetrical gaits, as in these gaits, "the left leg of a pair swings forward while the right leg swings back."

We further found that our robot model benefited from the same mechanistic effects that facilitate asymmetrical gaits in nature: the model exhibited improved leg recirculation, elastic energy storage in the spine, and enlarged stride lengths [50, 51, 5].

Leg Recirculation: The articulated model's improved leg recirculation manifested itself in two ways: it increased the top speeds that the model was able to achieve (Table 5.3) and it decreased the amount of negative work performed by the motors (Fig. 5.6). In the rigid model, the main body can only pitch in one direction. During phases of the gait in which the hind and front legs are moving in opposite directions (e.g. when the hind legs move backwards during stance to push off while the front legs move forwards to extend the stride and prepare for impact), the main body pitch can only aid one of these motions while impeding the other (Fig. 5.9). This leads to an increase in work that needs to be done by the hips, and eventually results in an increase in negative work that is done by the hip motors (Fig. 5.7). This negative work drives up the mechanical cost of transport for the rigid model. The decoupling of the front and back halves of the torso in the articulated model reduces the negative work done by the hip motors and minimizes the overall energetic cost. It further allowed the articulated model to move its legs quicker without violating torque constraints on the motors; resulting in higher maximal speeds than the rigid model instance. This

argument builds upon the hypothesis by [50] about leg recirculation where he states that the flexible spine helps by "advancing the limbs more rapidly." Here it is clear that the articulated spine also helps by *slowing* the limbs without removing excess energy from the system.

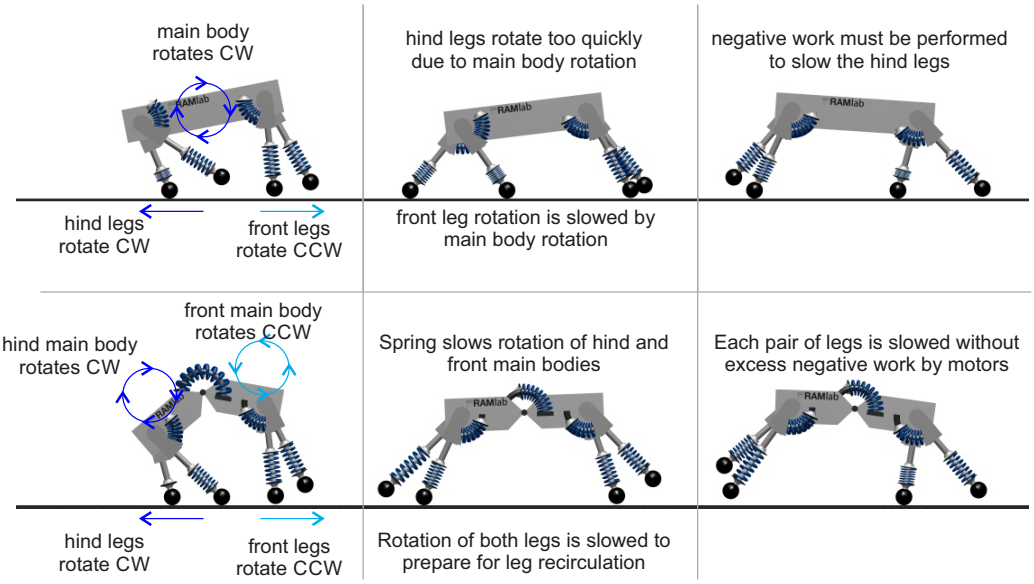

Figure 5.9: The figure shows an annotated version of a typical Galloping gait for both the rigid and articulated model instances at high speeds. For the rigid model (shown in the top row) the main body is only able to rotate in a single direction, moving the hind legs too quickly. As a result, excess negative work is performed by the hips to slow the legs. The articulated model (shown in the bottom row), in contrast, can have each half of the main body rotate, utilizing the spinal spring to slow the legs without performing excess negative work at the hips.

Elastic Energy Storage in the Spine: The articulated model was able to use the spinal spring to store and recover energy (Table 5.5), however, this value was small when compared to other sources of work in the joint. This is a surprising result, as quadrupedal mammals utilize their longissimus aponeurosis tendon to store energy [5]. Still, despite this lack of energy storage, the spinal joint still largely improves energetics. It achieves this improvement by producing a great deal more positive work than negative work (Fig. 5.8). That is, the joint is powering the gait by compensating for losses elsewhere. It is possible that a different string stiffness, one that is better tuned to the frequency of spine oscillation, would be more heavily utilized as an energy storage element.

Enlarged Stride Length: On average, the model instance with the articulated spine used longer strides than the model with the rigid spine (Table 5.4). This choice of

the optimizer, as compared for example to achieving higher speed motions by using the legs at a higher stride frequency, is also in agreement with what was observed in nature [51]. Hildebrand argues that this stride extension happens in concert with the improved leg recirculation. He states that by increasing the swing speed of the limbs, they cover more distance during the swing phase, and extend the duration of the stance phase, leading to longer strides.

Beyond the optimal control based approach, one of the main differences between this study and the existing work was the inclusion of four distinct legs in our model. While past studies have already indicated that a flexible spine is useful for quadrupedal robots, they have all lumped together the two front legs and two hind legs, and could thus only consider a bounding gait [5, 136, 66, 49, 21]. Our results support the finding that bounding with the articulated model is more economical than bounding with the rigid model. Yet, bounding was never the most economical gait for the articulated model instance. In fact, it was 6.26 % more costly than galloping on average. Having four legs was thus a crucial extension, as it allowed us to explore a broader variety of gaits. Confirming the results of our past work [130], minimizing energetic cost required switching between these different gaits as forward speed increased. The optimal gait sequence differed for the two model instances, but both required distinct motions for all four legs. For the rigid instance, the optimal gait sequence was walking, trotting, galloping, and grounded bounding. For the articulated instance, the optimal gait sequence was walking, trotting, galloping, and gallop bounding. The main difference between the two model instances was that, with the articulated spine, it paid off to switch from trotting to galloping at a much lower speed. This is a direct consequence of the fact that the articulated spine improved only the asymmetrical gaits (galloping) while leaving the energetics of the symmetrical gaits (trotting) unchanged.

Our simulation results strongly suggest that an articulated spinal joint can provide an energetic benefit for legged robots. Yet, before adding a spine to a robotic prototype, additional considerations should be taken into account. The addition of another motor, gearbox, spring, and mechanical joint will add complexity and weight to the robot which has to be compared to the potential energetic benefits. In particular the positive effects of the articulated spine did only manifest themselves at higher speeds, so hardware designers should carefully choose their desired operating speeds before implementing an articulated spinal joint. At low speeds the joint provided no benefit, and for four-beat walking, actually increased costs. In a hardware implementation, it might thus be useful to employ a physical clutch to disable the spinal joint during

slow and intermediate velocities, when using symmetrical gaits such as walking and trotting.

It is important to note that it was not a priori given that our optimization based approach would yield the same locomotion strategies that have been observed in nature. The optimizer did not know, for instance, how a typical galloping gait looks. It was not made aware of the differences between symmetrical and asymmetrical gaits and it could have chosen, for example, to not use the motor or spring in the spine or to not increase the articulated model's step length. Still, the optimizer found the exact same gaits to be optimal and discovered the same gait characteristics that are found in nature. For example, similar to quadrupeds in nature, both model instances transitioned from walking to trotting at normalized speeds between $0.5\sqrt{l_o g}$ and $0.7\sqrt{l_o g}$ [2]. Additionally, many quadrupeds in nature transition from symmetrical to asymmetrical gaits at normalized speeds between $1.4\sqrt{l_o g}$ and $1.7\sqrt{l_o g}$ [2]. The rigid and articulated model instances were slightly above and below this range respectively.

While our initial objective was to learn from nature how to build better robots, these findings let us also learn something about nature from robotics. These similarities add strong support to the mechanistic hypotheses that have been used to explain the observed motions of animals. By comparing the best possible motion of each model instance, we essentially removed the question of motion generation and control from the investigation, and our optimization approach thus established a direct causality between the mechanical dynamics of a certain morphology and the resulting motion. Such a causality is almost impossible to establish in comparative biology. In particular, animals have many considerations that can act as confounding factors. These other factors include reducing skeletal stresses [33], improving stability [14], and even predation evasion tactics [91]. For example, a cheetah may utilize its spine heavily at high speeds to facilitate compression of its lungs for oxygen exchange. By using optimization on robotic model instances, we were able to remove such physiological and neurological effects and could focus exclusively on the dynamical advantages of an articulated spine as they have been proposed by Hildebrand and Alexander. Our results seem to verify their hypotheses and highlight the importance of the natural mechanical dynamics in the spine.

Still, it is important to note that our model reflects just one out of many different possible implementations of a quadrupedal robot (see for example [34, 31, 99, 77]). In the process of developing the study presented in this paper, we made a substantial number of decisions when selecting model structure, specific model parameters, and the employed cost function. These choices affect the optimal motion. It is likely,

for example, that a different morphology would favor different asymmetrical gaits at high speeds. For example, in nature, bounding gaits tend to be preferred by animals with torsos that are relatively long when compared to leg length. These gaits can be particularly useful at high speeds, when the force output of the leg muscles is near saturation, as simultaneous push off of the hind feet provides a greater propulsive force (perhaps indicating why grounded bounding was favored by the rigid model instance at high speeds). Animals with shorter torsos compared to leg lengths, however, tend to prefer galloping gaits [54]. The effect of an articulated spine on gait energetics for these various morphologies is an area ripe for exploration. Still, regardless of the specific morphology, quadrupedal animals generally favor symmetrical gaits at low speeds and asymmetrical gaits at high speeds [54].

Therefore, even with the specific choices that we have made, our results seem to point in a more general direction. Despite the vast differences between our robot model and animals, our results closely resembled what has been observed in nature. These similarities point to fundamental causes for the improved performance with an articulated spine. This also likely means that our results will extend to a wide range of robotic prototypes beyond the specific model considered in this work. Future studies could aim to verify this claim and explore the range of possible parameter values and robot structures. However, we would actually advocate to go one step further and include these properties directly in the optimization. With the development of suitable optimization tools and computational power, this approach would turn the investigation of the benefit of a certain morphology directly into a design process that tells us how a quadrupedal robot should be built.

CHAPTER VI

Conclusions and Future Directions

Throughout this dissertation work, I have developed and implemented a methodology for the simultaneous optimization of motion and morphology in legged robots. I have investigated this methodology on sample legged robotic design questions. The explorations in these design questions inform future hardware development by roboticists and help explain why animals in nature move in the ways that they do. I first explored the notion of optimal motion and morphology in an initial comparison of series and parallel elasticity in a monoped hopper (Chapter II, published in [134]). In that work, the optimal motion cost landscape was mapped as a function of configurable parameters in the hoppers. I found that series was the better choice when optimizing for the positive motor work and the positive electrical work, and parallel was the slightly better choice when optimizing for electrical losses. I then built on this work by performing the comparison with parameters being chosen by the optimizer (Chapter III, published in [133]). Additionally, this project incorporated gear friction into the model. I found that for the most complete cost function, the positive electrical work, series was the better choice when the majority of the transmission was handled by a low friction rotary-to-linear transmission. Parallel was the better choice for smaller rotary-to-linear transmissions. The next study I performed extended this project to two dimensions and additional configurations, as I analyzed the optimal configuration of series and parallel elasticity in the hip and leg joints of a two-dimensional monoped (Chapter IV, published in [132]). In general, the most energetically economical configuration had a parallel elastic actuator at the hip, and a series elastic actuator at the leg. In the last study, I performed a discrete morphological comparison, comparing rigid and articulated spinal configurations in a four-legged quadrupedal robot (Chapter V, published in [135]). This study focused on a comparison of two discrete morphologies with fixed parameters, but included gait in the comparison. I found that the articulated spine led to large energetic sav-

ings for asymmetrical gaits at high speeds. The combination of these studies readily forms a methodology for the simultaneous optimization of motion and morphology. In this chapter I will focus on the significance of this work and discuss future research directions.

6.1 Discussion of Contributions

The study of the optimization of legged robot motion and morphology has three primary roles. First, it leads to answers to practical legged robot questions. The work in this dissertation addresses debates that have gone on in the legged robotic community for many years. Is series or parallel elasticity the more energetically favorable choice? Is an articulated spine in a quadruped energetically beneficial? If so, for which gaits? Furthermore, the methodology in this papers opens the door to letting researchers answer any question such as these. Broad questions such as, should legs be prismatic or articulated? Should robots have point feet or extended ankles? Not only does it provide a technique to obtain answers, though, it provides a way to make fair comparisons. Rather than comparing a particular implementation of one discrete morphological design to another particular implementation, researchers can instead compare the best version of each.

Second, it provides a methodology for fairly answering a broad range of design questions. While in this work, this tool has been applied specifically to legged robots, it can be expanded to a large variety of questions. Optimization is a tool that has expanded to use in fields as diverse as medicinal regimens [89] and exoskeleton control [73]. As these fields continue to advance, they will need a means by which to fairly compare different designs. The work presented here can be extended to aid in those efforts.

The third role of this type of legged robotic work is to provide insight into the way in which humans and animals move. Animal motion is subject to a variety of motivations. Animals have to simultaneously consider predator avoidance, stability, breathing technique, and force minimization, among many other driving factors. It can be difficult to isolate the role of a particular morphological variation. Moreover, often in nature, a perfect experiment is impossible to conduct. In the case of the articulated spine study, there is no animal that is identical to a cheetah in every way except for having a rigid spine. Optimization of legged robots does not suffer from these drawbacks. Morphological variations can be, in a sense, looked at completely independently from other driving factors. A particular structure's effect on energetics,

or any other cost function, can be explored.

6.2 Overview of Presented Work

The way that a legged system moves and the way that it is built are inherently coupled. Despite that, the vast majority of robotic work today seeks to improve these two facets independently [136, 10, 131, 45, 20]. In general, either the motion is optimized on a particular piece of robotic hardware, or, a specific hardware parameter is modified within a fixed motion strategy. The work that I have presented in this dissertation seeks instead to optimize these two facets simultaneously.

The simultaneous optimization of motion and morphology is a fundamentally difficult problem. Because the two are so intricately related, there is an overlap in their effect. For example, different mass and spring values can lead to the same natural frequencies, which in turn, will lead to similar preferred motion. As a result, any optimization method has to approach this problem with sufficient caution to assure that local minima are averted.

The work presented in Chapter II began a preliminary exploration into the question of simultaneous optimization of motion and morphology in legged robots. In that work, I compared one dimensional hoppers with series elasticity to those with parallel elasticity. Rather than include parameters directly within the optimization, and as a result being unsure of the particular effect of a set of parameters, I instead sought to map the optimal cost landscape as a function of parameters. These cost mappings were compared to theoretical predictions to ensure their accuracy. The contributions of this work were two-fold. First, it showed that the common mode of thinking about series and parallel elasticity required more nuance. Typically, a roboticist picks one of the two and justifies it by its respective advantage. For parallel, they often state that it is the better choice for minimizing motor torques. For series, they often state that it is the better choice for minimizing mechanical energy. In mapping the cost landscape, however, we were able to show that the argument is more subtle. For a variety of cost functions, the better choice between series and parallel elasticity depends on the parameter choice. The second main contribution is that this cost landscape mapping technique can be extended to any discrete morphological comparison. In the study, I performed a two-dimensional parameter sweep, finding the optimal motion cost as a function of no-load velocity and spring stiffness. This same technique could readily be performed for any cost function or parameter choice within the legged robot, such as mass distribution. Furthermore, it could be extended to other systems outside of

the legged robot domain to help understand the relationship between optimal motion and structure.

The work described in Chapter III builds on the preliminary exploration in Chapter II. In that work, I again looked at a simultaneous optimization of motion and morphology to compare serial and parallel elasticity in monoped hoppers, but this time, included morphological parameters directly within the optimization. Taking advantage of the lessons learned from Chapter II, I was able to look at a more complex model, now incorporating gear friction, in order to fairly compare the best possible parallel hopper to the best possible series hopper for a variety of cost functions. Yet again, the contribution is two-fold. First, it investigates the two most common motor and elasticity configurations, and gives a definitive method for deciding which is the most energetically economical configuration for an implementation. Second, it describes a methodology that allows future researchers to, within a single optimization, find the best possible motion and parameters simultaneously. Yet again, this is a technique that extends beyond incorporating transmission and stiffness parameters. It further extends beyond legged robots. Similar techniques, for example, were implemented by [56] for the optimal mass configuration and control of a sit-to-stand assistive device. This work extended on their efforts by incorporating a simultaneous optimization to perform a discrete design comparison. Researchers for any field can perform a similar fair comparison for any problem that can be formulated as a model-based optimization.

The work described in Chapter IV represents another step in the evolution towards a single optimization that incorporates both the continuous (motion within a particular gait) and discrete (a particular footfall sequence) aspects of motion, as well as both the continuous (parameters) and discrete (a discrete morphological comparison) aspects of morphology. In this study, I investigated the optimal motion and morphology of a two-dimensional monoped. There were now four possible configurations of series and parallel elasticity, and, forward speed was included as yet another element in the optimization. The work yet again lends insight into a practical question for roboticists. It also shows the potential for expanding the technique to more complex problems than simple in-place hopping.

The work discussed in Chapter V incorporates the last element, gait choice, into the simultaneous optimization of motion and morphology in legged robots. In that work, I compared two instances of a quadrupedal model, one with a rigid spine and one with an articulated spine, across a variety of common gaits. By incorporating gait, the work allows roboticists to see the types of motions for which the articulated

spine is energetically beneficial. Additionally, since there are no biological effects in my relatively simple robotic models, we can isolate the mechanistic effect of the spine, lending insight into its utility in nature. Lastly, the project represents the last element in a study that combines the simultaneous optimization of motion and morphology. By combining this study with the techniques from the previous studies detailed above, a roboticist could, in a single methodology, find the best discrete morphology, with the best continuous parameters, moving at the best possible gait, with the best motion strategy within that gait.

6.3 Limitations and Need for Future Research

The work presented in this dissertation presents a methodology for the simultaneous optimization of motion and morphology in legged robotic simulation. The methodology is a tool that gives roboticists a way to fairly compare discrete design variations in legged robots. Still, the methodology is not without its limitations, and there is room for exploration among future researchers.

The first area for future exploration is to continue to work on the techniques used for the conceptual models throughout the dissertation. In particular, future researchers could look to improve the optimization techniques used within this work. While these gradient-based tools are incredibly powerful, they are susceptible to local minima. In finding the solutions presented in the dissertation, I took great care to test all points with a variety of initial conditions. That included using motion found from other cost functions and gaits as initial seeds. Furthermore, many of my motions were compared to theoretical predictions to ensure that they were indeed reasonable. Still, ultimately there can be no guarantee of global optimality for the techniques we used. One source of future work could be to improve upon these optimization techniques. That improvement could also seek to incorporate the discrete aspects of motion directly within the optimization. That is, the footfall sequence of the legged robot could be chosen by the optimizer. While we attempted to do just that in our previous work [130], we found that the existing techniques were generally less accurate than the multiple shooting technique I used throughout the dissertation. Still, even with the improved multiple shooting technique, when I attempted to include morphological parameters directly within the optimization for a more complex problem, such as the quadrupedal work in Chapter V, we found that the optimizer had poor convergence. As a result, utilizing improved optimization techniques could allow researchers to leverage the methodology presented in this work for even more

complex design questions.

Improved techniques could open the door for researchers to build on the results of the studies presented throughout the dissertation. They could explore additional projects that can make use of the methodology presented. For example, these researchers could seek out the single set of parameters that is best, on average, for a large speed range. Or, they could see what single set of parameters are best across multiple gaits. Researchers could also consider exploring different cost functions. The variety of cost functions explored in Chapters II-IV could also be explored for more complex projects such as the work presented in Chapter V. These studies could incorporate the gear friction model from Chapter III and therefore quantify the effect of those frictional losses. Within any of these cost functions, sensitivity studies could also be conducted to see the effect of changes on a single parameter on the cost. For example, researchers could look at the effect of the ratio of main body to leg length on gait choice, and see if it has a similar effect as in nature [54]. The projects presented throughout this dissertation all look at energy-optimal motions. It is possible, however, that a roboticist, or an animal in nature, has different motivations. Researchers, could, for example, consider stability within the optimization. This stability could be explored through a Floquet analysis or could be implemented with stabilizing feedback controllers. The cost of this added stability could be incorporated into the cost functions.

The conceptual models used throughout this dissertation are of intermediate complexity. They are complex enough that they can model realistic robotic motion, such as swing leg dynamics and ground clearance. They are also simple enough that they can be used to make generalizable conclusions about robotic hardware as well as human and animal motion. Still, exploring the connection of these conceptual models to the simple and complex models around them would strengthen the utility of the results.

Exploring the connection of the conceptual models presented in this work to simpler models would help to shed more light on the interdependence of motion and morphology. There is a vast body of work that uses simplified models to find passive or nearly passive motions [15, 38, 41]. From these works, as well as from the various motions presented throughout the dissertation, it is clear that legged systems take advantage of their natural dynamics to move in an energetically economical manner. In a sense, the work presented here can be viewed as an optimal tuning of these natural dynamics. Optimizing the morphology can in turn lead to more favorable passive dynamics, which then lead to reduced energy costs. This area is ripe for exploration.

A detailed understanding of how the lossless motions that arise from the interplay of gravity, inertia, and oscillation are taken advantage of by more complex systems could open the door to not only building better robots, but to understanding why humans and animals move in the ways that they do. One means of exploring this connection is to add a parameter that scales all of the sources of loss in the conceptual models presented in this work. This parameter can then be varied to see how removing complexity from the models, and approaching a passive model, changes the motion. That is, researchers can see how more complex models take advantage of their natural dynamics to move economically. Ultimately, once this connection is understood, roboticsts can tune parameters in the natural dynamics, to obtain desired motion in the full robot.

It is also necessary to explore the connections of the conceptual models to more complex models and hardware. While the simulations discussed in this work can certainly give insight to roboticists, and motivate hardware development, it is simply impossible to fully capture the complexity of a hardware implementation in simulation. For example, implementing an articulated spine into a quadrupedal robot requires additional mechanical equipment and sensors. Moreover, many of the motion strategies chosen by the optimizer are sensitive to very specific parameter values. In reality, parameter values vary. We further assume in simulation that foot contacts can't slip, though in reality they might. There are also energetics associated with on-board computing performance and stabilizing feedback, among many other factors. Ultimately, all of these additional complexities can only be fully explored in a hardware implementation. One direction is to see if, despite all of these complexities, the same trends from the optimization can be seen in a robot. That is, a roboticist could map the optimal trajectories from simulation onto a hardware design, and see if a gait transition is still energetically beneficial. Another direction would be to have the hardware learn optimal motions. Through a reinforcement learning scheme, the hardware could explore motions within gaits, as well as different gaits, and find the most energetically favorable motion. The resulting hardware-optimal gaits could then be compared to simulation to see its utility. In these explorations, modeling is still a very powerful tool, and can used as a starting point towards a full implementation on hardware (see [120] for example).

6.4 Concluding Remarks

The combination of the project methodologies presented in this work gives robotic and animal researchers an important tool. The simultaneous optimization of motion and morphology paves the way for building better legged robots. It also provides a tool that can be extended to a variety of other fields. With it, researchers can compare not just particular versions of designs, but rather, the best versions of those designs. Lastly, it allows for a deeper understanding of nature and the fundamental principles that drive legged locomotion.

APPENDIX

APPENDIX A

Detailed Theoretical Predictions of Parallel and Series Elastic Actuated Hoppers

Detailed Theoretical Predictions

In order to determine whether PEA or SEA is more energetically economical, we must simultaneously optimize for the motion and morphology. Even for our simple hopper models, this is a convoluted task. Due to the interdependence of the many factors at play (type of actuator, cost function, spring stiffness, motor transmission, motor force, and hopper motion) the effect of an individual aspect, or of the basic principles of the underlying motion, can be inextricably lost in those highly interwoven relationships. Therefore, before analyzing a full optimization (where morphological parameters can be chosen by the optimizer), we begin with a simpler study that allows us to understand the underlying motion strategies that are optimal for each cost function. In this study, parameters were set to predefined values; the only exception is the no load speed of the motor $\bar{u}$, which was systematically varied. For a wide range of no load speeds and for three different cost functions, we developed predictions of the hopping motion that the optimizer output. These predictions begin with an analysis of a simpler model with a mass-less foot and no damping. We then extend those predictions to the actual model presented earlier.

The mass-less foot was approximated in the numerical optimizations by a very small mass: $m_2 = 0.0001\,\mathrm{m}_o$ (with $m_1 = 0.9999\,\mathrm{m}_o$), as compared to the regular mass distribution of $m_2 = 0.05\,\mathrm{m}_o$ and $m_1 = 0.95\,\mathrm{m}_o$. Removing the foot mass eliminates foot collision losses as well as damping in the springs. The remaining parameter

values were fixed at the following values: hopping height $h = 1.3\,l_o$, spring-stiffness $k = 20\,m_o g/l_o$, damping ratio $\zeta = 0.2$, and motor offset $u_{offset} = 0\,l_o$.

Positive Motor Work

PEA

For PEA with a massless foot, the only source of losses is the touchdown collision that acts on the inertia of the motor:

$$E_{p,mc} = \frac{1}{2}\left(\frac{j_{mot} m_1}{m_1 + j_{mot}}\right) \cdot (\dot{y}_{TD} - \dot{l}_{TD})^2. \tag{A.1}$$

This equation expresses the energy that is needed to make the leg velocity equal to the main body velocity at touch-down. $\dot{y}_{TD}$ ($\dot{l}_{TD}$) is the velocity of the main body (leg) right before touch-down. The collision losses thus vanish when the leg velocity is equal to the main body velocity. With PEA, there is a simple strategy to ensure this: 'clutching the leg'. This strategy initiates at the moment of lift-off, when the leg is extending exactly as fast as the main body is moving upwards. Right after lift-off, the parallel spring will passively slow down this leg extension while storing the associated kinetic energy. Once $\dot{l}$ has reached a value of zero, the motor 'clutches' the spring at this extended length by applying a constant force to keep its length fixed. No work is required in the process, since there is always either no force or no velocity. Shortly before touchdown, the motor 'unclutches' by applying zero force. This allows the spring to passively contract the leg. The stored energy is converted back into kinetic energy and the leg will reach the same velocity that it had at lift-off. In the mean time, the main body was undergoing a purely ballistic flight and will thus also have the same velocity at touch-down as it had at lift-off. When the 'unclutching' is timed right, the leg velocity will thus equal exactly the main body velocity at the moment of touch-down. No collision losses occur and $E_{p,mc} = 0$. This process is illustrated in Figure A.1.

Since we enforce limits on maximal leg extension, this strategy does fail for low no-load speeds (and a high associated reflected motor inertia). In these cases, the spring cannot stop the leg extension passively before the leg length limit ($l_{max} = 1.15\,l_o$) is violated. In other words: there is more kinetic energy in the leg than can be stored in the spring. The motor must perform negative work to remove excess energy from the system. That energy must be replaced later. By taking the difference between the kinetic energy stored in the motor $\frac{1}{2} j_{mot} \dot{l}_{LO}^2$ and the potential energy that can be

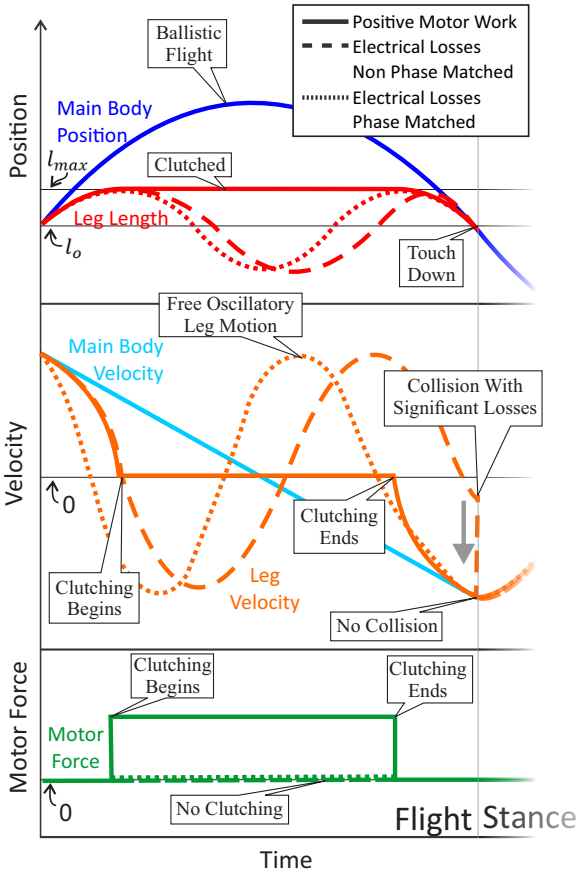

Figure A.1: Shown is a simplified hand-drawn cartoon illustrating the motion strategies of a hopper with PEA. In the idealized case of having no foot mass and no damping, losses arise only through collision losses in the motor inertia and from negative motor work. The PEA hopper can eliminate *positive motor work* (solid lines) by ensuring that the leg and the main body have the same velocity at touchdown. The associated motion strategy lets the leg extend passively during flight until the spring naturally stops it, and then uses the motor force to 'clutch' it. This 'clutching' is released shortly before touchdown to match the leg velocity to the main body velocity. When optimizing for *electrical losses* (dashed lines) the necessary 'clutching' force would lead to high costs. It is thus more efficient to allow the spring to oscillate freely during flight. That strategy can lead to collision losses that require active forces to re-inject energy. Only for selected values of the no load speed $\bar{u}$, the leg spring oscillation and ballistic motion of the main body are matched in phase, such that the leg and the main body have the same velocity at touchdown (dotted lines).

stored in the spring $\frac{1}{2}k(l_{max} - l_o)^2$, we can compute this negative motor work as:

$$E_{p,nm} = max\left(\frac{1}{2}\left(j_{mot}\dot{l}_{LO}^2 - k\left(l_{max} - l_o\right)^2\right), 0\right), \tag{A.2}$$

where j_{mot} is the reflected motor inertia, $\dot{l}_{LO}$ is the leg velocity at liftoff, and l_{max} is the maximum leg length. Since during stance, the leg and the main body move together, the lift-off velocity of the leg is equal to the lift-off velocity of the main body. For simplicity, we assume that lift-off and touchdown happen with an un-extended leg of length l_o. This velocity can then be computed from the hopping height h as:

$$\dot{l}_{LO} = \dot{y}_{LO} = \sqrt{2g\left(h - y_{TD}\right)} = \sqrt{2g\left(h - l_o\right)}, \tag{A.3}$$

Overall, the positive motor work for PEA with a massless foot is given by:

$$\widetilde{C}_{p,mot} = E_{p,nm}, \tag{A.4}$$

where $E_{p,nm}$ is defined by Equation (A.2). Figure A.2a compares this prediction with the cost values obtained from the numerical optimization. The motion that resulted from the optimization with $\bar{u} = 1.5\sqrt{l_o g}$ is shown in Figure A.3. In both cases, the numerical results closely match the theoretical prediction.

When we add mass to the foot, we also introduce foot collision losses and damping in the spring. Following the same strategy as above can completely eliminate the foot collision losses. The damping losses can be approximated by assuming that during stance the hopper undergoes a sinusoidal motion of frequency $\omega_o = \sqrt{\frac{k}{j_{mot}+m_1}}$. We can represent these losses $c_{p,1}\left(\bar{u}\right)$ as a function of the no-load speed $\bar{u}$. To calculate $c_{p,1}\left(\bar{u}\right)$, we begin by assuming that lift-off and touchdown happen with an unextended leg of length l_o. To calculate the damping losses for the PEA hopper with a foot with mass, we assumed that the hopper undergoes a purely sinusoidal motion during stance. The leg velocity for the sinusoidal motion is given by:

$$\dot{l}_o = A_o \omega_o \cos\left(\omega_o t + \alpha_o\right), \tag{A.5}$$

where

$$A_o = \frac{m_1 g}{k \sin(\alpha_o)}, \tag{A.6}$$

and

$$\tan\left(\alpha_o\right) = \frac{\omega_o m_1 g}{k \dot{y}_{TD}}. \tag{A.7}$$

The natural frequency is given by $\omega_o = \sqrt{\frac{k}{j_{mot}+m_1}}$. The damping losses are calculated

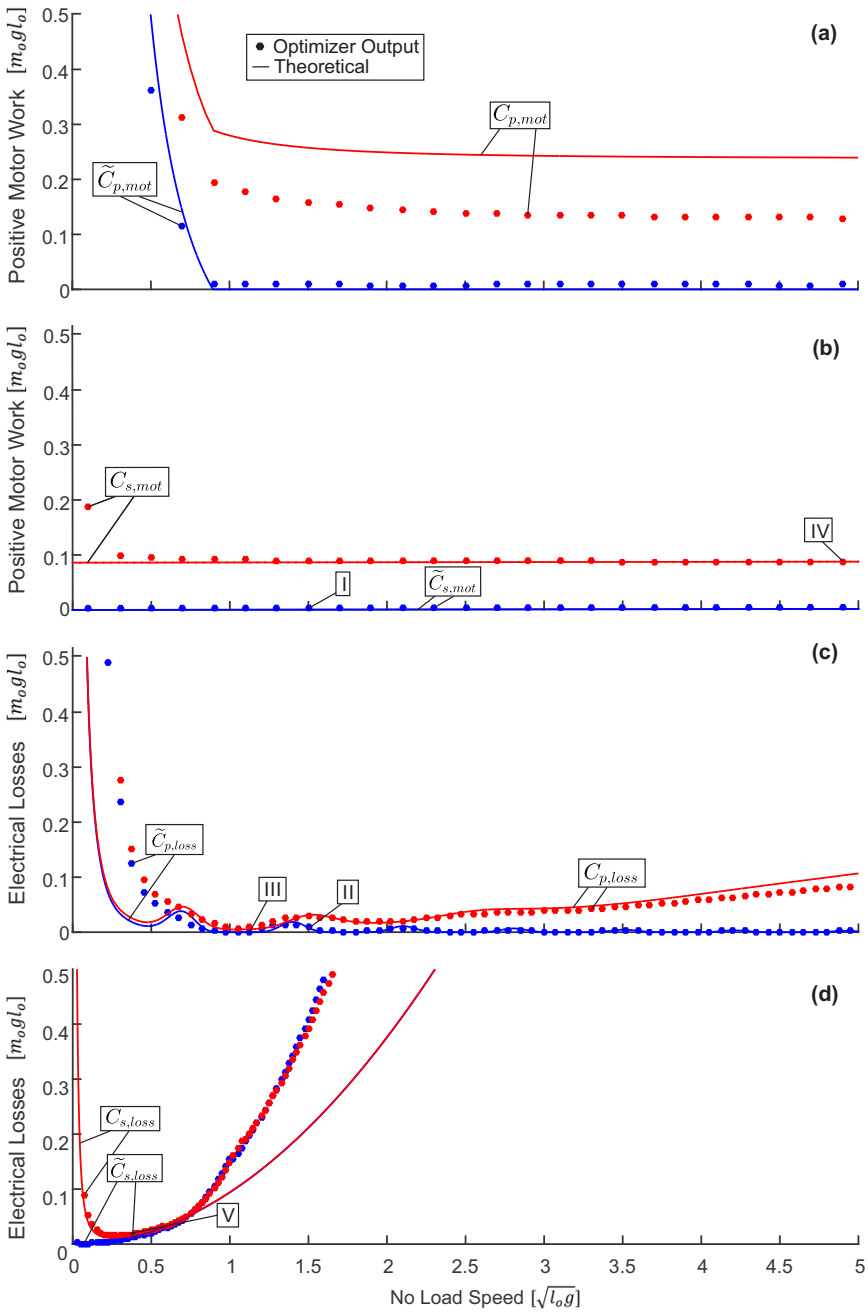

Figure A.2: Comparison of theoretical cost predictions (solid lines) with numerical optimization results (dots). Shown are: PEA positive motor work (a), SEA positive motor work (b), PEA electrical losses (c), and SEA electrical losses (d). Results for hopping with a massless foot are shown in blue and for a foot with mass in red. The labels I-V refer to the examplary optimal motions shown in Figures A.3 and A.4. In general the theoretical predictions closely match the optimizer output. This confirms that the optimizer is outputting realistic results.

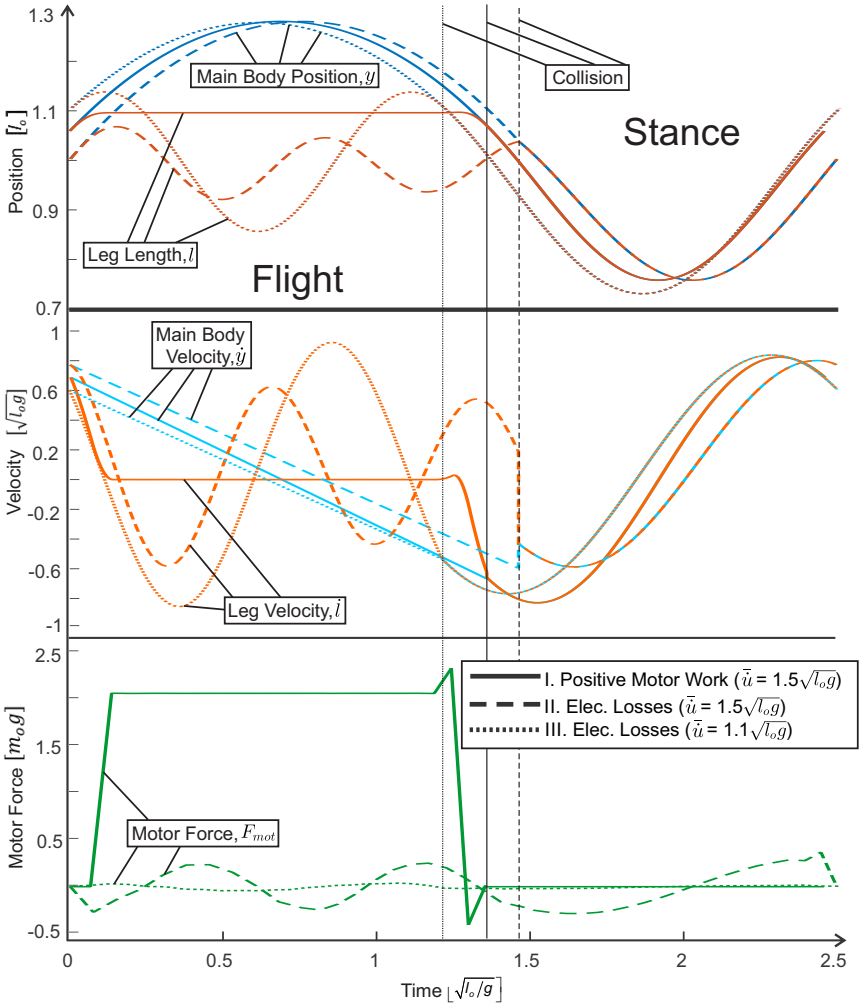

Figure A.3: Shown are optimal motion and force profiles for PEA with a massless foot. When optimizing for positive motor work, the actuator 'clutches' the spring during flight (shown for $\bar{u} = 1.5\sqrt{\mathrm{l_o g}}$). In contrast, when optimizing for electrical losses, the leg is oscillating freely during flight. For $\bar{u} = 1.5\sqrt{\mathrm{l_o g}}$, leg and main body motion are not matched in phase and a collision occurs. Such a phase matching can be achieved, for example, when the no-load speed is reduced to $\bar{u} = 1.1\sqrt{\mathrm{l_o g}}$. In this case, no collision happens at touchdown and no energy is lost. Consequently, there is almost no motor force needed to sustain a continuous hopping motion. These numerical results closely match the predictions shown in Figure A.1

by integrating the damping power ($P_{damp} = b\dot{l}_o^2$) over the stance time:

$$c_{p,1} = \int_0^{T_{stance}} P_{damp} dt \tag{A.8}$$

The positive motor work for PEA with a foot with mass is thus given by:

$$C_{p,mot} = E_{p,nm} + c_{p,1}\left(\bar{\dot{u}}\right), \tag{A.9}$$

which is compared to the numerical results in Figure A.2a. The approximation is an overestimate of the mechanical work. This is to be expected, since a smart choice of actuation can likely reduce damping losses; for example, by injecting energy only at the very end of stance.

SEA

For SEA, no collision losses can occur in the motor inertia. The positive motor work $C_{s,mot}$ can be driven to zero simply by keeping the motor at rest ($u \equiv 0$). Since there is also no inertia added to the leg, the hopper will not approach the leg length limits and no negative motor work is necessary. We therefore have:

$$\widetilde{C}_{s,mot} = 0\,\mathrm{m_o g l_o} \tag{A.10}$$

The numerical optimization reveals that the positive motor work is indeed close to zero (Figure A.2b). The small differences can be attributed to the foot having a slightly non-zero mass in the numerical model.

Giving the foot mass introduces collision and damping losses. We approximate these losses with a constant value that is fit to the optimization results:

$$C_{s,mot} = 0.086\,\mathrm{m_o g l_o}, \tag{A.11}$$

The comparison of theoretical and numerical results in Figure A.2b shows that the assumption of a constant loss term fails for low no-load speeds. Similar to the PEA case (Equation (A.2)), this is due to negative work that becomes necessary when a higher motor inertia causes the leg length limits to be violated.

With respect to the optimal motion profile, [108] argues that in order to avoid collision losses, a SEA hopper should retract its leg shortly before impact. To avoid excess negative motor work and damping losses, the motor must also stay motionless during the first half of stance, and then move to keep $(\dot{l} - \dot{u})$ constant during the second half of stance. All these strategies are implemented in the solution obtained by the optimizer (Figure A.4). In addition, we observe that the motor stays near its maximum position during flight to decrease the effective hopping height. Since SEA is able to move its motor up to a distance of $0.15\,l_o$, its effective hopping height is

half that of PEA. The positive motor work is thus roughly twice as high for PEA as for SEA.

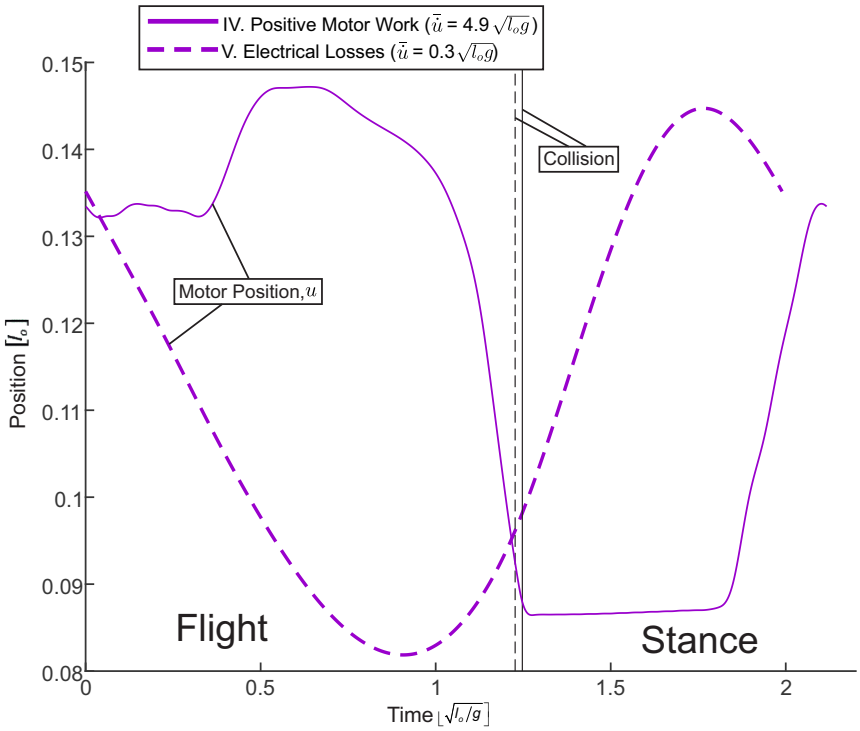

Figure A.4: Shown is the optimal motor position u for SEA with a foot with mass. For positive motor work, the foot remains motionless during the first half of stance and injects energy in the second half. It is also almost maximally extended towards the limit of $u_{max} = 0.15\, l_o$. This motion is in close agreement with the predictions in [108]. When optimizing for electrical losses, the motor moves in a much smoother way and inputs energy throughout the entirety of stance.

Electrical Losses

PEA

The electrical losses as defined by Equation (2.10) are solely a function of the motor force F_{mot}. Actuator work is only accounted for indirectly, as motor forces are needed to perform work.

For PEA, 'clutching' the leg (as discussed earlier) would require significant motor force F_{mot} during flight. Consequently, it is not an option when electrical losses constitute the cost function. Instead, it is better to let the leg oscillate freely. For a massless foot (without damping), the leg undergoes a natural spring-mass oscillation

with a velocity $\dot{l}_n(t)$ of:

$$\dot{l}_n(t) = -A_n \omega_n \sin(\omega_n t - \alpha_n). \tag{A.12}$$

The amplitude A_n and phase α_n are derived by again assuming that lift-off and touchdown happen with an un-extended leg of length l_o. Equation A.12 is derived from solving the equations of motion of an undamped spring-mass oscillator with mass equal to j_{mot}. As the foot is massless, we ignore the fact that the oscillator is in an accelerated frame. The amplitude is defined by:

$$A_n = \sqrt{l_o^2 + \left(\frac{\dot{l}_{TD}}{\omega_n}\right)^2} \tag{A.13}$$

and the phase offset is defined by

$$\tan(\alpha_n) = \frac{\dot{l}_{LO}}{\omega_n l_o} \tag{A.14}$$

and $\omega_n = \sqrt{\frac{k}{j_{mot}}}$.

The natural frequency of this oscillation is $\omega_n = \sqrt{\frac{k}{j_{mot}}}$. From this equation, the leg velocity at touchdown $\dot{l}_{TD}$ can be computed using the time of flight:

$$T_{flight} = 2\frac{\dot{y}_{LO}}{g} \tag{A.15}$$

The collision losses in the motor inertia depend on the relative phase of leg motion and main body motion. They can be computed from Equation (A.1) using $\dot{l}_{TD} = \dot{l}_n(T_{flight})$. The result depends on ω_n and j_{mot}, and is thus a function of $\bar{u}$. As $\bar{u}$ varies, the size of the collision losses in the motor fluctuates. Figure A.1 sketches out two examples of such a free oscillation in which the phase is matched (dotted lines) and not matched (dashed lines). For the matched phase, the hopping motion is loss-less and does not require any force input. In this case, $\widetilde{C}_{P,loss}$ is zero. Otherwise, the lost energy must be replaced to reach back to the same original height at the end of the hop. This replacement requires a force input, which will lead to electrical losses.

In approximation, we can assume that the required motor force F_{mot} is proportional to these energetic losses. This assumption is true if the motion of the hopper is not changed substantially from the ideal case in the presence of losses (approxi-

mately free oscillation during flight, followed by a sinusoidal stance phase). We further assume that the thermal electric losses are proportional to $(F_{mot}\bar{\dot{u}})^2$ (motivated by Equation (2.10)). We can thus approximate the electrical losses as:

$$\widetilde{C}_{p,loss} = \widetilde{c}_{p,2}\bar{\dot{u}}^2 \left(E_{p,nm} + E_{p,mc}\right)^2, \tag{A.16}$$

in which $E_{p,nm}$ and $E_{p,mc}$ are calculated from Equations (A.1) and (A.2), respectively.

Applying Equation (A.16) with $\widetilde{c}_{p,2} = 0.12\, m_o g l_o$ yields the comparison shown in Figure A.2c. Our theory can accurately predict the fluctations in $\widetilde{C}_{p,loss}$ as a function of $\bar{\dot{u}}$. The prediction only fails for low no-load speeds. This is not surprising, given that for these cases the larger amounts of negative motor work violate our earlier assumption that $\dot{l}(t)$ is not substantially changed. Sample optimal motions are shown in Figure A.3. The motion strategy is very similar to the predictions presented in Figure A.1. The notable exception is that the motor force is not zero as predicted, but rather, oscillates slightly. These small force inputs are likely a way to shift the phase of the leg while simultaneously injecting energy without applying a large force.

When giving the foot mass, we represent the sum of damping and collision losses by $c_{p,3}$, a constant chosen to fit the optimizer output. $\dot{l}(t)$ is calculated assuming that we have a mass-spring damper.

Yet again assuming that lift-off and touchdown happen with an un-extended leg of length l_o. The leg velocity $\dot{l}_d t$ is derived from solving the equations of motion of a damped spring-mass oscillator with mass equal to $m_{tot} = j_{mot} + m_2$

$$\dot{l}_d(t) = -A_d e^{-\gamma t}\left(\omega_d \sin\left(\omega_d t - \alpha_d\right) + \gamma \cos\left(\omega_d t - \alpha_d\right)\right). \tag{A.17}$$

The amplitude is given by:

$$A_d = \left((l_{LO} - l_o)^2 + \frac{(\dot{l}_{LO} + \gamma(l_{LO} - l_o))^2}{w_d^2}\right)^{1/2} \tag{A.18}$$

and the phase offset is given by:

$$\tan\left(\alpha_d\right) = \frac{\dot{l}_{LO}}{w_d(l_{LO} - l_o)} + \frac{\gamma}{w_d} \tag{A.19}$$

where the damping coefficient is given by $\gamma = \frac{b}{2(m_{tot})}$, the natural frequency is $\omega_n = \sqrt{\frac{k}{m_{tot}}}$, and the natural damped frequency is given by $w_d = \sqrt{w_n^2 - \gamma^2}$.

Note that the effects of gravity and main body acceleration are neglected, as the

foot mass is significantly smaller than the main body.

Following the same reasoning as in the massless foot case, the thermal electric losses are given by:

$$C_{p,loss} = c_{p,2}\bar{\dot{u}}^2 \left(E_{p,nm} + E_{p,mc} + c_{p,3}\right)^2 \tag{A.20}$$

Applying Equation (A.20) with $c_{p,2} = \widetilde{c}_{p,2} = 0.12$, and $c_{p,3} = 0.18\, m_o g l_o$ yields the results shown in Figure A.2c. Once again, a high motor inertia accounts for the differences at low values of $\bar{\dot{u}}$.

SEA

For SEA, the leg force must balance the weight of the robot on average, and -since there is no net motion- the average actuator acceleration must be zero:

$$\int_0^T F dt = \int_0^T \left(F_{mot} - j_{mot}\ddot{u}\right) dt = \int_0^T F_{mot} dt = m_1 g T. \tag{A.21}$$

The force-square optimal actuation strategy is to have a nearly constant motor force $F_{mot} = m_1 g + F_{mot}^{act}(t)$, in which F_{mot}^{act} is only a small fluctuating force that creates a net-positive work to compensate for losses [108]. The electrical losses associated with this strategy are:

$$\widetilde{C}_{s,loss} = C_{s,loss} = \frac{T}{P_{max}} \left(\left(m_1 g \bar{\dot{u}}\right)^2 + \left(\frac{j_{unsc}}{\bar{\dot{u}}}\right)^2 \sigma^2\left(\ddot{u}_{act}\right) \right), \tag{A.22}$$

in which $\ddot{u}_{act}$ is the acceleration caused by F_{mot}^{act}. T is the time of a hop, and $\sigma^2\left(\ddot{u}_{act}\right)$ is the variance of the active motor acceleration. If there are no mechanical losses associated with the motion, no active forces are required and $\tilde{\sigma}^2\left(\ddot{u}_{act}\right) = 0\, m_o^2 \sqrt{g^3 l_o}$. Applying Equation (A.22) with $\widetilde{T} = 2.5\sqrt{l_o/g}$ yields the results in Figure A.2d.

This prediction underestimates the electrical losses at higher no load speeds. This results from the fact that in addition to the 'active' motor acceleration $\ddot{u}_{act}$ (caused by F_{mot}^{act}), there is also a 'passive' motor acceleration $\ddot{u}_{pas}$ that is caused by the difference between the constant motor force term $m_1 g$ and the leg force F:

$$\ddot{u}_{pas} = \frac{1}{j_{mot}} \left(m_1 g - F\right). \tag{A.23}$$

This passive acceleration scales inversely with the reflected motor inertia and is thus proportional to $\bar{\dot{u}}^2$. For higher values of $\bar{\dot{u}}$, this motor acceleration would lead to violations of the motor position limits, which requires the motor to deviate from the optimal force profile causing $\tilde{\sigma}^2\left(\ddot{u}_{act}\right) > 0\, m_o^2 \sqrt{g^3 l_o}$.

Giving the foot mass leads to losses, meaning that $\sigma^2(\ddot{u}_{act})$ must be non-zero. Applying Equation (A.22) with $T = 2.5\sqrt{l_o/g}$ and $\sigma^2(\ddot{u}_{act}) = 0.01\, m_o^2\sqrt{g^3 l_o}$ yields the results in Figure A.2d. Again the prediction underestimates electrical losses at high no load speeds where motor position limits come into play.

Contrary to the positive motor work optimization, the motor motion should now be distributed over the full stride, as is confirmed in Figure A.4.

When the foot has mass, both actuator types have an energetic minimum with respect to $\bar{\dot{u}}$. This minimum implies that there is a trade-off between low and high no-load speeds. For SEA, that trade-off stems from the motor force needed to accelerate the reflected inertia j_{mot} of the motor. Since this inertia is inversely proportional to $\bar{\dot{u}}^2$, it prohibits a no-load-speed that is too close to 0. A high no-load speed leads to increased losses because $\bar{\dot{u}}^2$ directly scales c_{loss} (Equation (2.10)). For PEA, the trade-off arises because a large no-load-speed would lead to large thermal losses if the required motor force is non-zero. Decreasing the no-load speed, however, introduces other unwanted effects. Collision losses depend on the reflected motor inertia according to Equation (A.1) and increase for smaller $\bar{\dot{u}}$. Also, as detailed above, higher values of $\bar{\dot{u}}$ lead to increased negative motor work.

Positive Electrical Work

Due to the complexity of positive electrical work as cost function, it is not possible to perform a detailed theoretical analysis. However, minimizing positive electrical work represents a trade-off between minimizing positive motor work and electrical losses. We thus expect that the result for this cost function combines the characteristics of both previously discussed cases.

BIBLIOGRAPHY

BIBLIOGRAPHY

[1] Alexander, R.: Mechanics of bipedal locomotion. Perspectives in experimental biology **1**, 493–504 (1976)

[2] Alexander, R.: Optimization and gaits in the locomotion of vertebrates. Physiological reviews **69**(4), 1199–1227 (1989)

[3] Alexander, R., Dimery, N.J., Ker, R.: Elastic structures in the back and their role in galloping in some mammals. Journal of zoology **207**(4), 467–482 (1985)

[4] Alexander, R.M.: The gaits of bipedal and quadrupedal animals. The International Journal of Robotics Research **3**(2), 49–59 (1984)

[5] Alexander, R.M.: Why mammals gallop. American zoologist **28**(1), 237–245 (1988)

[6] Alexander, R.M.: 3 uses for springs in legged locomotion. The International Journal of Robotics Research **9**(2), 53–61 (1990)

[7] Alexander, R.M.: Three uses for springs in legged locomotion. The International Journal of Robotics Research **9**(2), 53–61 (1990)

[8] Alexander, R.M.: A model of bipedal locomotion on compliant legs. Philosophical Transactions of the Royal Society of London. Series B: Biological Sciences **338**(1284), 189–198 (1992)

[9] Alexander, R.M.: Principles of animal locomotion. Princeton University Press (2003)

[10] Ananthanarayanan, A., Azadi, M., Kim, S.: Towards a bio-inspired leg design for high-speed running. Bioinspiration & biomimetics **7**(4), 046,005 (2012)

[11] Bertram, J.E., Gutmann, A.: Motions of the running horse and cheetah revisited: fundamental mechanics of the transverse and rotary gallop. Journal of the Royal Society Interface pp. rsif–2008 (2008)

[12] Bhounsule, P.A., Cortell, J., Grewal, A., Hendriksen, B., Karssen, J.D., Paul, C., Ruina, A.: Low-bandwidth reflex-based control for lower power walking: 65 km on a single battery charge. The International Journal of Robotics Research **33**(10), 1305–1321 (2014)

[13] Bhounsule, P.A., Cortell, J., Ruina, A.: Design and control of ranger: an energy-efficient, dynamic walking robot. In: Proc. CLAWAR, pp. 441–448 (2012)

[14] Birn-Jeffery, A.V., Hubicki, C.M., Blum, Y., Renjewski, D., Hurst, J.W., Daley, M.A.: Don't break a leg: running birds from quail to ostrich prioritise leg safety and economy on uneven terrain. Journal of Experimental Biology **217**(21), 3786–3796 (2014)

[15] Blickhan, R.: The spring-mass model for running and hopping. Journal of biomechanics **22**(11-12), 1217–1227 (1989)

[16] Blickhan, R., Full, R.: Similarity in multilegged locomotion: bouncing like a monopode. Journal of Comparative Physiology A **173**(5), 509–517 (1993)

[17] Bock, H.G., Plitt, K.J.: A multiple shooting algorithm for direct solution of optimal control problems. PROCEEDINGS OF THE IFAC WORLD CONGRESS (1984)

[18] Bramble, D.M., Carrier, D.R.: Running and breathing in mammals. Science **219**(4582), 251–256 (1983)

[19] Brodbeck, L., Hauser, S., Iida, F.: Morphological evolution of physical robots through model-free phenotype development. PloS one **10**(6), e0128,444 (2015)

[20] Buss, B.G., Hamed, K.A., Griffin, B.A., Grizzle, J.W.: Experimental results for 3d bipedal robot walking based on systematic optimization of virtual constraints. In: American Control Conference (ACC), 2016, pp. 4785–4792. IEEE (2016)

[21] Cao, Q., Poulakakis, I.: On the energetics of quadrupedal bounding with and without torso compliance. In: Intelligent Robots and Systems (IROS 2014), 2014 IEEE/RSJ International Conference on, pp. 4901–4906. IEEE (2014)

[22] Cavagna, G.A., Heglund, N.C., Taylor, C.R.: Mechanical work in terrestrial locomotion: two basic mechanisms for minimizing energy expenditure. American Journal of Physiology-Regulatory, Integrative and Comparative Physiology **233**(5), R243–R261 (1977)

[23] Cavagna, G.A., Thys, H., Zamboni, A.: The sources of external work in level walking and running. The Journal of physiology **262**(3), 639 (1976)

[24] Chatzakos, P., Papadopoulos, E.: Bio-inspired design of electrically-driven bounding quadrupeds via parametric analysis. Mechanism and Machine Theory **44**(3), 559–579 (2009)

[25] Chevallereau, C., Aoustin, Y.: Optimal reference trajectories for walking and running of a biped robot. Robotica **19**(5), 557–569 (2001)

[26] Collins, S.H., Wiggin, M.B., Sawicki, G.S.: Reducing the energy cost of human walking using an unpowered exoskeleton. Nature **522**(7555), 212–215 (2015)

[27] Collins, S.H., Wisse, M., Ruina, A.: A three-dimensional passive-dynamic walking robot with two legs and knees. The International Journal of Robotics Research **20**(7), 607–615 (2001)

[28] Dean, J.C., Kuo, A.D.: Energetic costs of producing muscle work and force in a cyclical human bouncing task. Journal of Applied Physiology **110**(4), 873–880 (2011)

[29] Di Prampero, P.: The energy cost of human locomotion on land and in water. International journal of sports medicine **7**(2), 55–72 (1986)

[30] Diehl, M., Leineweber, D.B., Schäfer, A.A.: MUSCOD-II User's Manual. IWR (2001)

[31] Eckert, P., Spröwitz, A., Witte, H., Ijspeert, A.J.: Comparing the effect of different spine and leg designs for a small bounding quadruped robot. In: Robotics and Automation (ICRA), 2015 IEEE International Conference on, pp. 3128–3133. IEEE (2015)

[32] Fallon, M.F., Marion, P., Deits, R., Whelan, T., Antone, M., McDonald, J., Tedrake, R.: Continuous humanoid locomotion over uneven terrain using stereo fusion. In: Humanoid Robots (Humanoids), 2015 IEEE-RAS 15th International Conference on, pp. 881–888. IEEE (2015)

[33] Farley, C.T., Taylor, C.R.: A mechanical trigger for the trot-gallop. Geochim. Cosmochim. Acta **53**, 2101 (1989)

[34] Folkertsma, G.A., Kim, S., Stramigioli, S.: Parallel stiffness in a bounding quadruped with flexible spine. In: Intelligent Robots and Systems (IROS), 2012 IEEE/RSJ International Conference on, pp. 2210–2215. IEEE (2012)

[35] Gabrielli, G., Von Karman, T.: What price speed?: specific power required for propulsion of vehicles (1950)

[36] Galis, F., Carrier, D.R., Van Alphen, J., Van Der Mije, S.D., Van Dooren, T.J., Metz, J.A., Ten Broek, C.M.: Fast running restricts evolutionary change of the vertebral column in mammals. Proceedings of the National Academy of Sciences **111**(31), 11,401–11,406 (2014)

[37] Gan, Z., Remy, C.D.: A passive dynamic quadruped that moves in a large variety of gaits. In: Intelligent Robots and Systems (IROS), 2014 IEEE/RSJ International Conference on, p. Accepted for publication. IEEE (2014)

[38] Gan, Z., Wiestner, T., Weishaupt, M.A., Waldern, N.M., Remy, C.D.: Passive dynamics explain quadrupedal walking, trotting, and tölting. Journal of Computational and Nonlinear Dynamics (2015)

[39] Garcia, M.S.: Stability, scaling, and chaos in passive-dynamic gait models. Ph.D. thesis, Cornell University (1999)

[40] Geijtenbeek, T., van de Panne, M., van der Stappen, A.F.: Flexible muscle-based locomotion for bipedal creatures. ACM Transactions on Graphics (TOG) **32**(6), 206 (2013)

[41] Geyer, H., Seyfarth, A., Blickhan, R.: Compliant leg behaviour explains basic dynamics of walking and running. Proceedings of the Royal Society B **273**(1603), 2861–2867 (2006)

[42] Gomes, M., Ruina, A.: Walking model with no energy cost. Physical Review E **83**(3), 032,901 (2011)

[43] Gregorio, P., Ahmadi, M., Buehler, M.: Design, control, and energetics of an electrically actuated legged robot. IEEE Transactions on Systems, Man, and Cybernetics, Part B (Cybernetics) **27**(4), 626–634 (1997)

[44] Griffin, B., Grizzle, J.: Nonholonomic virtual constraints and gait optimization for robust walking control. The International Journal of Robotics Research **36**(8), 895–922 (2017)

[45] Grimmer, M., Eslamy, M., Gliech, S., Seyfarth, A.: A comparison of parallel- and series elastic elements in an actuator for mimicking human ankle joint in walking and running. In: Robotics and Automation (ICRA), 2012 IEEE International Conference on, pp. 2463–2470. IEEE (2012)

[46] Grizzle, J., Hurst, J., Morris, B., Park, H.W., Sreenath, K.: Mabel, a new robotic bipedal walker and runner. In: American Control Conference, 2009. ACC'09., pp. 2030–2036. IEEE (2009)

[47] Ha, S., Coros, S., Alspach, A., Kim, J., Yamane, K.: Task-based limb optimization for legged robots. In: Intelligent Robots and Systems (IROS), 2016 IEEE/RSJ International Conference on, pp. 2062–2068. IEEE (2016)

[48] Haeufle, D., Taylor, M., Schmitt, S., Geyer, H.: A clutched parallel elastic actuator concept: towards energy efficient powered legs in prosthetics and robotics. In: Biomedical Robotics and Biomechatronics (BioRob), 2012 4th IEEE RAS & EMBS International Conference on, pp. 1614–1619. IEEE (2012)

[49] Haueisen, B.M.: Investigation of an articulated spine in a quadruped robotic system. Ph.D. thesis, The University of Michigan (2011)

[50] Hildebrand, M.: Motions of the running cheetah and horse. Journal of Mammalogy **40**(4), 481–495 (1959)

[51] Hildebrand, M.: Further studies on locomotion of the cheetah. Journal of mammalogy **42**(1), 84–91 (1961)

[52] Hildebrand, M.: Symmetrical gaits of horses. Science **150**(3697), 701–708 (1965)

[53] Hildebrand, M.: Analysis of asymmetrical gaits. Journal of Mammalogy **58**(2), 131–156 (1977)

[54] Hildebrand, M.: The adaptive significance of tetrapod gait selection. American Zoologist **20**(1), 255–267 (1980)

[55] Hildebrand, M.: Walking and running. Functional vertebrate morphology **3**, 38–57 (1985)

[56] Hoang, K.L.H., Mombaur, K.D.: Optimal design of a physical assistive device to support sit-to-stand motions. In: Robotics and Automation (ICRA), 2015 IEEE International Conference on, pp. 5891–5897. IEEE (2015)

[57] Hoyt, D.F., Taylor, C.R.: Gait and the energetics of locomotion in horses. Nature **292**(5820), 239–240 (1981)

[58] Hubicki, C., Grimes, J., Jones, M., Renjewski, D., Spröwitz, A., Abate, A., Hurst, J.: Atrias: Design and validation of a tether-free 3d-capable spring-mass bipedal robot. The International Journal of Robotics Research **35**(12), 1497–1521 (2016)

[59] Hurst, J., Rizzi, A.: Series compliance for an efficient running gait. Robotics & Automation Magazine, IEEE **15**(3), 42–51 (2008)

[60] Hutter, M., Gehring, C., Jud, D., Lauber, A., Bellicoso, C.D., Tsounis, V., Hwangbo, J., Bodie, K., Fankhauser, P., Bloesch, M., et al.: Anymal-a highly mobile and dynamic quadrupedal robot. In: Intelligent Robots and Systems (IROS), 2016 IEEE/RSJ International Conference on, pp. 38–44. IEEE (2016)

[61] Hutter, M., Gehring, M., Bloesch, M., Mark, A.H., Remy, C.D., Siegwart, R.Y., Mark, A.H., Mark, A.H., Siegwart, R.Y., Siegwart, R.Y.: StarlETH: A compliant quadrupedal robot for fast, efficient, and versatile locomotion. Autonomous Systems Lab, ETH Zurich (2013)

[62] Hutter, M., Remy, C.D., Hoepflinger, M.A., Siegwart, R.: Scarleth: Design and control of a planar running robot. In: Intelligent Robots and Systems (IROS), 2011 IEEE/RSJ International Conference on, pp. 562–567. IEEE (2011)

[63] Hutter, M., Remy, C.D., Siegwart, R.: Design of an articulated robotic leg with nonlinear series elastic actuation. In: International Conference on CLimbing And WAlking Robots, CLAWAR, pp. 645–652 (2009)

[64] Ilg, W., Berns, K., Jedele, H., Albiez, J., Dillmann, R., Fischer, M., Witte, H., Biltzinger, J., Lehmann, R., Schilling, N.: Bisam: From small mammals to a four legged walking machine. In: Proceedings of the Fifth International Conference on Simulation of Adaptive Behaviour, pp. 400–407 (1998)

[65] James, J., Ross, P., Ball, D.: Comparison of elastic configurations for energy efficient legged locomotion (2015)

[66] Kani, M.H.H., Ahmadabadi, M.N.: Comparing effects of rigid, flexible, and actuated series-elastic spines on bounding gait of quadruped robots. In: Robotics and Mechatronics (ICRoM), 2013 First RSI/ISM International Conference on, pp. 282–287. IEEE (2013)

[67] Karssen, J.: Robotic bipedal running: Increasing disturbance rejection. Ph.D. thesis (2013)

[68] Karssen, J., Wisse, M.: Running robot phides. In: Dynamic Walking Conference (2012)

[69] Karssen, J.D., Haberland, M., Wisse, M., Kim, S.: The effects of swing-leg retraction on running performance: analysis, simulation, and experiment. Robotica **33**(10), 2137–2155 (2015)

[70] Khoramshahi, M., Sprowitz, A., Tuleu, A., Ahmadabadi, M.N., Ijspeert, A.: Benefits of an active spine supported bounding locomotion with a small compliant quadruped robot. In: Proceedings of 2013 IEEE International Conference on Robotics and Automation, EPFL-CONF-186299 (2013)

[71] Kiguchi, K., Kusumoto, Y., Watanabe, K., Izumi, K., Fukuda, T.: Energy-optimal gait analysis of quadruped robots. Artificial life and robotics **6**(3), 120–125 (2002)

[72] Koepl, D., Hurst, J.: Force control for planar spring-mass running. In: Intelligent Robots and Systems (IROS), 2011 IEEE/RSJ International Conference on, pp. 3758–3763. IEEE (2011)

[73] Koller, J.R., Gates, D.H., Ferris, D.P., Remy, C.D.: 'body-in-the-loop'optimization of assistive robotic devices: A validation study. In: Robotics: Science and Systems (2016)

[74] Kuindersma, S., Deits, R., Fallon, M., Valenzuela, A., Dai, H., Permenter, F., Koolen, T., Marion, P., Tedrake, R.: Optimization-based locomotion planning, estimation, and control design for the atlas humanoid robot. Autonomous Robots **40**(3), 429–455 (2016)

[75] Kuo, A.D.: Choosing your steps carefully. Robotics & Automation Magazine, IEEE **14**(2), 18–29 (2007)

[76] Laughton, M.A., Warne, D.: Electrical engineer's reference book. Newnes (2002)

[77] Leeser, K.F.: Locomotion experiments on a planar quadruped robot with articulated spine. Ph.D. thesis, Massachusetts Institute of Technology (1996)

[78] Leineweber, D.: Efficient reduced sqp methods for the optimization of chemical processes described by large sparse dae models (1999)

[79] Lichtwark, G.A., Wilson, A.M.: In vivo mechanical properties of the human achilles tendon during one-legged hopping. Journal of Experimental Biology **208**(24), 4715–4725 (2005)

[80] Lohmeier, S., Buschmann, T., Ulbrich, H., Pfeiffer, F.: Modular joint design for performance enhanced humanoid robot lola. In: Robotics and Automation, 2006. ICRA 2006. Proceedings 2006 IEEE International Conference on, pp. 88–93. IEEE (2006)

[81] Ma, W.L., Kolathaya, S., Ambrose, E.R., Hubicki, C.M., Ames, A.D.: Bipedal robotic running with durus-2d: Bridging the gap between theory and experiment. In: Proceedings of the 20th International Conference on Hybrid Systems: Computation and Control, pp. 265–274. ACM (2017)

[82] Maxon Motor: Maxon Program 2010/2011 (2010-2011)

[83] McGeer, T., et al.: Passive dynamic walking. I. J. Robotic Res. **9**(2), 62–82 (1990)

[84] McGuigan, M.P., Wilson, A.M.: The effect of gait and digital flexor muscle activation on limb compliance in the forelimb of the horse equus caballus. Journal of Experimental Biology **206**(8), 1325–1336 (2003)

[85] Minetti, A., Ardigo, L., Reinach, E., Saibene, F.: The relationship between mechanical work and energy expenditure of locomotion in horses. The Journal of Experimental Biology **202**(17), 2329–2338 (1999)

[86] Minetti, A.E.: The biomechanics of skipping gaits: a third locomotion paradigm? Proceedings of the Royal Society of London. Series B: Biological Sciences **265**(1402), 1227–1233 (1998)

[87] Mochon, S., McMahon, T.A.: Ballistic walking: An improved model. Mathematical Biosciences **52**(3-4), 241–260 (1980)

[88] Mombaur, K.: Using optimization to create self-stable human-like running. Robotica **27**(03), 321–330 (2009)

[89] Moore, H.: How to mathematically optimize drug regimens using optimal control. Journal of pharmacokinetics and pharmacodynamics pp. 1–11 (2018)

[90] Moore, J.M., McKinley, P.K.: Evolving flexible joint morphologies. In: Proceedings of the 14th annual conference on Genetic and evolutionary computation, pp. 145–152. ACM (2012)

[91] Moore, T.Y., Biewener, A.A.: Outrun or outmaneuver: Predator–prey interactions as a model system for integrating biomechanical studies in a broader ecological and evolutionary context. Integrative and comparative biology p. icv074 (2015)

[92] Muraro, A., Chevallereau, C., Aoustin, Y.: Optimal trajectories for a quadruped robot with trot, amble and curvet gaits for two energetic criteria. Multibody System Dynamics **9**(1), 39–62 (2003)

[93] Owaki, D., Kano, T., Nagasawa, K., Tero, A., Ishiguro, A.: Simple robot suggests physical interlimb communication is essential for quadruped walking. Journal of The Royal Society Interface **10**(78), 20120,669 (2013)

[94] Owaki, D., Koyama, M., Yamaguchi, S., Kubo, S., Ishiguro, A.: A two-dimensional passive dynamic running biped with knees. In: Robotics and Automation (ICRA), 2010 IEEE International Conference on, pp. 5237–5242. IEEE (2010)

[95] Paine, N., Oh, S., Sentis, L.: Design and control considerations for high-performance series elastic actuators. Mechatronics, IEEE/ASME Transactions on **19**(3), 1080–1091 (2014)

[96] Park, H.W., Wensing, P.M., Kim, S.: High-speed bounding with the mit cheetah 2: Control design and experiments. The International Journal of Robotics Research **36**(2), 167–192 (2017)

[97] Paul, C., Bongard, J.C.: The road less travelled: Morphology in the optimization of biped robot locomotion. In: Intelligent Robots and Systems, 2001. Proceedings. 2001 IEEE/RSJ International Conference on, vol. 1, pp. 226–232. IEEE (2001)

[98] Posa, M., Tedrake, R.: Direct trajectory optimization of rigid body dynamical systems through contact. In: Algorithmic Foundations of Robotics X, pp. 527–542. Springer (2013)

[99] Pouya, S., Khodabakhsh, M., Spröwitz, A., Ijspeert, A.: Spinal joint compliance and actuation in a simulated bounding quadruped robot. Autonomous Robots **41**(2), 437–452 (2017)

[100] Pratt, G.A., Williamson, M.M.: Series elastic actuators. In: Intelligent Robots and Systems 95.'Human Robot Interaction and Cooperative Robots', Proceedings. 1995 IEEE/RSJ International Conference on, vol. 1, pp. 399–406. IEEE (1995)

[101] Pratt, J., Chew, C.M., Torres, A., Dilworth, P., Pratt, G.: Virtual model control: An intuitive approach for bipedal locomotion. The International Journal of Robotics Research **20**(2), 129–143 (2001)

[102] Pratt, J., Krupp, B.: Design of a bipedal walking robot. In: SPIE defense and security symposium, pp. 69,621F–69,621F. International Society for Optics and Photonics (2008)

[103] Raibert, M.H.: Legged robots that balance. MIT press (1986)

[104] Raibert, M.H., Brown, H.B., Chepponis, M.: Experiments in balance with a 3d one-legged hopping machine. The International Journal of Robotics Research **3**(2), 75–92 (1984)

[105] Ralston, H.J.: Energy-speed relation and optimal speed during level walking. Internationale Zeitschrift für angewandte Physiologie einschließlich Arbeitsphysiologie **17**(4), 277–283 (1958)

[106] Rebula, J.R., Kuo, A.D.: The cost of leg forces in bipedal locomotion: a simple optimization study. PloS one **10**(2), e0117,384 (2015)

[107] Reher, J., Cousineau, E.A., Hereid, A., Hubicki, C.M., Ames, A.D.: Realizing dynamic and efficient bipedal locomotion on the humanoid robot durus. In: Robotics and Automation (ICRA), 2016 IEEE International Conference on, pp. 1794–1801. IEEE (2016)

[108] Remy, C.D.: Optimal exploitation of natural dynamics in legged locomotion. Ph.D. thesis, Eidgenssische Technische Hochschule (2011)

[109] Remy, C.D., Buffinton, K., Siegwart, R.: A matlab framework for efficient gait creation. In: Intelligent Robots and Systems (IROS), 2011 IEEE/RSJ International Conference on, pp. 190–196. IEEE (2011)

[110] Remy, C.D., Buffinton, K., Siegwart, R.: Comparison of cost functions for electrically driven running robots. In: Robotics and Automation (ICRA), 2012 IEEE International Conference on, pp. 2343–2350. IEEE (2012)

[111] Remy, C.D., Buffinton, K.W., Siegwart, R.Y.: Stability analysis of passive dynamic walking of quadrupeds. The International Journal of Robotics Research **29**(9), 1173–85 (2010)

[112] Remy, C.D., Hutter, M., Hoepflinger, M., Bloesch, M., Gehring, C., Siegwart, R.: Quadrupedal robots with stiff and compliant actuation. Automatisierungstechnik **60**(11), 682–691 (2012)

[113] Robinson, D.W., Pratt, J.E., Paluska, D.J., Pratt, G.A.: Series elastic actuator development for a biomimetic walking robot. In: Advanced Intelligent Mechatronics, 1999. Proceedings. 1999 IEEE/ASME International Conference on, pp. 561–568. IEEE (1999)

[114] Rosendo, A., Nakatsu, S., Narioka, K., Hosoda, K.: Pneupard: A biomimetic musculoskeletal approach for a feline-inspired quadruped robot. In: Intelligent Robots and Systems (IROS), 2013 IEEE/RSJ International Conference on, pp. 1452–1457. IEEE (2013)

[115] Schilling, N., Fischer, M.: Kinematic analysis of treadmill locomotion of tree shrews, tupaia glis (scandentia: Tupaiidae). Zeitschrift fur Saugetierkunde **64**, 129–153 (1999)

[116] Semini, C., Barasuol, V., Goldsmith, J., Frigerio, M., Focchi, M., Gao, Y., Caldwell, D.G.: Design of the hydraulically actuated, torque-controlled quadruped robot hyq2max. IEEE/ASME Transactions on Mechatronics **22**(2), 635–646 (2017)

[117] Seyfarth, A., Geyer, H., Gunther, M., Blickhan, R.: A movement criterion for running. Journal of Biomechanics **35**(5), 649–55 (2002)

[118] Seyfarth, A., Iida, F., Tausch, R., Stelzer, M., von Stryk, O., Karguth, A.: Towards bipedal jogging as a natural result of optimizing walking speed for passively compliant three-segmented legs. The International Journal of Robotics Research **28**(2), 257–265 (2009)

[119] Sims, K.: Evolving 3d morphology and behavior by competition. Artificial life **1**(4), 353–372 (1994)

[120] Smit-Anseeuw, N., Gleason, R., Vasudevan, R., Remy, C.D.: The energetic benefit of robotic gait selectiona case study on the robot ramone. IEEE Robotics and Automation Letters **2**(2), 1124–1131 (2017)

[121] Spröwitz, A., Tuleu, A., Vespignani, M., Ajallooeian, M., Badri, E., Ijspeert, A.J.: Towards dynamic trot gait locomotion: Design, control, and experiments with cheetah-cub, a compliant quadruped robot. The International Journal of Robotics Research **32**(8), 932–950 (2013)

[122] Srinivasan, M.: Fifteen observations on the structure of energy-minimizing gaits in many simple biped models. Journal of The Royal Society Interface p. rsif20090544 (2010)

[123] Srinivasan, M., Ruina, A.: Computer optimization of a minimal biped model discovers walking and running. Nature **439**(7072), 72–75 (2006)

[124] Thomson: Lead screws, ball screws, and ball splines catalog (2016)

[125] Tsujita, K., Kawakami, M., Tsuchiya, K.: A study on optimal gait pattern of a quadruped locomotion robot. In: Systems, Man and Cybernetics, 2004 IEEE International Conference on, vol. 1, pp. 745–749. IEEE (2004)

[126] Tucker, V.A.: The energetic cost of moving about: Walking and running are extremely inefficient forms of locomotion. much greater efficiency is achieved by birds, fishand bicyclists. American Scientist **63**(4), 413–419 (1975)

[127] Westervelt, E.R., Grizzle, J.W., Chevallereau, C., Choi, J.H., Morris, B.: Feedback control of dynamic bipedal robot locomotion, vol. 28. CRC press (2007)

[128] Wisse, M., Schwab, A.L., van der Linde, R.Q., van der Helm, F.C.: How to keep from falling forward: elementary swing leg action for passive dynamic walkers. Robotics, IEEE Transactions on **21**(3), 393–401 (2005)

[129] Xi, W., Remy, C.D.: Optimal gaits and motions for legged robots. In: Intelligent Robots and Systems (IROS), 2014 IEEE/RSJ International Conference on, p. Accepted for publication. IEEE (2014)

[130] Xi, W., Yesilevskiy, Y., Remy, C.D.: Selecting gaits for economical locomotion of legged robots. The International Journal of Robotics Research **35**(9), 1140–1154 (2016)

[131] Yang, T., Westervelt, E., Schmiedeler, J.P., Bockbrader, R.: Design and control of a planar bipedal robot ernie with parallel knee compliance. Autonomous robots **25**(4), 317–330 (2008)

[132] Yesilevskiy, Y., Gan, Z., Remy, C.D.: Optimal configuration of series and parallel elasticity in a 2d monoped. In: 2016 IEEE International Conference on Robotics and Automation (ICRA), pp. 1360–1365. IEEE (2016)

[133] Yesilevskiy, Y., Gan, Z., Remy, C.D.: Energy-optimal hopping in parallel and series elastic 1d monopeds. ASME. J. Mechanisms Robotics (2018)

[134] Yesilevskiy, Y., Xi, W., Remy, C.D.: A comparison of series and parallel elasticity in a monoped hopper. In: Robotics and Automation (ICRA), 2015 IEEE International Conference on, pp. 1036–1041. IEEE (2015)

[135] Yesilevskiy, Y., Yang, W., Remy, C.D.: Spine morphology and energetics: How principles from nature apply to robotics. Bioinspiration & biomimetics (2018)

[136] Zhao, Q., Ellenberger, B., Sumioka, H., Sandy, T., Pfeifer, R.: The effect of spine actuation and stiffness on a pneumatically-driven quadruped robot for cheetah-like locomotion. In: Robotics and Biomimetics (ROBIO), 2013 IEEE International Conference on, pp. 1807–1812. IEEE (2013)